A geological and geophysical description of the Arc Mounds, southwest Porcupine Bank

INFOMAR
Integrated Mapping for the Sustainable Development of Ireland's Marine Resource

Final Report

July 2013

Fiona Stapleton*

John Murray

Anthony Grehan

Garret Duffy

Mike Williams

*f.stapleton1@nuigalway.ie

Earth & Ocean Sciences
School of Natural Sciences
NUI Galway
OÉ Gaillimh

In collaboration with: Ifremer

Contents

Abstract

Deep-water cold-water coral carbonate mounds occur worldwide and are prominently developed along the European margin, where they constitute an important marine ecosystem. Such ecosystems are the focus of considerable research efforts at present - in particular, trying to understand their initiation and maintenance processes. This project involves a description of what have been termed the 'Arc Mounds'; a previously undescribed region situated on the south-western margin of the Porcupine Bank, which features coral mounds aligned along scarps. The geological and geomorphological setting of these bioherms was characterised geophysically using ship- and ROV-mounted multibeam and subbottom profiler data. Mapping the extent and location of the Arc Mounds has revealed over 40 carbonate build-ups, tens to a few hundreds of metres long and generally 50 m high, grouped mainly in water depths of between 630 m and 850 m. It appears that the living coral frameworks are located along these topographic highs, facing the main flow of the bottom currents, where hard and firm substrata and/or failure-related sediment bedforms occur. This information was augmented with sedimentological and palaeontological data from two piston cores; recovered from the summit of a carbonate mound, and from laterally equivalent off-mound facies on the adjacent seafloor. The differences between the two cores illustrate the role cold-water corals play in constructing large 3-dimensional structures on the seabed. Such mound-like morphologies are thus interpreted as a result of sediment accreted by coral growth and consequent sediment trapping; their burial prevented by bottom currents. A prominent sub-mound reflector and sediment recovered from the equivalent depth indicates that the mounds initially developed on a carbonate hardground. The development of the coral mounds, in this area of the Porcupine Bank, appears to be the result of an interaction between drift deposition and biological growth processes which are influenced by both the local topography and current regime.

Keywords: cold-water coral; carbonate mound; multibeam; NE Atlantic

Acknowledgements

We are deeply indebted to INFOMAR for providing the main financial support for this research endeavour.

The geophysical and geological data presented in this report was collected by IFREMER on the BobEco cruise, onboard the RV *Pourqoui Pas?* IFREMER is thanked for making this data available to us and for providing considerable assistance and advice with the sediment core analysis at Brest. Additionally, a *Thomas Crawford Hayes Research Award* was awarded by the NUI Galway School of Natural Sciences to Ms. Stapleton and was used to travel to the IFREMER institute in France in order to log the cores. Ms. Stapleton wishes to sincerely thank Jean-Francois Bourreliet and Matthieu Veslin for their contribution to this work and for their help during her stay at IFREMER. We also sincerely thank Louise Allcock and Patrick Collins of the Ryan Institute in NUI Galway for identification of shell material.

Chapter 1: Introduction

Cold-water corals have been known to science since Linnaeus' *Systema Naturae* in 1758; yet, there is still a paucity of information on cold-water coral biology, distribution, behaviour and ecology. However, interest in cold-water corals has escalated with technological developments and improvements in deep-water research. It is only within the last few decades that, due to the increased use of deep-water acoustics, the spatial extent (distribution) of cold-water corals is being realised. It is now known that cold-water corals form reefs from the polar to tropical habitats (Wood, 1999) including: continental shelves, slopes, banks, on seamounts, in fjords and on submarine canyon walls (van der Land, 2011).

It was only in the 1960s that deep-sea exploration lead to the discovery of mound-like structures colonised by corals (Stetson *et al.*, 1962). Cold-water coral mounds develop through successive build-ups of in-situ (autochthonous) coral debris and related trapped or baffled externally supplied (allochthonous) sediment. (Mazzini *et al.*, 2012). Cold-water coral mounds represent unique habitats in terms of biodiversity, providing records of climate fluctuations and also carbon sinks (Klages *et al.*, 2004). As much information about the palaeoenvironmental conditions in which the cold-water corals existed is needed in order to adequately predict their ability to survive in the future. Additionally, as carbonate mounds are well known from the fossil record (see Wood, 1999 and references therein), studying contemporary examples may aid in their interpretation.

1.1: Project Motivation

Designated Area of Conservation

The controls on the growth and decline of corals on carbonate mounds have yet to be fully understood. In order to elucidate these processes, mound genesis, topography and morphology must be investigated. This work sets out to describe the Arc Mounds in such a context and aims to support designating the region as a Special Area of Conservation under the Habitats Directive. Reasons for conserving such habitats include:

(i) The mound habitats are biodiversity centres

(ii) These bioherms play an important role in the carbon cycle *and*

(iii) The skeletons of the corals themselves are important archives for climate and environmental change

(i) *Biodiversity centre*

Cold-water coral reefs occurring on coral carbonate mounds are as rich in associated fauna as their tropical reef counterparts (e.g. van der Land, 2011) making them high biodiversity centres (Wheeler *et al.*, 2011). Sponges, molluscs, bryozoa, gastropods, anemones, and fishes are commonly found using the coral framework as a nursery, refuge or stable substrate to grow upon (van der Land, 2011).

(ii) *Carbonate budget estimations*

Reefs are major producers of carbonate sediment and therefore may be significant sinks for inorganic carbon, which is important for global carbon budget estimations (Titschack *et al.*, 2009). If coral reefs act as significant storehouses of carbon and regulators of atmospheric CO_2, then they may have a role in the control of climate and sea-level fluctuation.

(iii) *Corals as archives*

The skeletons of reef-builders record the local temperature and chemical characteristics of the sea water in which they grew (Wood, 1999). Therefore corals are one of a limited number of archives that record deep-sea conditions at very high resolution. Understanding how the earth's climate has changed naturally in the past will aid in prediction of the future but will also help in quantifying how much man influences the environment.

Possible threats to cold-water coral habitats

Immediate threats

Coral has a slow habitat recovery rate (Connell, 1997). Human activities such as trawling, oil and gas exploration, and undersea pipe-laying constitute some of the greatest threats to cold-water corals. The documented destruction of deep-water corals by trawling (e.g. Hall-Spencer *et al.*, 2002) necessitates the implementation of protective measures in order to ensure the long-term survival of these habitats.

Longer-term threats

Carbonate chemistry determines whether it is physically possible for corals to calcify, thus future global warming and ocean acidification also pose a threat to these ecosystems. Orr *et al.* (2005) demonstrated that the depths at which hard corals are able produce their skeletons are likely to decrease within the timescale of the present century. Guinotte *et al.* (2006) overlaid the predicted shallowing on the current distribution of cold-water corals, and found that many of the cold-water coral habitats may soon be in corrosive seawater.

1.2: Project Objectives

This project involves the analysis of a combination of geophysical and geological (sedimentological and palaeontological) data acquired from the Arc mound province in the Porcupine Bank. The aims are to:

(i) Create multi-scale digital terrain models, backscatter mosaics and bathymetric terrain analysis rasters of the carbonate mound structures.

(ii) Conduct a detailed analysis of the sedimentology and (macro- and micro-) faunal content of the cores.

(iii) Interpret the geological setting and its importance as a contributing factor to present day coral growth and type and distribution of the mounds.

1.3: Materials and Methods

A program of multibeam sounding, sidescan sonar, sub-bottom profiling, coring, and video dives was completed on the west Porcupine Bank During Leg two of the BobEco (**B**ay **O**f **B**iscay – **ECO**logy) cruise on the French Research Vessel *Pourqoui Pas?* (23rd September - 10th October 2011).

Two shipborne and one ROV (remotely operated vehicle) multibeam datasets were acquired. ROV multibeam backscatter data were acquired simultaneously with the bathymetric data. Video data was acquired along an ROV route at 70 m altitude and also along the OTUS transect (black and white camera) at 10 m altitude for long range optical imaging. The data

was added to the ArcMap Geographic Information System (GIS) for map creation, geospatial manipulation and analysis.

The precise methodologies employed are described in the following sections of this report:

		Section:
Geophysical (Chapter 3)	Creation of multi-scale bathymetric terrain models & analysis rasters	**3.1**
	Interpretation of sidescan data	**3.2**
	Interpretation of chirp data	**3.3**
Geological (Chapter 4)	Deployment of Multi-Sensor Core Logger	**4.2**
	cm-scale logging of the sedimentary facies variation	**4.3**
	Sub-sampling of sediments and coral from the cores	
	Laser & sieve-based grain size analysis of the core sediment subsamples	**4.4**
	Thin-section petrography (of base-cutter sediment)	**4.5**
	Thin-section petrography (of *in-situ* dropstones recovered from sediment)	**4.6**

Chapter 2: Location and Environmental Context

2.1: Area of Interest

The area examined during this research was located in the Arc Mounds province in the southwest Porcupine Bank in the North Atlantic (Fig. 2.1). The Porcupine Bank forms a raised area of seabed lying between the Porcupine Seabight and Rockall Trough water basins (Fig. 2.1). The Porcupine Bank is positioned between 51°N – 54°N and 12°W – 15°W and covers an area of approximately 10,000 km^2 (Scoffin and Bowes, 1988). Approximately 110 km^2 of seafloor was examined, located from 51°15'N – 51°22'N and 14°50'W – 14° 39'W.

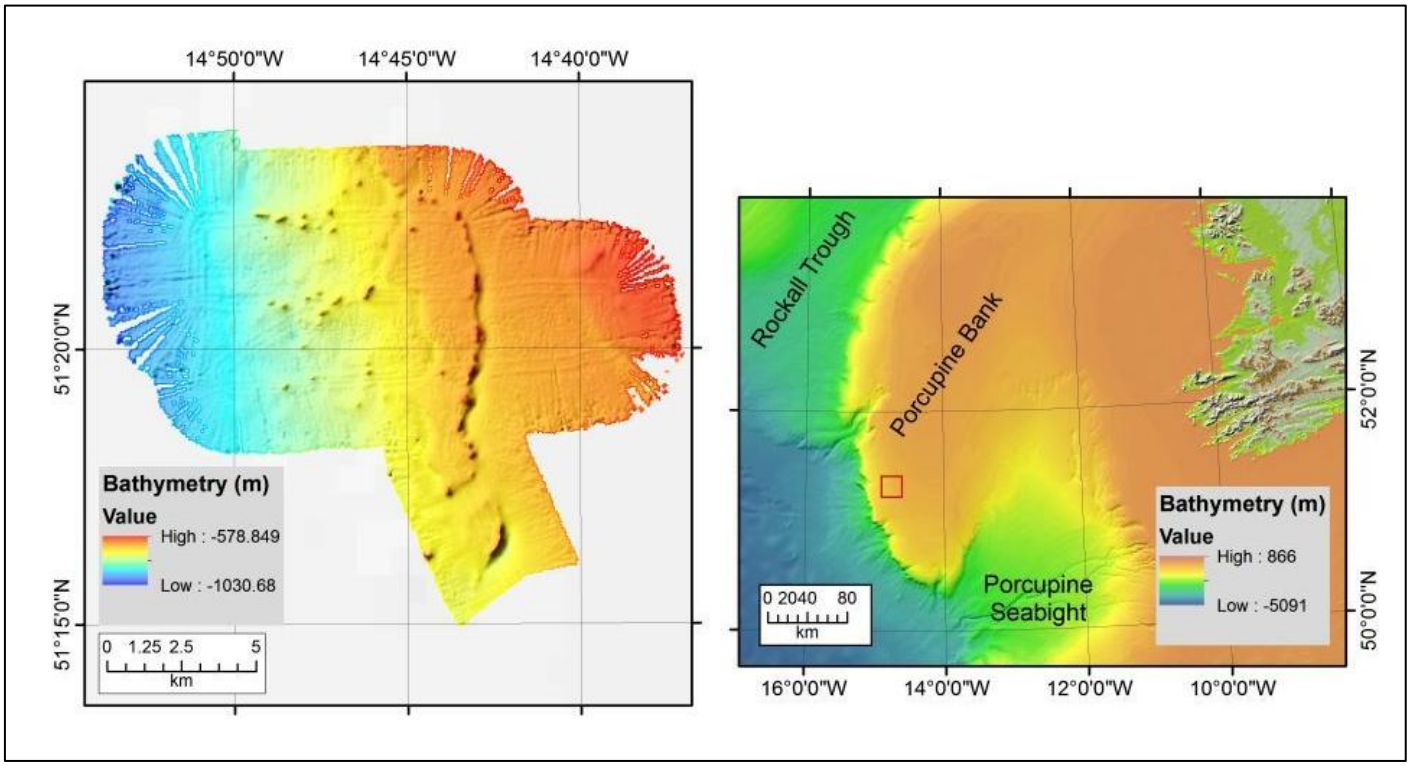

Fig. 2.1: Location of area of interest. Bathymetry of seafloor using GEBCO (General Bathymetric Chart of the Ocean) data with horizontal grid spacing of 30 arc seconds, WGS 1984). The location of the detailed survey map Reson 7150 50 m BASE overlain on hillshade (on left) is indicated by the red inset box in the general location map (on right).

2.2: Hydrography

The Porcupine Basin and its surrounding margins have been below sea level since the late Cretaceous, the exception being a period of exposure during the early Eocene (Shannon *et al.*, 2001). Water depths on the Bank range from less than 50 m to greater than 500 m (Scoffin and Bowes, 1988) and the Irish Shelf break is located at approximately 600 m water depth (Øvrebø *et al.*, 2006). The southern, western and northern margins of the Porcupine Bank are steep, whereas the east margin, towards the Porcupine Seabight, is gentle (Fig. 2.1). The depth of the permanent thermocline in the NE Atlantic lies between 600 and 1000 m, forming below the winter mixed layer (White and Dorschel, 2010).

The hydrodynamic regime at the Porcupine Bank is dominated by the presence of Eastern North Atlantic Water [ENAW]. ENAW is that part of Central water (500 – 1000 m water depth) that is more saline than the Western North Atlantic Water [WNAW], and overlies Labrador Sea Water [LSW] which re-circulates at depth below 1200 m (Frank *et al.*, 2009). ENAW forms in the Bay of Biscay (Pollard *et al.*, 1996) and is advected northwards, along the Porcupine Bank into the southern Rockall Trough by the poleward, 50 km-wide, Shelf Edge Current [SEC] with average speeds of 15 – 30 cm/s^{-1} (New and Smythe-Wright, 2001). The Slope Current [SC] flows along the continental slope from south of the Porcupine Bank to the Faroe-Shetland Channel (Hackett and Petter Røed, 1998). The SEC is the strongest and most shoreward filament of the SC (Gyory *et al.*, 2003).

The inferring of the south to north current is based on:

(i) *Bedform geometries* - Kenyon *et al.* (2003) noted medium-sized sand waves between the mounds on the Porcupine Bank, indicating possible current velocities of 40-50cm/s.

(ii) *Modern current meter data* (e.g. White and Bowyer, 1997) and

(iii) *Pattern of scour around the upper-slope carbonate mounds* (Øvrebø, 2005). The presence of the Porcupine Bank accelerates the contour-following currents as they flow along the margin (Wheeler *et al.*, 2005).

2.3: Geology

The Porcupine Bank is a remnant of the palaeocontinent of Pangaea; that split-off as a failed rift during the opening of the proto-North Atlantic in the Middle to Late Jurassic (Naylor and Mounteney, 1975, Van Rooij *et al.*, 2007b). The bank is still connected to the Irish continental margin in the northeast by the underlying Slyne Ridge (Dorschel *et al.*, 2010).

The bedrock geology of the Porcupine Bank is poorly constrained at present. It consists of a metamorphic basement overlain by Upper Palaeozoic siltstones and sandstones, with patches of Mesozoic (Lower Cretaceous) shallow-marine deposits (Masson *et al.*, 1989). The only cored section of this basement, retrieved by a MEBO ("Meeresboden-Bohrgerät", German for "sea floor drill rig") shallow borehole in 2006, showed it to be a granitic orthogneiss. U-Pb Zircon geochronology indicated a crystallisation age of ~1.3 Ga and it was likely metamorphosed during the Grenvillian Orogeny (Daly *et al.*, 2008). Upper Palaeozoic sediments, along with plutonic and metamorphic rocks, have been collected from the western margin of the Porcupine Bank by the submersible *Cyana* (Tate and Dobson, 1989).

The surrounding deeper waters to the west, north and south, and the broad Irish Shelf to the east (Fig 2.1) results in the Porcupine Bank being significantly removed from terrigenous sedimentation, resulting in carbonate sediment accumulation on the bank (at present) and mixing with relict quartz sands and other glacial material (Scoffin and Bowes, 1988). These workers produced a depth-related facies model for modern open-sea temperate carbonate sediments which predicted that in water depths greater than 500 m, planktonic foraminifera would be the primary bioclastic constituent, whereas water depths of 200 – 500 m were associated with benthic foraminifera and *Lophelia* coral patches.

2.4: Carbonate Mounds

Carbonate mounds are common in deep offshore areas to the west of Ireland. White and Dorschel (2010) produced a map of the North East Atlantic carbonate mound provinces based on Irish National Seabed Survey data (Fig. 2.2). 1013 individual mounds were documented on the continental slopes in water depths of 500 – 1,500 m. The size and shape of the mounds vary considerably, from simple cones hundreds of metres wide to complex amalgamated ridge features with some having a 5 km base diameter (footprint) and rising to 300 m above the seafloor (e.g. De Mol *et al.*, 2002, White and Dorschel, 2010).

On the Porcupine Bank these carbonate mounds are developed between 500 – 1200 m water depths (Klages *et al.*, 2004), with numerous examples hundreds of metres in height (Wheeler *et al.*, 2005). Many of these bioherms are believed to have initiated on common erosional surfaces, tentatively dated as Pliocene (Kenyon *et al.*, 2003, van Weering *et al.*, 2003). The Pelagia Mounds of the northern Porcupine Bank are noted as relatively isolated, discrete structures existing in a strong current regime (Kenyon *et al.*, 2003, van Weering *et al.*, 2003). Kenyon *et al.* (2003) found the Pelagia mounds to be made up of interbedded layers of foraminiferal ooze and coral debris, with thickets of living coral and associated benthic organisms covering the upper parts of the mounds.

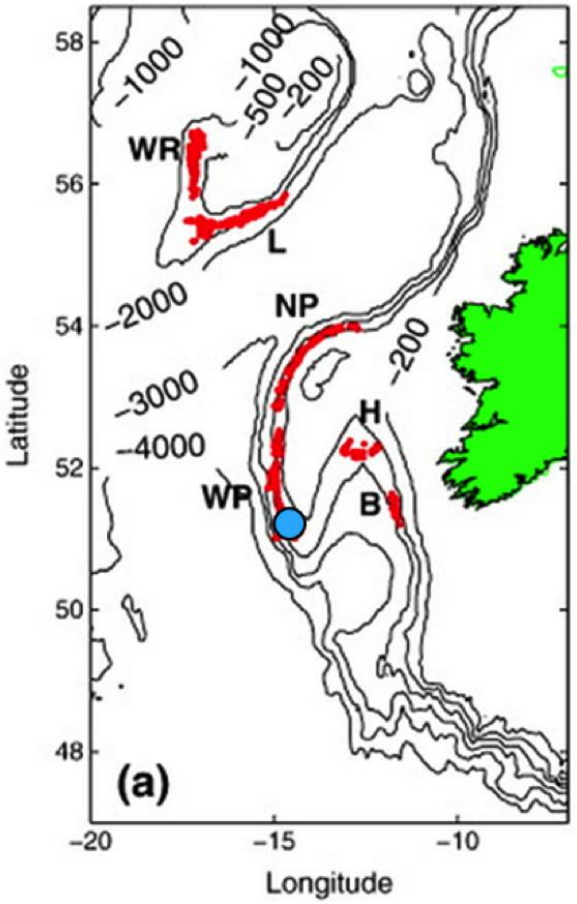

Fig 2.2: Location of the carbonate mound provinces in the North East Atlantic produced by (White and Dorschel, 2010) and based on Irish National Seabed Survey data. 1013 individual mounds were documented, ranging from 10s to 100s of meters high with some having a 5km base diameter. The mound provinces, indicated by the letters, occur on the upper continental slopes: WR- west Rockall, L = Logachev, NP- north Porcupine, WP-west Porcupine, Hovland, B- Belmount. Arc Mounds region indicated by blue dot.

2.4.1: Ecology of mounds

The Porcupine Bank corals currently exist in well-ventilated, near-thermocline waters of temperature 4 – 12 °C, close to, or within, the oxygen minimum zone reflecting high concentrations of suspended organic material (Frank *et al.*, 2009, Wheeler *et al.*, 2007). High surface productivity has been measured over the bank and is ascribed to water circulation around the bank causing nutrient accumulation (White *et al.*, 2005). It has been suggested that, due to high surface productivity and the downslope transport of this organic matter to the benthic flank regions, there is enhanced nutrient availability for coral growth (White *et al.*,

2005). Intermediate nepheloid layers (Dickson and McCave, 1986, Kenyon *et al.*, 2003) have also been cited as a mechanism of providing a food supply.

2.4.2: Scarps and Hardgrounds

Porcupine Bank mounds predominantly occur on sub-parallel topographic ridges that overlie boundary faults, interpreted as fault scarps (Wheeler *et al.*, 2005). The scarp investigated by Klages *et al.*, (2004) at the Porcupine Bank[1], was composed of a 10 cm capping-layer of limestone hardground, coated with a thin layer of manganese oxide, which was protecting softer carbonate-rich rocks beneath and was littered with ice-rafted debris [IRD] on its top surface. The IRD implies that the scarps predate the last glaciation and the formation of the metal precipitate indicates that the rock was exposed at the seabed for a considerable period of time. Notwithstanding, the non-lithified nature of the underlying sediment suggested to Klages *et al.*, (2004) that they were Quaternary in age. The coincidence of the topographic scarps with the inferred Rockall Trough boundary faults suggested to these workers that hydrocarbon seepage along these faults may have stimulated mound development; however, an alternative suggestion put forward was that the scarps may have formed by preferential seabed erosion (due to a lack of evidence for neo-tectonic activity in the area).

Mazzini *et al.* (2012) also identified calcite, dolomite and phosphatic hardgrounds in samples from a scarp framing the eastern part of the Porcupine Bank Canyon region. They suggested that water column stratification, enhanced bottom currents, and upwelling facilitated the deposition of organic matter and that subsequent phosphatisation lead to the formation of phosphate-glauconite deposits.

(Noé *et al.*, 2006) also found hardgrounds associated with carbonate mounds in the Porcupine Seabight and the Rockall Bank. [2] These were composed of mid-Pleistocene lithified carbonates, ranging from chalks to micritic limestones, which were exhumed during the Holocene. Current-induced sedimentary structures, a non-luminescing matrix indicating oxic pore fluids, and a marine isotopic signature lacking a depleted carbon regime indicated to Noé *et al.*, (2006) that these hardgrounds clearly differed from bacterially induced authigenic carbonate crusts, typical of hydrocarbon seep settings. Carbonate lithification was ascribed to carbonate ion diffusion from supersaturated seawater into pore fluids, with vigorous bottom currents the ultimate control.

[1] , This work was part of Expedition ARKTIS XIX/3 and was conducted on the research vessel POLARSTERN in 2003.

[2] This work was completed during the RV Meteor cruises M161-1 and M161-3 in 2004.

The Challenger Mound basal firmground separates underlying, Miocene glauconitic siltstones from the (Plio-) Pleistocene mound sequence above (Thierens *et al.*, 2010). A late Miocene to late Pliocene erosion event, attributed to major oceanographic changes at the onset of Northern Hemisphere glaciation and the associated re-introduction of Mediterranean Ocean Water, is considered to have created this feature (Thierens *et al.*, 2010).

In fact, many occurrences of hardgrounds have been documented on erosive mound flanks (van Weering *et al.*, 2003). Noé *et al.* (2006) concluded that hardgrounds are an essential element of carbonate mound growth as they provide a substrate for the mound-building invertebrates to colonise and stabilise the inclined mound flanks.

Hardgrounds develop when carbonate production and sedimentation rates are low, a condition that would, for example, be promoted during glacial periods (Dorschel *et al.*, 2005, Smeulders, 2011, van Weering *et al.*, 2003). The mechanism of hardground formation is still under investigation but the two main hypotheses, as summarised by Noé *et al.*, (2006), are:

1. Fine-grained pelagic sediments accumulate in off-mound sites in areas protected from currents. The sediments become trapped (baffled) within the coral framework on the mound flanks and top and become lithified by early-diagnetic physicochemical processes.
2. Bacteria contribute to a syndepositional mound stabilisation by metabolic products which induce carbonate precipitation at the base and within the mounds.

Chapter 3: Geophysical Investigation

3.1: Multibeam

3.1.1: Acquisition

The remotely operated vehicle [ROV] was deployed on the 12th September 2011 at 1633 hrs and reached sea-bottom at 1720 hrs. MMR-OTUS (photography) was acquired at 10 m from the bottom in order to determine coral cover. Following coral presence determination, multibeam data was acquired at 50 – 70 m altitude by VICTOR 6000 during dive PL474-12, using the Reson 7125/400 kHz echosounder.

The ROV dive was approximately 23.5 hours in duration and distance travelled was 18 km. Bathymetric datasets from the ship multibeam, Reson7150/24 kHz and Reson7111/100 kHz, were then obtained in the same area. The echosounder attributes are listed in Table 3.1.1 (below).

Manufacturer	Model	Frequency (kHz)	Max Depth Range	Swath Coverage
Reson	SeaBat 7150	24 kHz	15 km	150°
Reson	SeaBat 7111	100 kHz	1 km	150°
Reson	SeaBat 7125 (ROV)	400 kHz	600 m	128°

Table 3.1.1: Echosounder attributes

ROV VICTOR

The SeaBat 7125 multi-beam echo-sounder system has up to 128° swath coverage to an altitude of at least 100 m. The maximum slant range is greater than 200 m. 512 equally spaced bathymetry soundings are generated per ping. The soundings may then be corrected for refraction, mechanical offsets between the projector and hydrophone, sensor offsets, attitude, heading, depth and tide. The performance attributes of the ROV Victor are listed in Table 3.1.2 (below)

Depth	6000 m
Frequency	400 kHz
Beams	512 equidistant
Bathymetric accuracy	0.2% altitude ROV
Resolution	5% altitude ROV
Swath width	3.4 × altitude ROV (< 200 m)

Table 3.1.2: Performance attributes of the ROV Victor

3.1.2: Processing

Tide corrections were applied onboard in real time for the ship's multibeam, using SHOM predictions. Multibeam data quality can be affected by several variables during acquisition; survey speed, weather conditions, water column composition, and vessel type can all produce 'noise' artefacts in multibeam datasets.

The program CARIS HIPS & SIPS 7.1 was used in NUI Galway to manually clean and quality-check the survey data and to create Digital Terrain Models [DTMs] for 3D viewing of the sea floor. The multibeam data was cleaned in CARIS using the subset editor (area-based cleaning), swath editor (line-based cleaning) and the attitude editor. Swath editor and attitude editor were opened simultaneously in order to investigate noise at perpendicular lines. 20 cm to 1 m grid size Bathymetry Associated with Statistical Error [BASE] surfaces were created for the ROV data depending on the quality of the data and the ROV altitude. At 70 m altitude and ~200 m corridor, DTMs were processed to a 50 cm grid size. 75 m to 25 m grid size DTMS were created from the shipborne multibeam. Fig. 3.1.1 shows the overall effect of cleaning the data in CARIS.

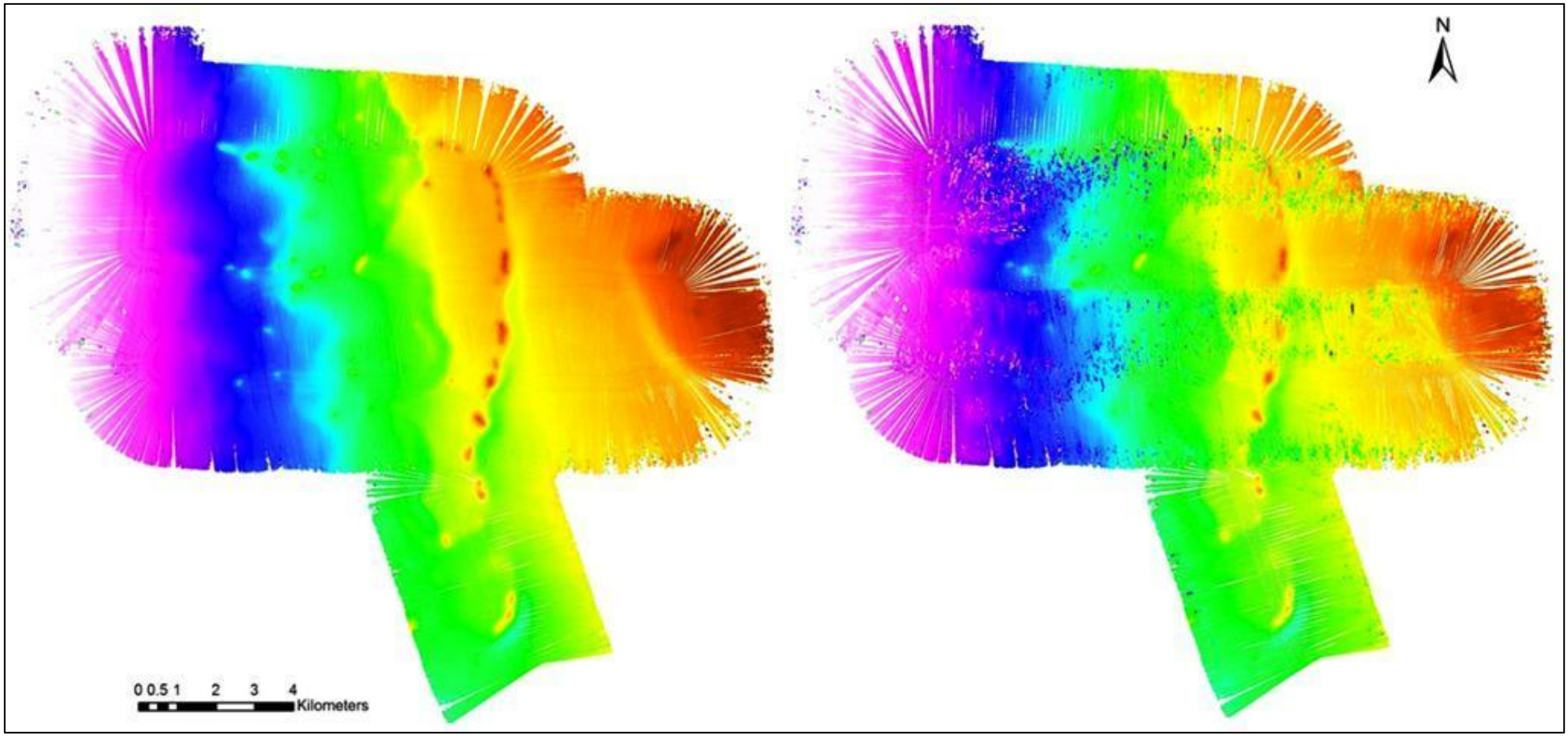

Fig. 3.1.1: Reson 7150 (24 kHz) 50 m grids. Cleaned BASE (left) and non-cleaned BASE surface (right). Images are non-sun illuminated to best display the effect of cleaning.

Error in navigation information

During conversion of the ROV multibeam files, an error caused a survey line to verge for hundreds of km to the southeast. To correct for this, the bounds in the manual navigation were filtered to contain only readings within (N51°24', W14°35') – (N51°15', W14°53'), and the error was removed. Quality soundings that lay outside the 1 and 2 quality flags were also rejected.

Correcting the depth information

Creating a BASE surface in CARIS showed water depths to be greater than expected. The GPS height (actual depth) was found to be correct in the attitude editor but the BASE showed the area to be twice as deep. Depth information in the raw data (s7k file) includes the depth of the ROV vehicle. However, the depth of the vehicle data is also included in the delta draft telegram. During the Merge process in CARIS the delta draft data was added to the measured depths. This resulted in the depth of the vehicle being added twice (once during creation of the s7k file and again within CARIS). Correction involved using the *Generic Data Parser*.

Correcting for GPS tide using Generic Data Parser

1. In CARIS all lines were selected and the process function was used to compute the GPS tide. In the Attitude Editor, the sensor layout was opened and the GPS tide was brought over to 'active'. The GPS tide was then exported using the Export Wizard 'HIPS tide' and opened to view in TextPad (Fig. 3.1.2)

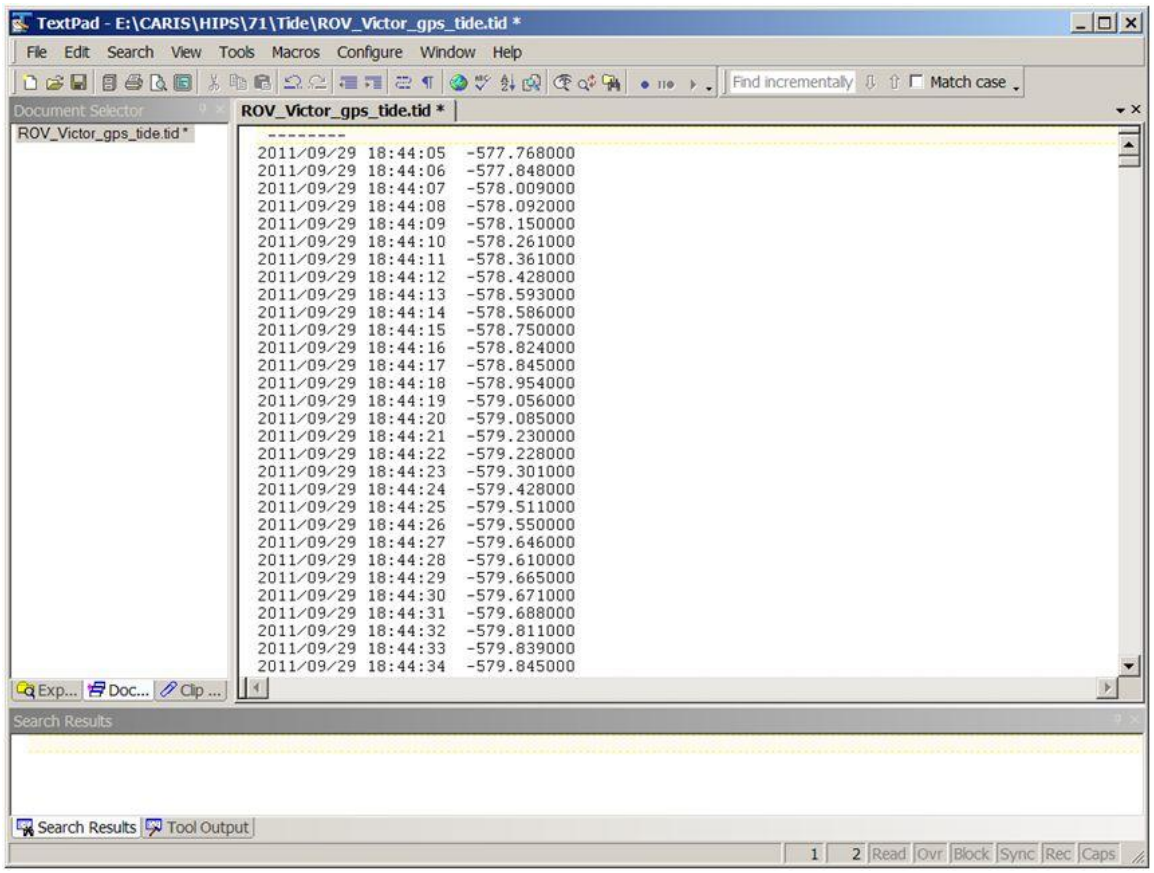

Fig. 3.1.2: A GPS tide file

2. In CARIS the Generic Data Parser (GDP) was opened in the Import functions and the raw data (i.e. the exported GPS tide file) was opened. The File Header, File Date and Time Stamps were defined and the GDP was then used to multiply the GPS tide data by -1 (Fig 3.1.3). The GDP could then be run, updating the existing survey lines. The GDP was closed and the session in CARIS was saved.

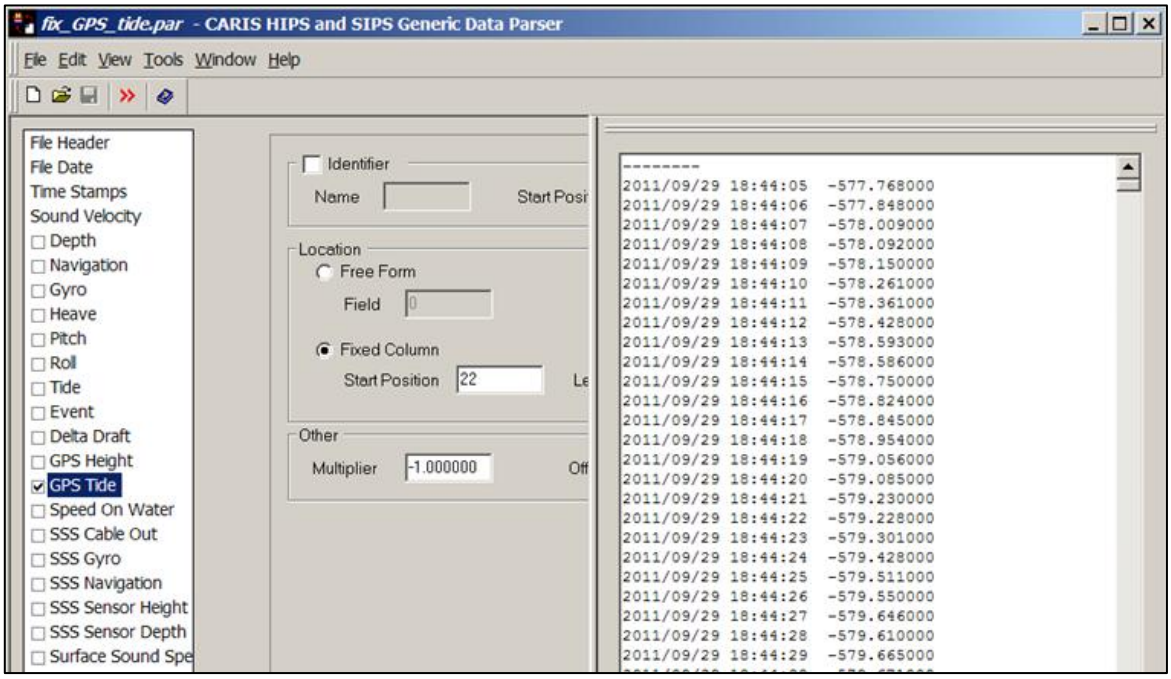

Fig. 3.1.3: Multiplying the GPS tide by -1 in the Generic Data Parser. Before this is done the File Header, Date and Time Stamps must be defined

3. The CARIS session was reopened and the lines were remerged, applying the GPS tide. A new BASE surface was created. The depths were checked and found to be correct (Fig 3.1.4.). Correcting the depth reduced the error threshold. The pre-corrected BASE had a pronounced 'groove' in the southeast which was greatly lessened by correcting the depth (Fig. 3.1.5).

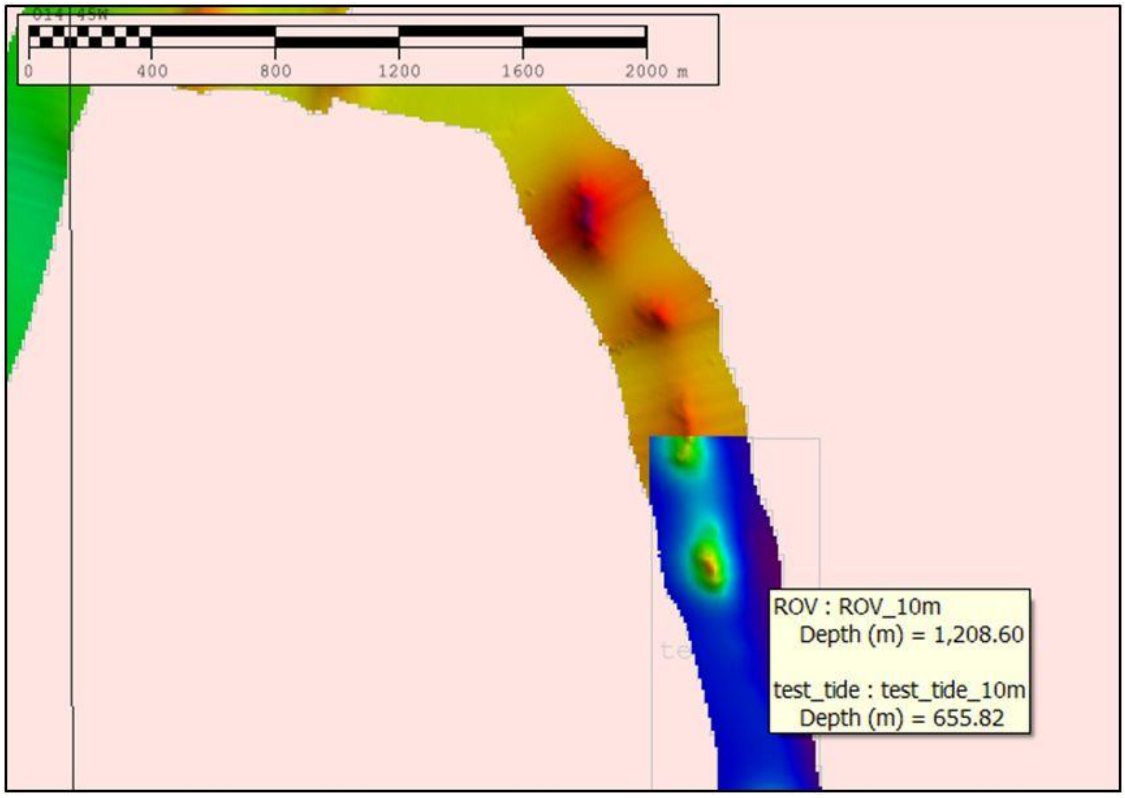

Fig. 3.1.4: The pre-corrected BASE surface (ROV_10m) shows deeper depths (1208.6m) and the corrected BASE surface (test_tide_10m), created using remerged lines with the GPS tide multiplied by -1, shows the true shallower depths (655.82m)

Correcting axial noise using attitude editor

The Navigation editor was initially used to try to remove anomalous turnabouts of the ROV, but it was through rejecting gyro in the Attitude editor that these spiral artefacts were removed (Fig. 3.1.6)

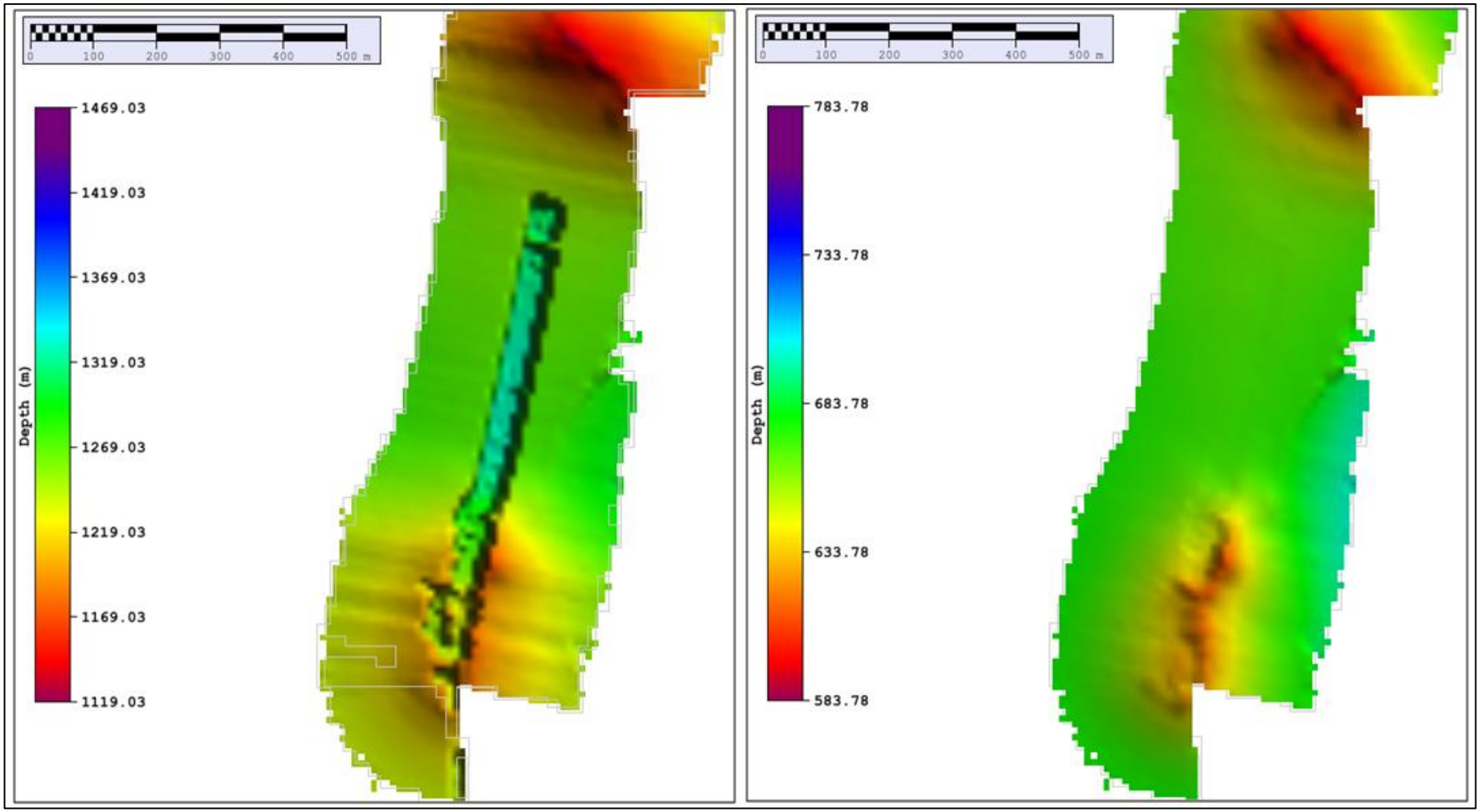

Fig. 3.1.5 Left: BASE of incorrect depth, 10 m resolution, showing groove with deeper soundings. Right: Depth-corrected BASE, 10 m resolution, showing groove greatly lessened.

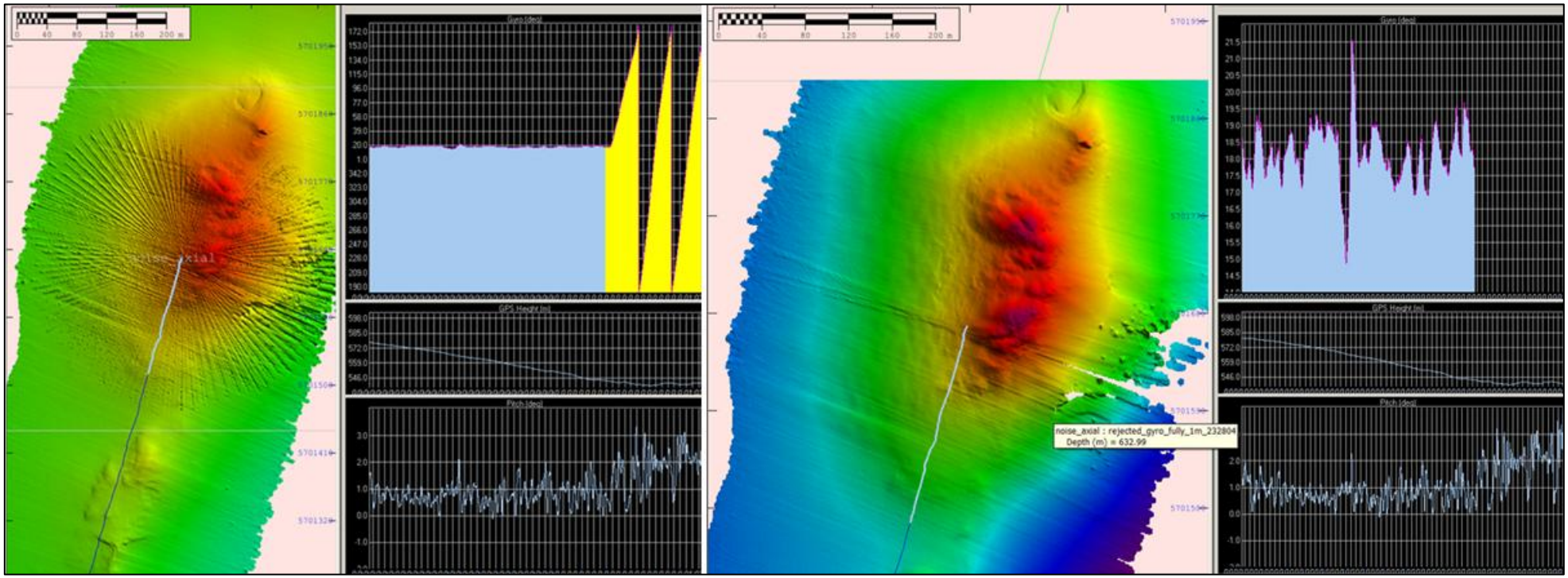

Fig. 3.1.6 Left shows the axial noise pattern caused by gyro anomalies (highlighted in yellow in the Attitude editor). Right shows the Cleaned data after the anomalies were manually removed (with interpolation).

Removing spikes in the data using subset editor and swath editor

The subset and swath editors were both used to remove spikes in the data which, if left uncleaned, produced circular artefacts in the DTMs (Figs. 3.1.7 and 3.1.8).

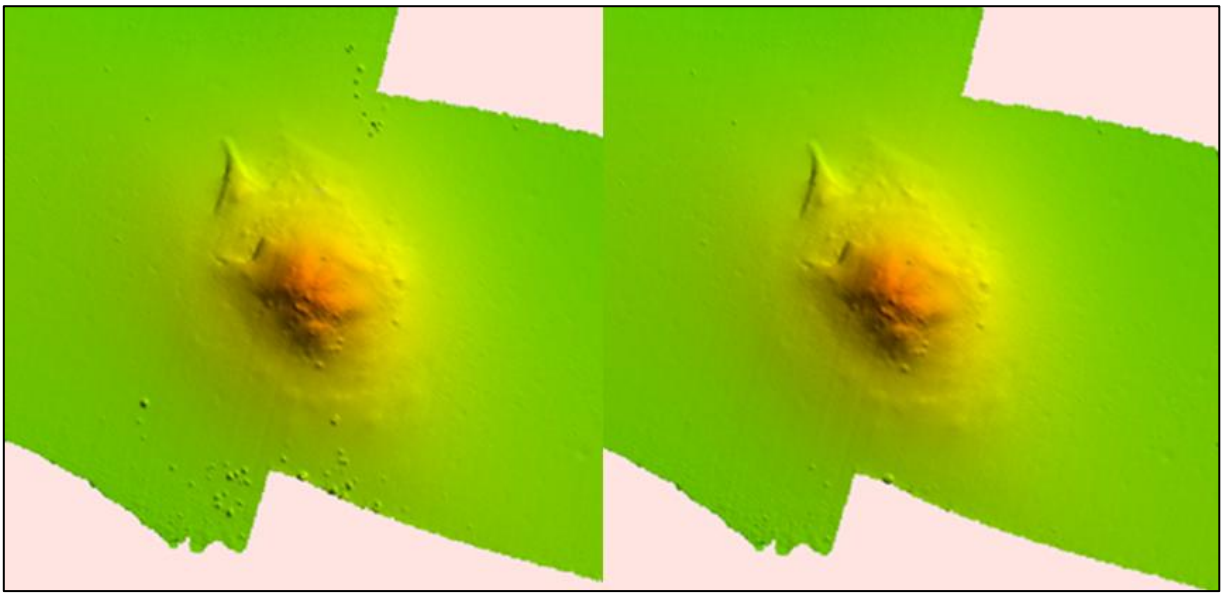

Fig. 3.1.7: Cleaning in subset editor removed the circular artefacts (left uncleaned, right cleaned). Removing the spikes removed the circular artefacts seen around the mound.

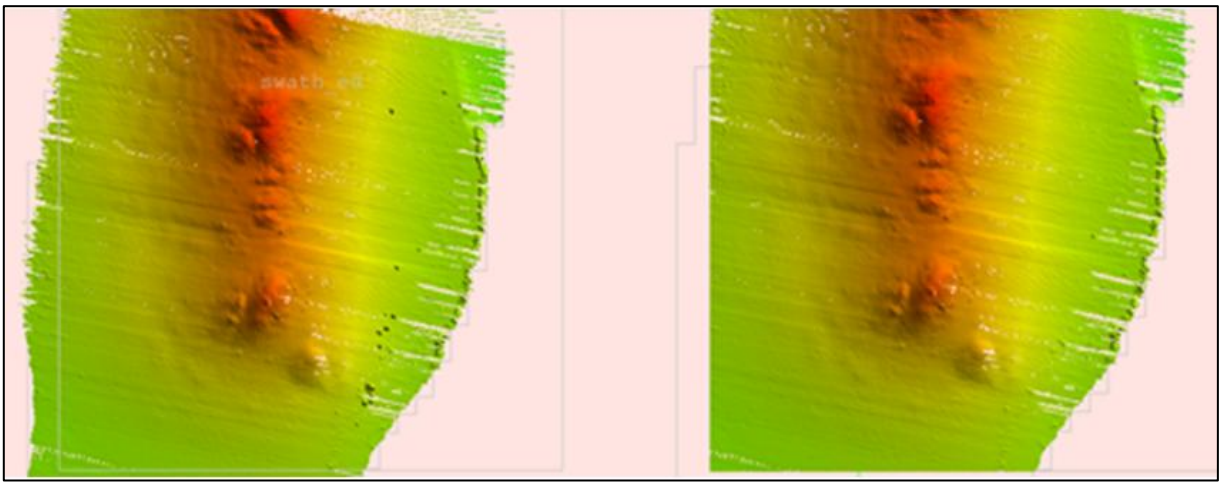

Fig. 3.1.8: Pre-cleaning area (left) and area post-cleaned (right) using swath editor. Removing the spikes removed the circular artefacts seen to the right of the mound.

The mounds themselves also showed circular features displaying a lumpy 'cauliflower-like' texture. In swath editor these lumps do not show up as anomalous spikes but as coherent undulations (Fig. 3.1.9), indicating that these are real topographical or geomorphological features – in this case, coral colonies. As the subset editor is area-based it was the preferred

cleaning method because it could remove anomalous soundings more efficiently. However, as the mounds are 3-dimensional structures they could interfere with cleaning, because in some cases it was not possible to select the anomalies without also selecting part of the mound (i.e. the noise features were too close to the true sounding surface). In these instances the spikes were cleaned line by line in swath editor.

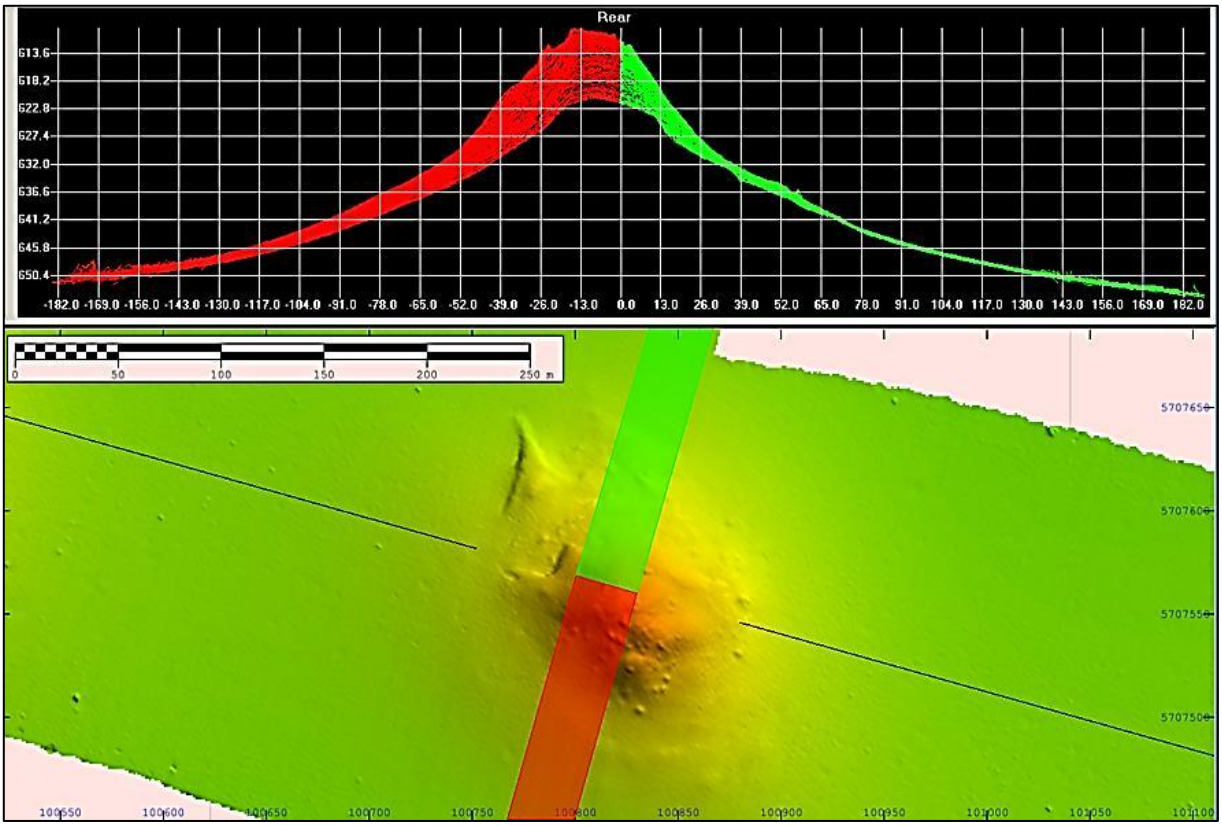

Fig. 3.1.9: 'Lumpy' texture (circular features) on the mound is shown as smooth undulations in swath editor (top), as opposed to the spikes associated with circular artefacts off the mound. This indicates that the 'cauliflower' texture represents real features – interpreted as coral colonies based on video evidence from the area.

Noise in the Shipborne 7111

Theoretically Reson 7111 (100 kHz) produces better resolution images in comparison to the 7150 (24 kHz) as it is higher frequency data. However, the Reson 7111 Shipborne Multibeam was discovered to contain large gaps and a lot of noise (Fig. 3.1.10). In the cruise report the poor quality is noted as '*signal quality and breadth of coverage degrades very rapidly to a depth not exceeding 400m*.'

Fig. 3.1.10: BASE, 25 m resolution, of the noisy 7111 100 kHz data.

The swath editor showed gaps in the data with parts of the survey lines containing little or no information (Fig. 3.1.11). The subset editor showed the noise to be composed of shallower anomalies (Fig. 3.1.12) ~ 420 m deep. Thus, even though a 25 m BASE of the 7111 data (Fig. 3.1.13) shows the mounds in higher resolution in comparison to the 7150 25 m BASE, it is largely unusable due to data gaps. A 50 m BASE shows less data gaps than the 25 m BASE (Fig. 3.1.14) but inherently involves loss of resolution. A 75 m BASE of the 7111 data produced the cleanest image (Fig. 3.1.15).

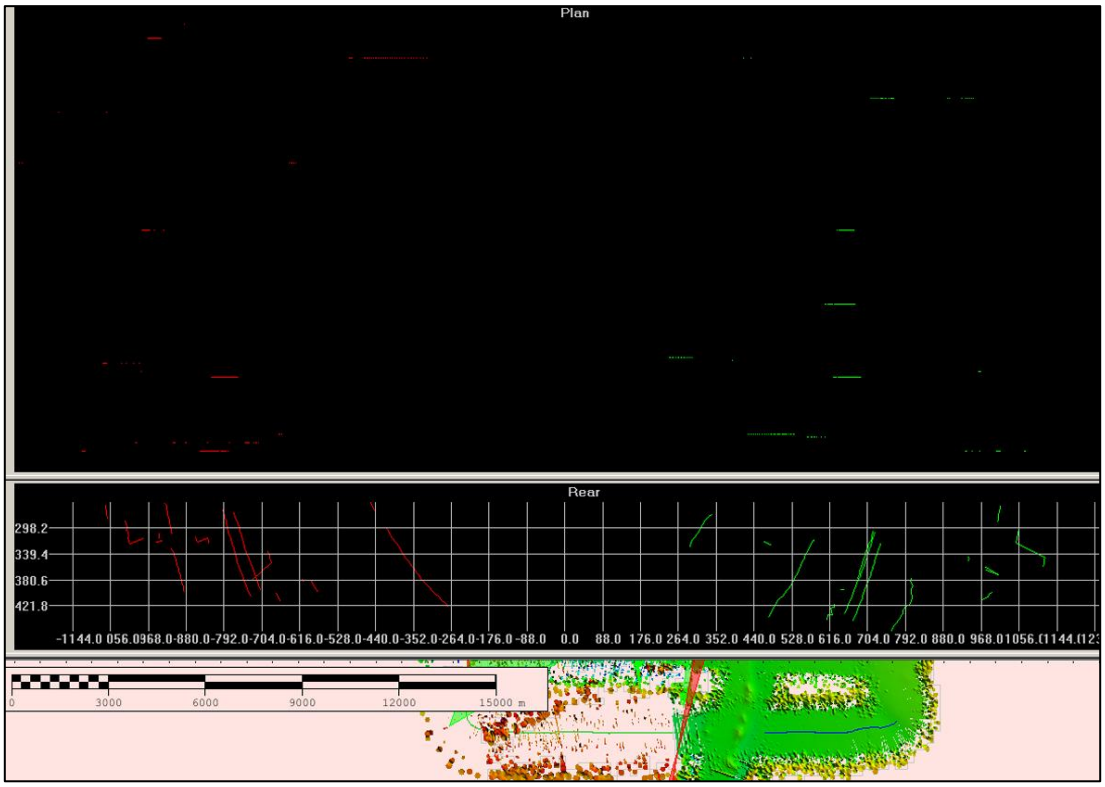

Fig. 3.1.11: The swath editor in plan and rear views(top and middle of figure) shows the lack of data acquired by the Reson 7111 100 kHz shipborne multibeam in the southwest of the survey area which explains the gaps in the BASE surface (75 m resolution) (bottom).

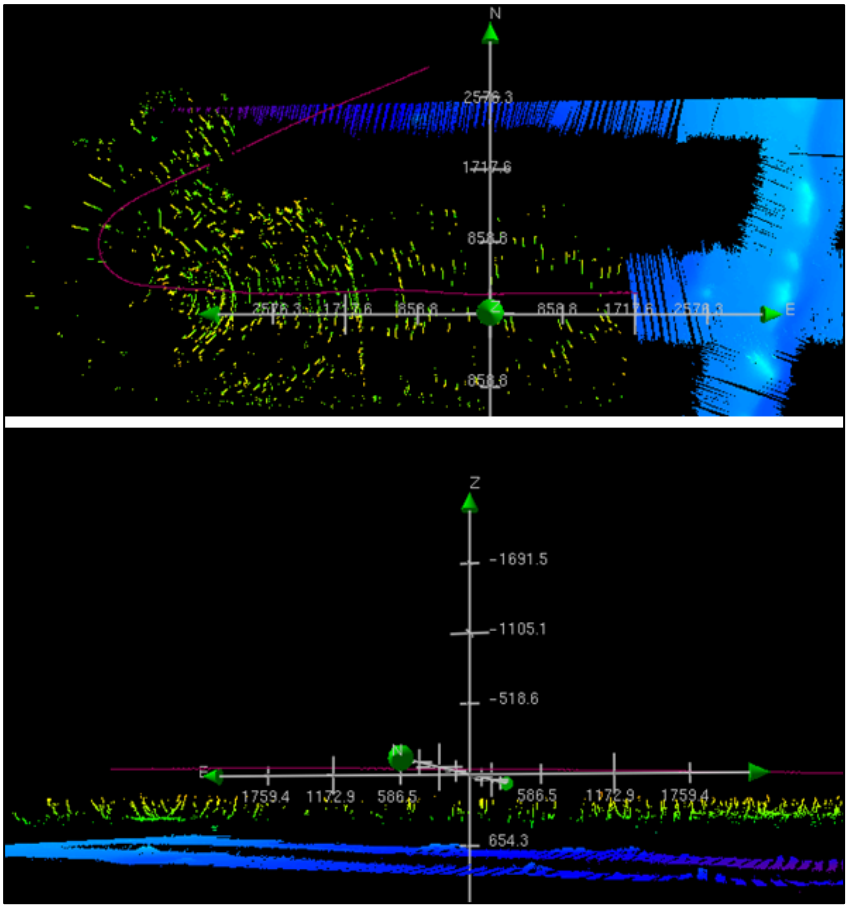

Fig. 3.1.12: The subset editor shows this part of the survey line has little/no information and that the noise is shallower than the true seabed surface, which can be observed in the adjacent survey line. Reson 7111 (100 kHz) shipbourne multibeam.

Top: Subset Editor aerial view of BASE surface (25 m resolution) showing the difference between the normal line and a line with noise.

Bottom: lateral view.

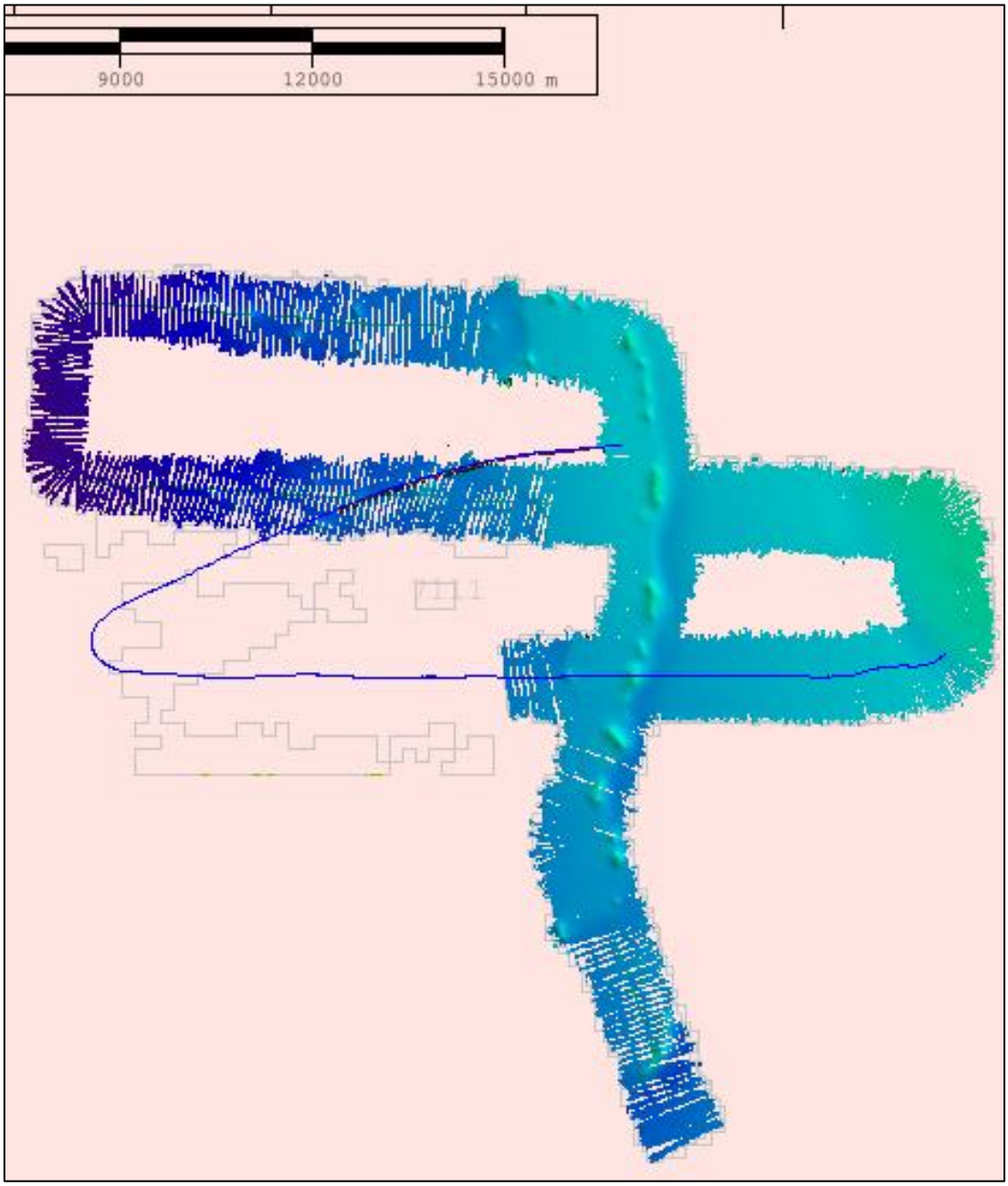

Fig. 3.1.13: 7111: 25 m BASE with many gaps in data coverage.

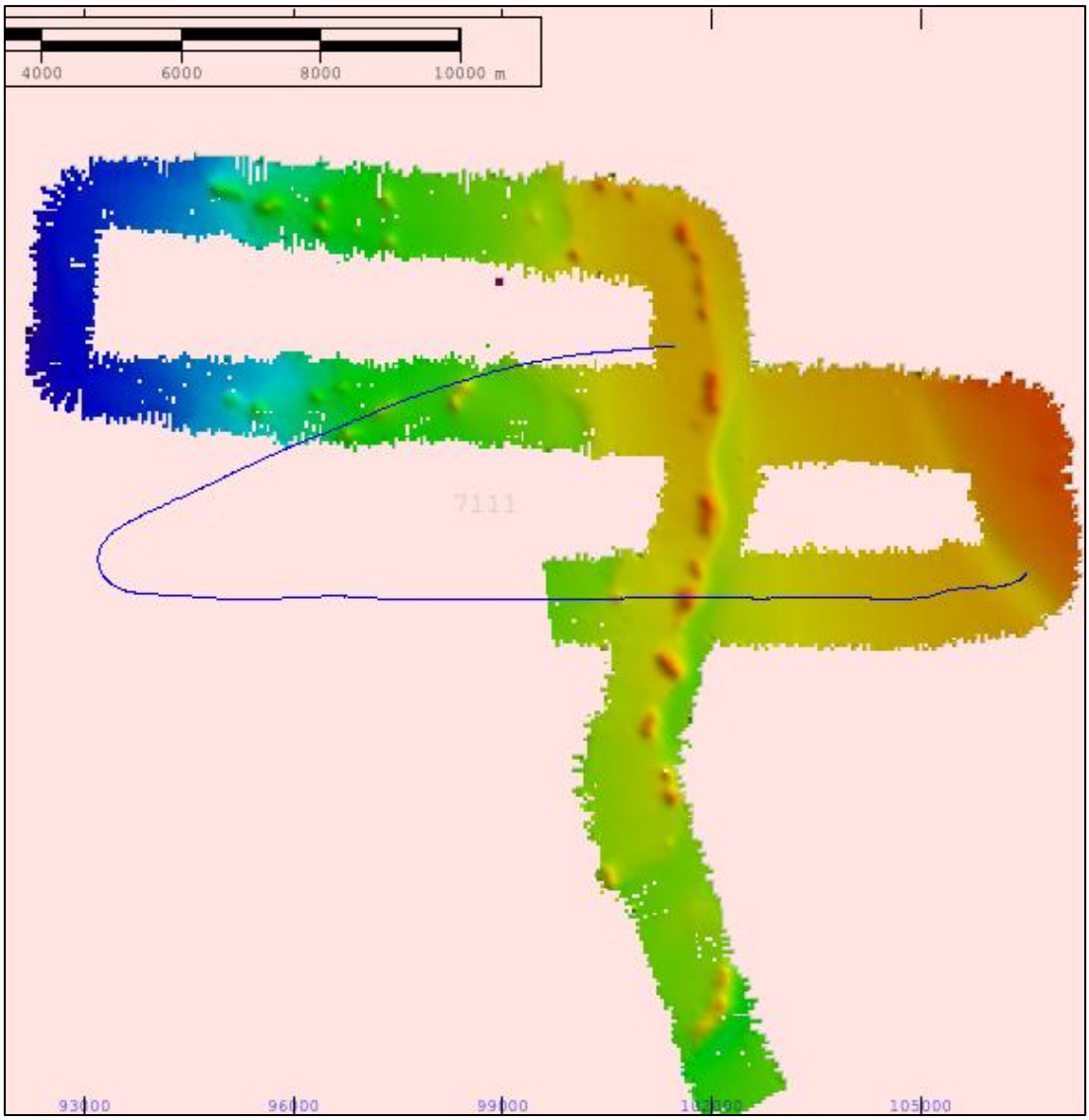

Fig. 3.1.14: Reson 7111, 50 m BASE shows less data gaps than the 25m Base but loss of resolution (compare with Fig. 3.1.13).

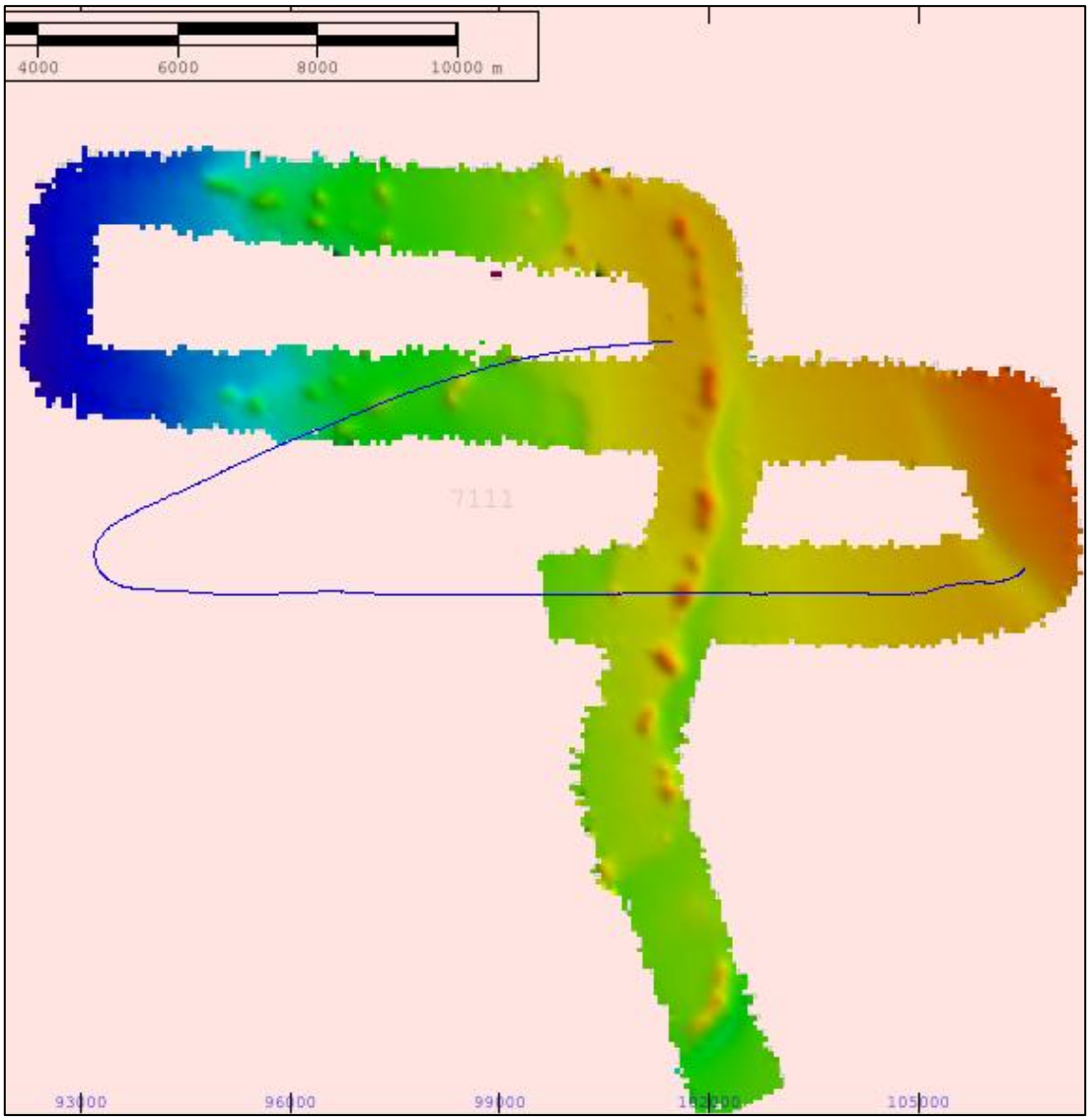

Fig. 3.1.15: Reson 7111, 75m BASE produces the cleanest image without data gaps, but resolution is poor

Map Production

Using ArcMAP sun-illuminated imagery (hillshades), slope and contour maps were created. Creating hillshades of resampled bathymetry (cubic technique) produced the best maps, due to its smoother appearance (Fig. 3.1.16).

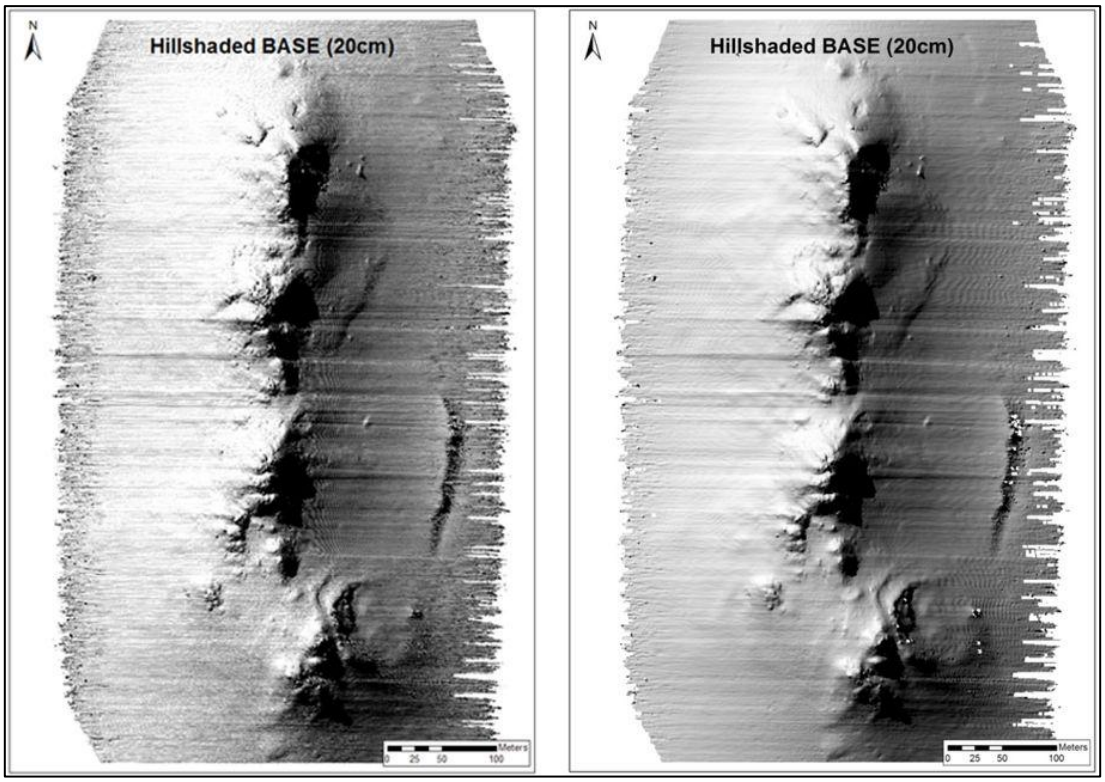

Fig. 3.1.16: ROV 7125 (400 kHz) data: Left - Hillshaded BASE 20 cm. Right - Hillshade of the resampled bathymetry data (using cubic technique); produced a smoother image with little loss of information.

3.1.3: Results

A range of corrected and finished multibeam bathymetric maps were produced for the Arc Mound study area. These are presented in Figs. 3.1.17-23. The high resolution of the ROV bathymetric map produced allowed identification of 17 mounds/mound complexes in great detail (Fig. 3.1.16) along an ~18 km transect, and the shipborne multibeam resolved > 40 mounds in lower resolution in an area approximately 110 km^2 (Figs. 3.1.17-18).

Both the shipborne and ROV multibeam data imaged the scarps that clearly occur in association with the mounds. Hillshaded multibeam data best imaged the scarp features (Fig. 3.1.19). Producing slope rasters of the bathymetry was also effective in highlighting the mounds and the scarps (Fig 3.1.20).

In Fig. 3.1.24 a bathymetric profile of the mounds is shown. This transect (based on ROV data) runs from NW to SE and demonstrates that the Arc mounds are generally over 50 m in elevation. A detailed mound contour map in Fig. 3.1.25 shows the location of one of the sediment cores.

.

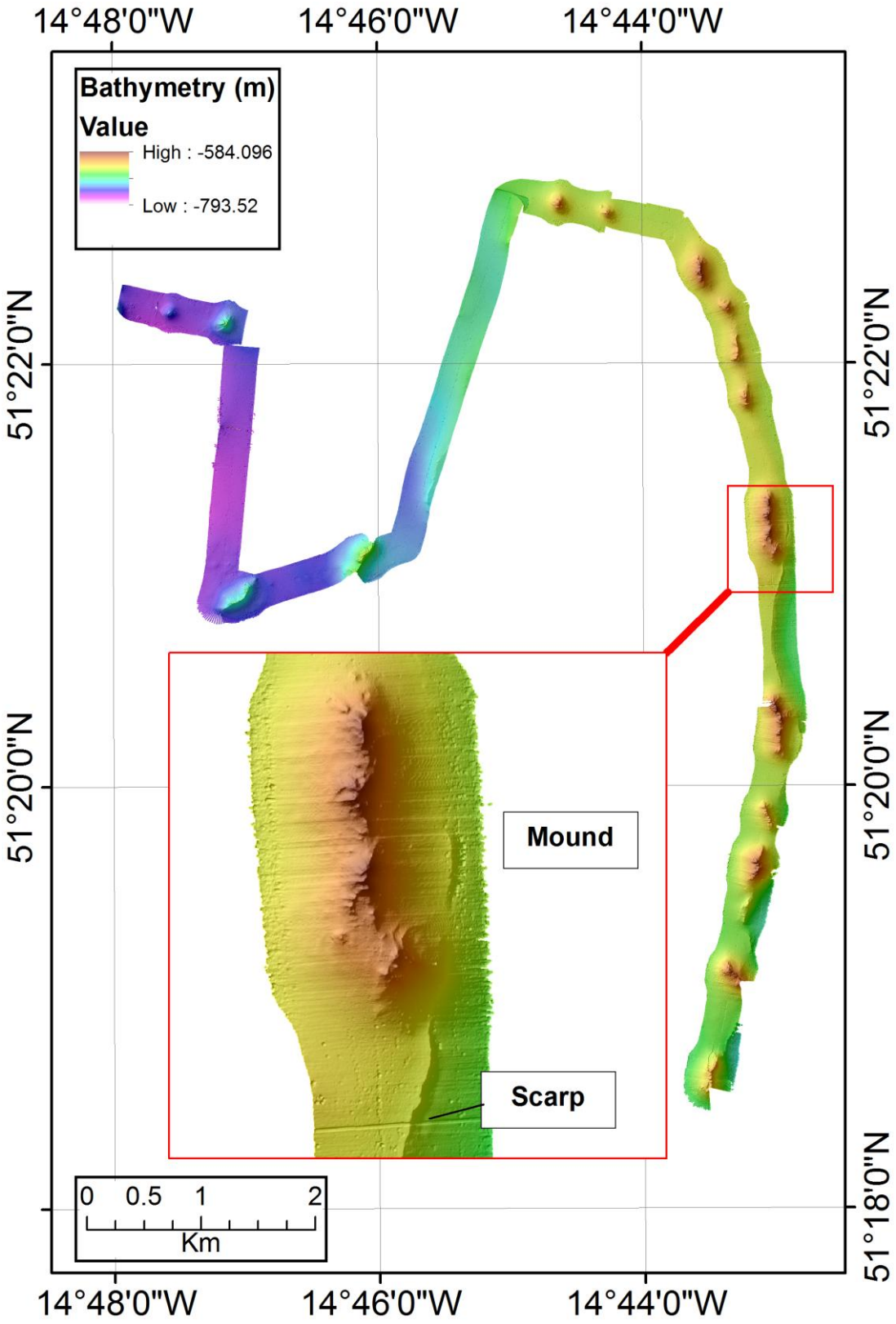

Fig. 3.1.17: 7125 1 m BASE with cored mound inset and associated scarp highlighted.

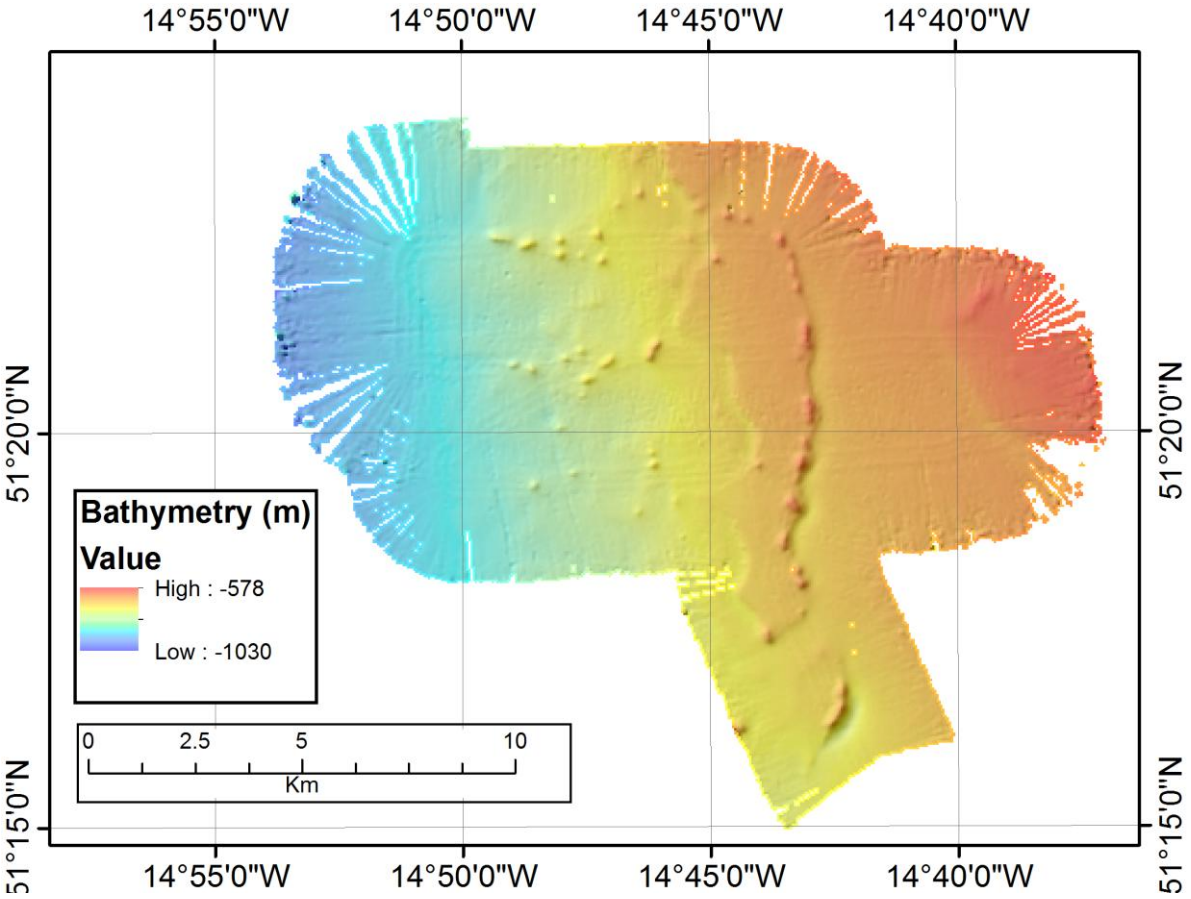

Fig. 3.1.18: Reson 7150 50 m BASE overlain on hillshade. Multibeam data shows the mounds to be aligned along the scarp to the east.

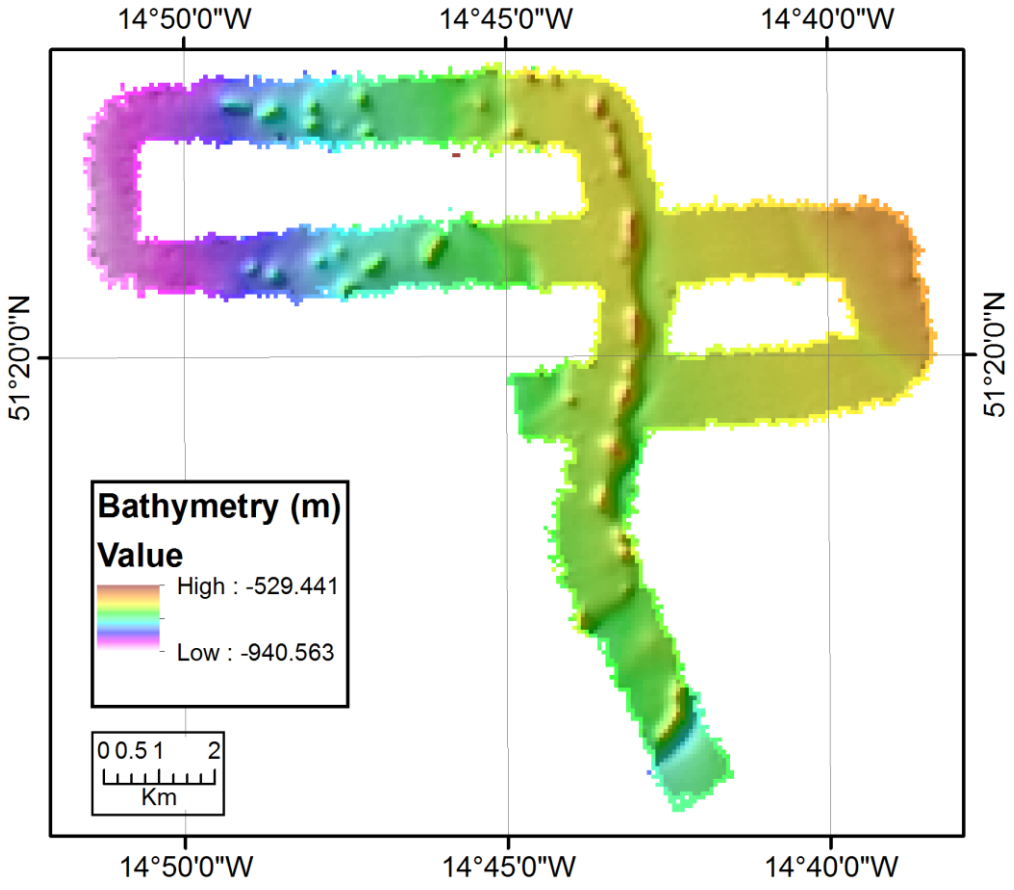

Fig. 3.1.19: 7111 shipborne multibeam data, 75 m resolution.

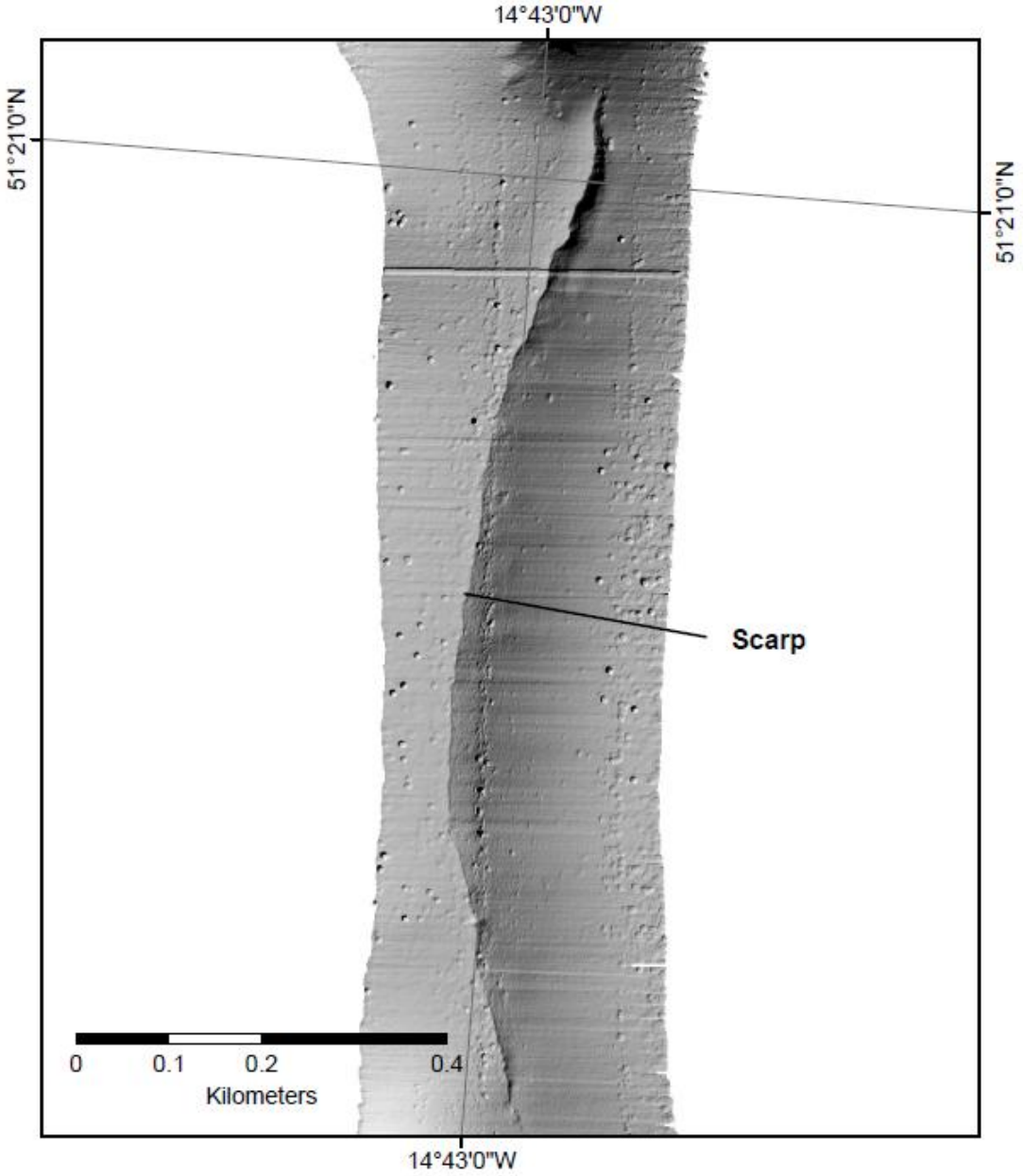

Fig. 3.1.20: Hillshading the bathymetry best imaged the scarps. ROV 7125 400 kHz, 1 m resolution.

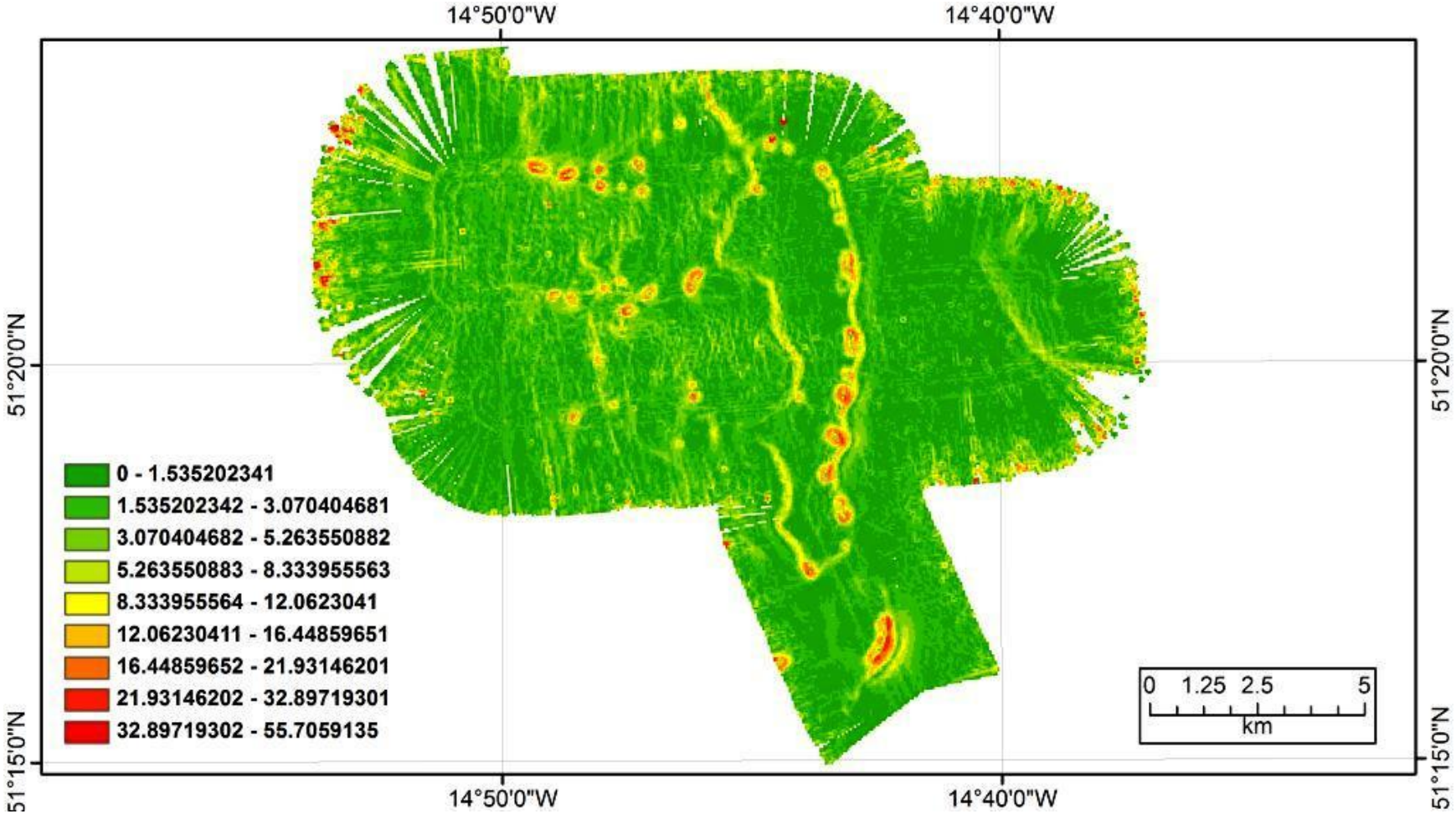

Fig. 3.1.21: Slope of Reson 7150 bathymetry (24 kHz), 50 m grid. The lower the slope value, the flatter the terrain; the higher the slope value the steeper the terrain. The slope is effective in highlighting the mounds and scarp.

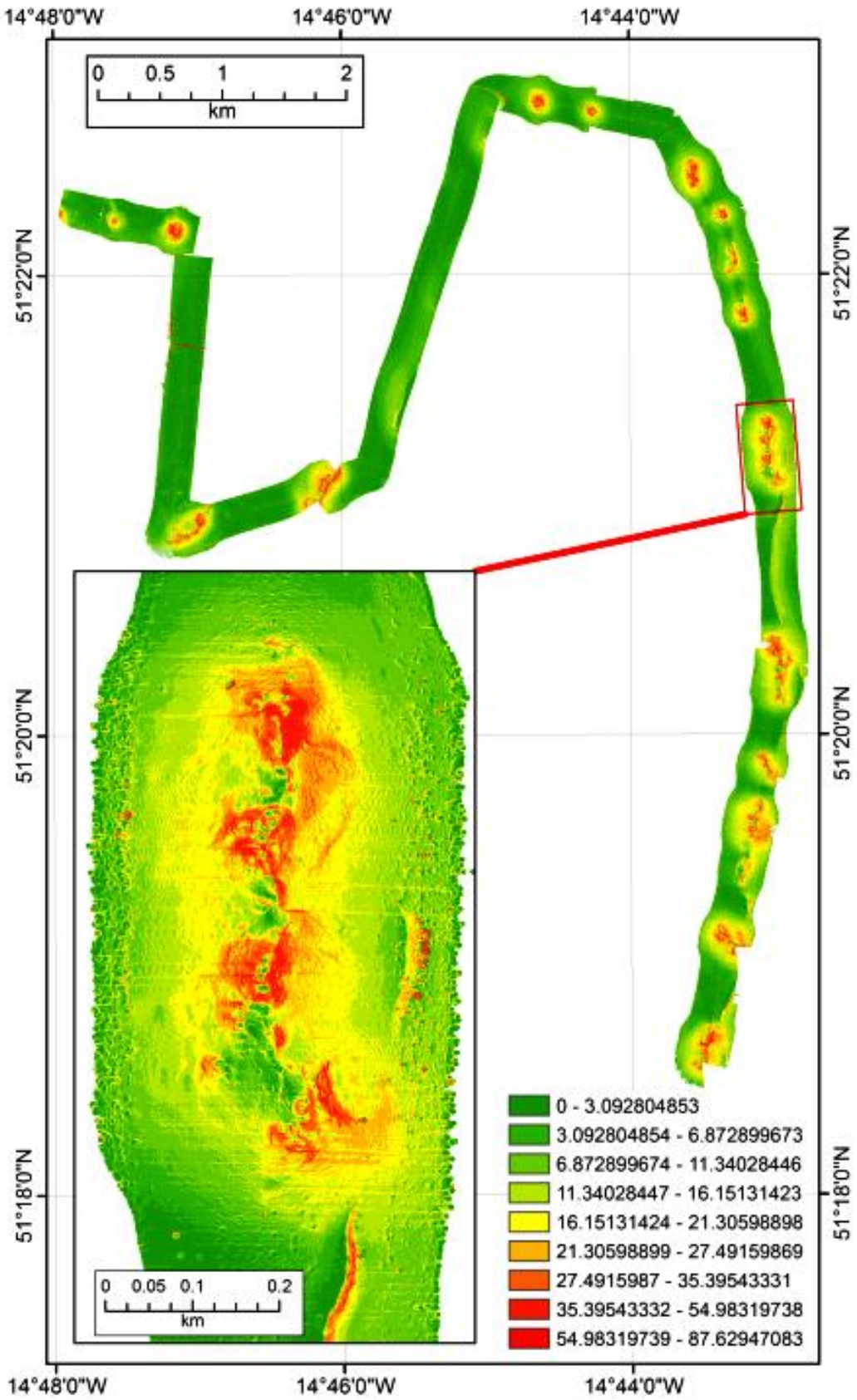

Fig. 3.1.22: Slope of ROV Reson 7125 bathymetry (400 kHz), 1 m grid, with slope of cored mound inset. The lower the slope value the flatter the terrain; the higher the slope value the steeper the terrain.

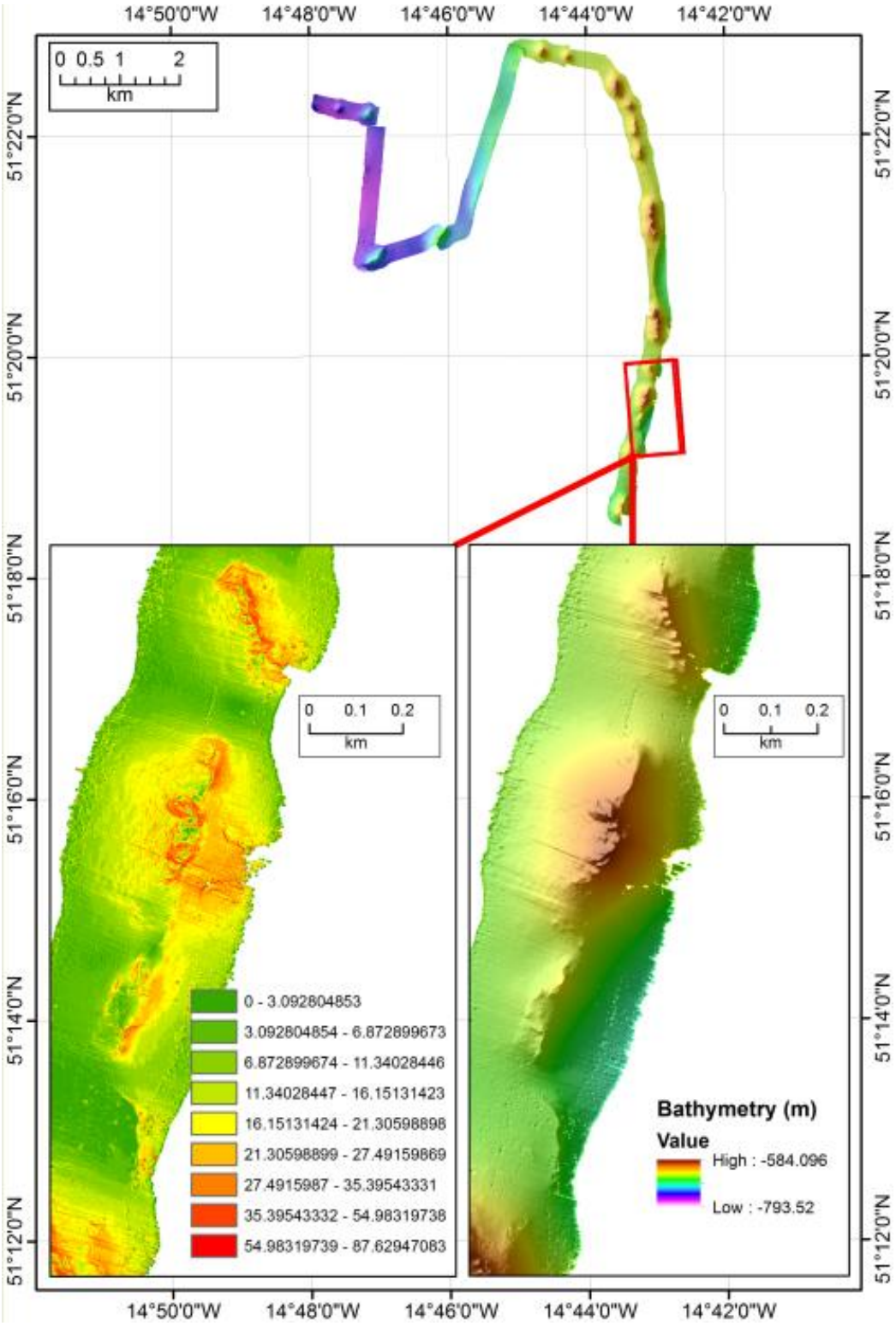

Fig. 3.1.23: The slope (left) was used with the multibeam hillshaded bathymetry (right) in order to discern geomorphology of the mound features. Reson 7125 (400 kHz), 1 m grid.

.

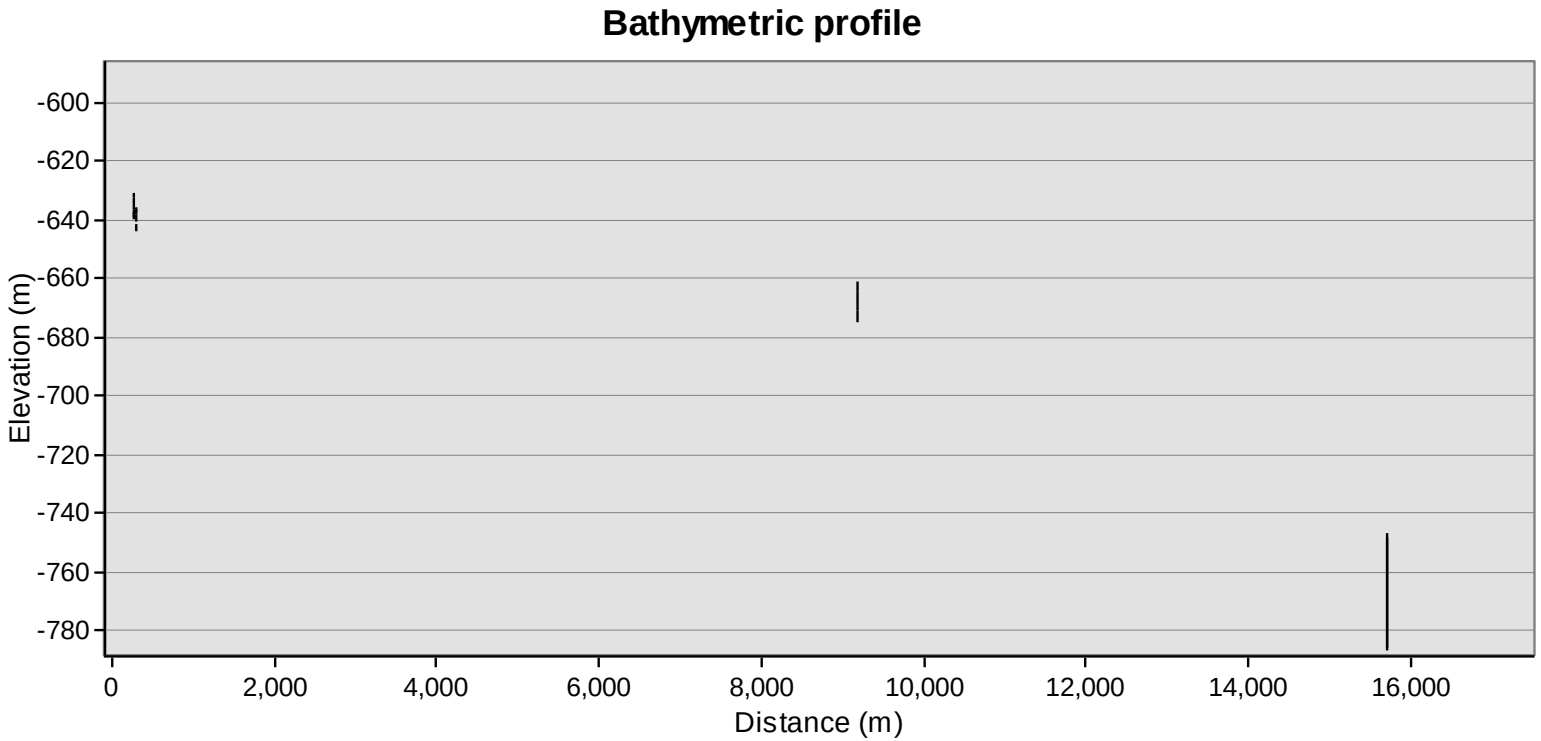

Fig. 3.1.24: Bathymetric profile of mounds in a transect of the ROV data from NW-SE. This cross-section shows the mounds are mostly over 50m in elevation from the adjacent seafloor. Note mounds are highly vertically exaggerated.

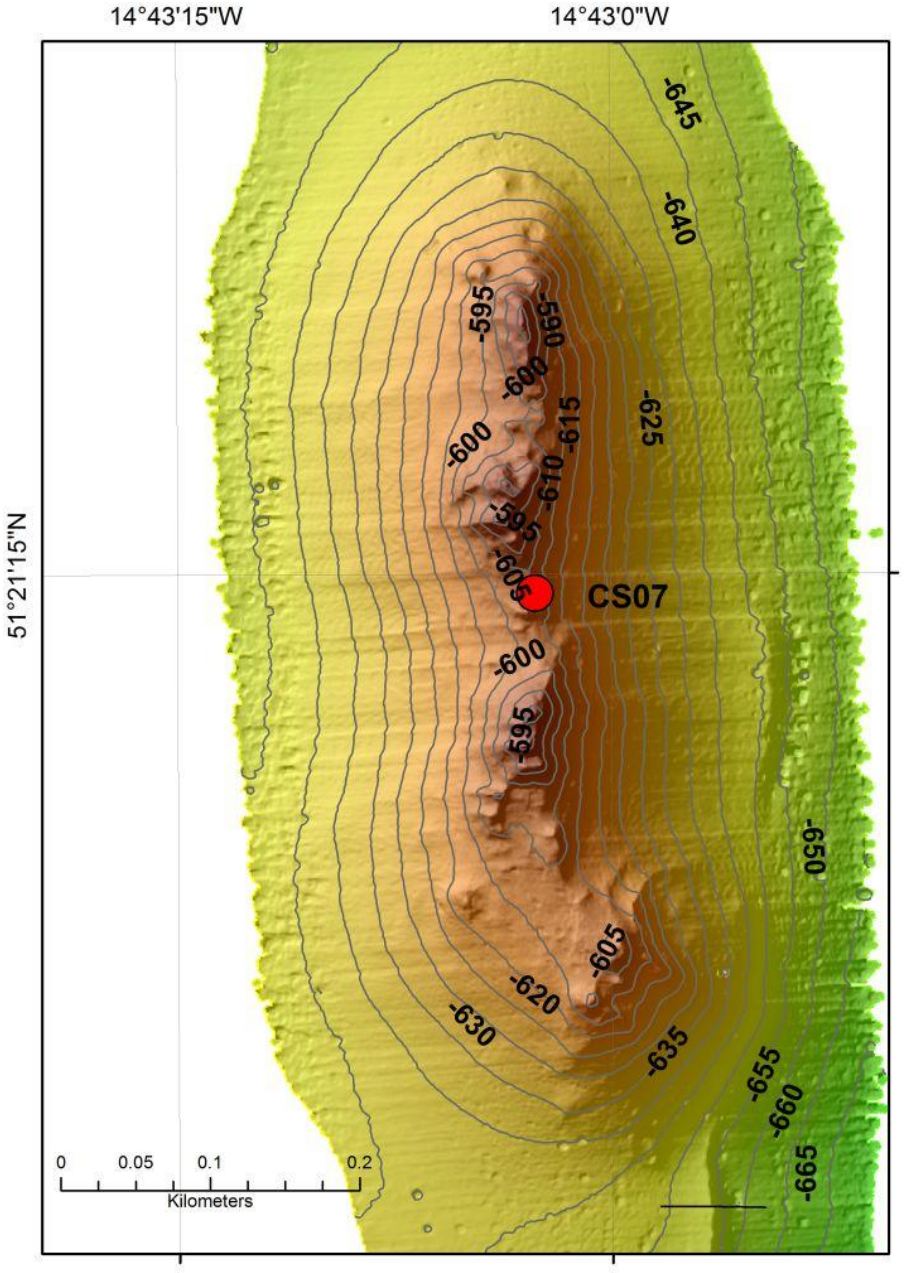

Fig. 3.1.25: Contour map of the cored mound. Core location indicated by red dot.

3.1.4: Discussion of mound morphology

Visualisation and description of the geomorphology of the carbonate mounds is carried out using multibeam data. The coral bioherms covered by the ROV survey include 17 rounded elongate mound complexes, each of which is over 100 m long - with the largest complex greater than 750 m in length.

A topographic cross-section from the northwest to the southeast (Fig 3.1.24) shows the mounds are mostly over 50 m high, in comparison to the adjacent seafloor, but heights range from 10 to 80 m. Contour maps (e.g. Fig 3.1.25) show the mounds have relatively sharp summits with the steepest slopes on the upper flanks becoming smoother towards the base. The bases of the mounds are broader than the rest of the structure. This may indicate that initial coral development occurred during a period of low sedimentation. In the later phases the coral growth kept pace with the sedimentation and developed in an upward direction (vertical accretion). Equally, it could mean that as the mound developed vertically the rubble migrated downslope due to gravity, resulting in lateral build-up.

Many of the Arc mounds are positioned flanking a fault scarp to the east; and occur on projections to the west – possibly due to water deflection off the western face of this scarp (Fig. 3.1.24). These features may suggest that there is a strong interaction of topography with local current dynamics and that this is influencing the coral mound distribution. Wheeler *et al.* (2007) distinguished cold-water coral carbonate mounds as those exhibiting:

Inherited morphology	Where carbonate mound morphology reflects the morphology of the (antecedent) seafloor topography.
Developed morphology	Where carbonate mound assume their own gross morphology mainly reflecting hydrodynamic controls.

The Arc Mounds appear to exhibit *both* inherited and developed morphological characteristics. The N–S alignment, parallel to the presumed fault scarps, indicates a morphology influenced by the pre-existing (antecedent) seafloor topography. However, mound growth may also be strongly controlled by the prevailing N-S current regime; thus it could be argued that this alignment is therefore also a developed morphology. The differences between the individual mounds also reflect their developed morphology related to local hydrodynamic controls, with the observation of more circular plan-view mounds located further west from the scarps (e.g. Fig. 3.1.18). Depressions along the mounds are interpreted as scouring structures created by currents and a reduction of sedimentation.

One point to note is that it may not be possible to decouple seafloor topography (geomorphology) from patterns of current flow (hydrodynamics), in which case the discrimination of the two discrete mound morphologies is not possible. The Arc mounds do

not apparently conform to either morphological division, but rather are incorporated under both categorisations and must be considered as such.

3.2: Sidescan backscatter

Backscatter data was recorded within Reson *.s7k raw data files. CARIS uses the snippet format (which incorporates the bathymetric data to remove water column noise); therefore the S7K raw data files were unusable in the Caris Geocoder program. The backscatter was thus processed separately by Garret Duffy (NUI Galway) in PDS2000 and made available in a raster format for inclusion in ArcMap.

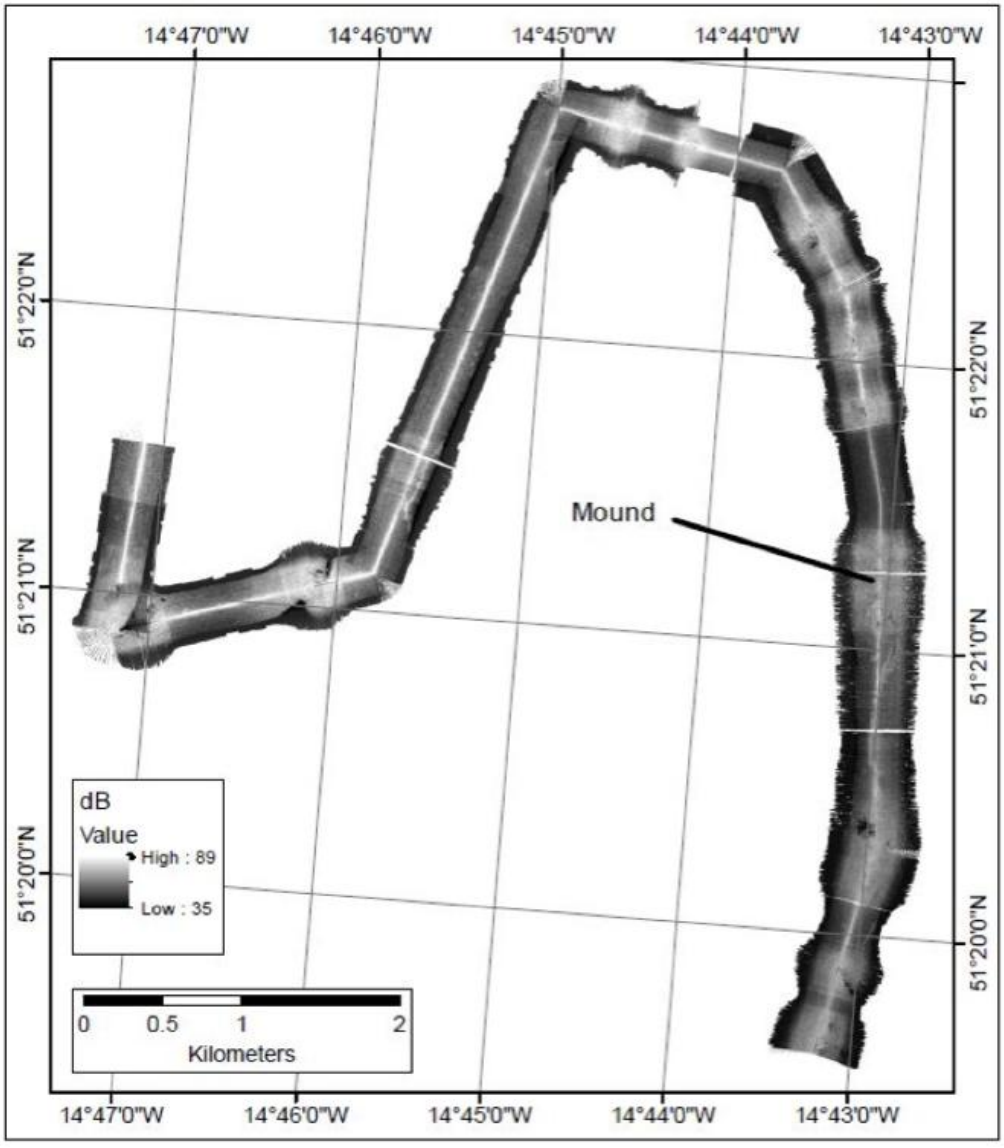

Fig 3.2.1: Sidescan data acquired along the ROV transect showing the mound complexes to have a higher backscattering signal.

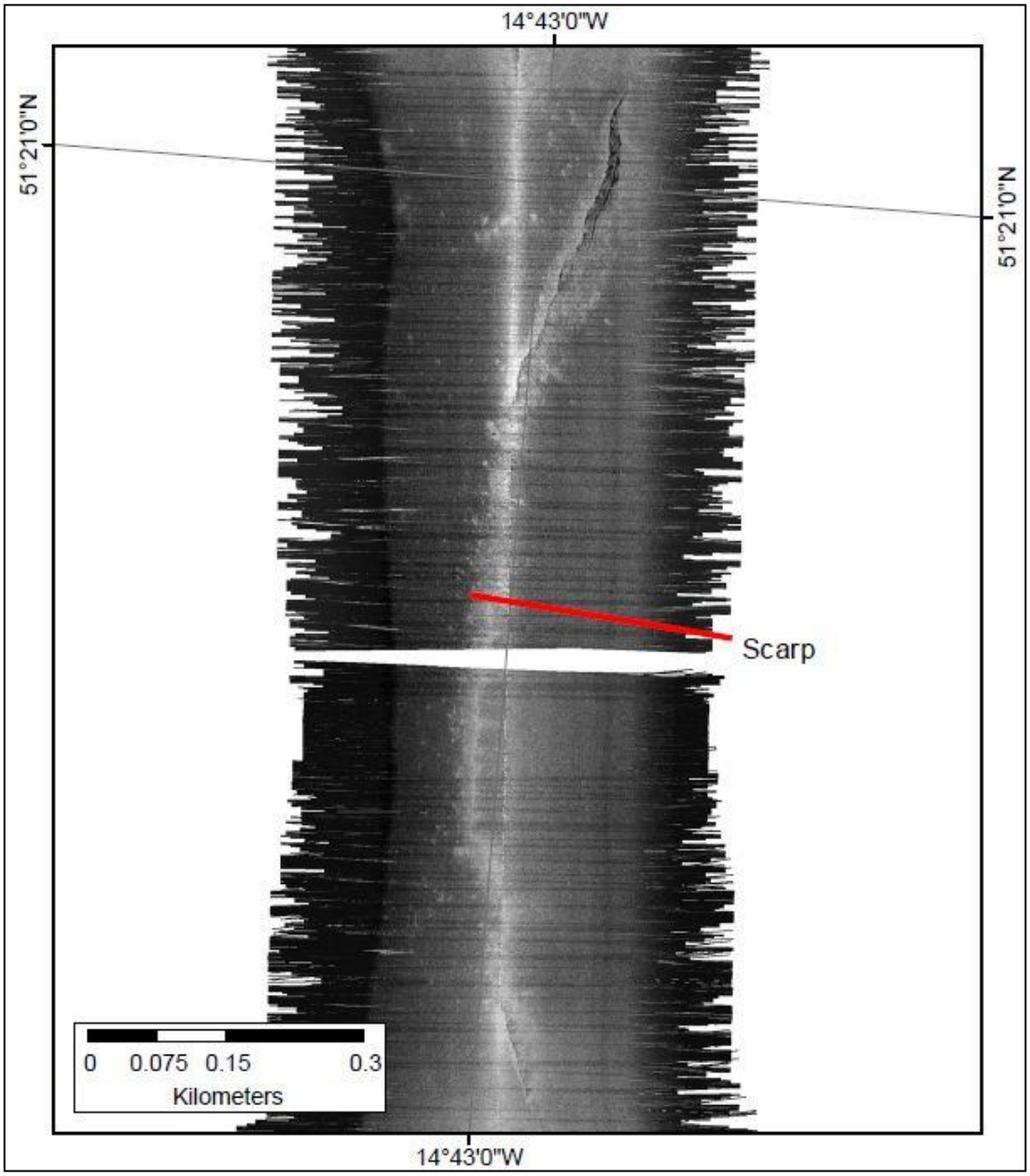

Fig 3.2.2: Backscatter signal in the sidescan images the scarps of the area.

3.2.1: Results and discussion

The sidescan data shows the mound complexes to have a higher backscattering signal (Fig 3.2.1) and was also successful in imaging the scarps (Fig. 3.2.1).

In this way, the sidescan augmented the multibeam data as it proved that the irregular linear features present in the multibeam data were not a source of noise.

3.3: Chirp

3.3.1: Acquisition

The Chirp sediment sounder was used simultaneously with the multibeam on the 29th September 2011. The SUBOP acquisition system was used with a circular array of 7 Tonpilz transducers used for transmission and reception (the diameter of each transducer was ~30 cm). The penetration depth can reach about 100 m in soft sediments and the vertical resolution is lower than 30 cm. The frequencies ranged from 1.7 – 5.3 kHz and eight profiles were obtained, but for this study only two profiles were investigated.

The chirp data was processed onboard using MATLAB and offshore in the IFREMER institute by Mathieu Veslin. Pdf results of the data from line BOBECO122A (from west to east) and an intersecting line BOBECO119A (from south to north), and the associated navigation data txt. files, were made available to NUIG.

3.3.2: Method

Bathymetric maps of the transects were produced and inset in the chirp results. The shotpoints from the apexes of the mound-like features were assigned coordinates from the navigation data and plotted on the multibeam data. This was completed in order to ensure the features correlated to the mounds seen on the multibeam and were not artefacts of acquisition.

3.3.3: Results and discussion

The west to east chirp data from line BOBECO122A (Figs. 3.3.1-2) and the intersecting south to north line BOBECO119A (Figs. 3.3.3-4) show eight and five carbonate mound-like features respectively. Plotting the coordinates of the mound-like features in the Chirp data (Tables 3.3.1 and 3.3.2) shows that they readily correlate to the mounds resolved by the multibeam data (Fig. 3.3.5).

The acoustically homogenous hyperbolic features, illustrated in Figs. 3.3.1-4, indicate the presence of mounds but it is important to note that, since the acoustic energy travels from the transducer in a broad cone with a footprint in the order of 50 to 100 m, highly sloping topographic features that are not directly below the device can be detected by sideswipe. This

is quite clearly occurring in the S-N chirp line where the bathymetric data shows the line to be west of the mounds (Fig. 3.3.3).

Depositional processes ultimately determine the facies (sedimentological) architecture of carbonate mounds and these possess different physical properties which, in turn, define the (geo)acoustic response. The CHIRP data shows the mounds to have a conspicuously different geophysical structure to the surrounding sediment, indicating a different composition in off-mound areas. The laterally equivalent (off-mound) sediments, from which core CS06 was acquired, show conformable, horizontal, stratified, sub-bottom reflectors which onlap the flanks of the mounds. These draping deposits are provisionally interpreted as contourites, with low-amplitude reflectors interpreted as fine-grained sediment and high-amplitude reflectors interpreted as being coarser in nature.

The carbonate mounds appear as acoustically homogenous dome-shaped structures. This lack of internal reflectors indicates a uniform facies (in geophysical terms) with little or no internal acoustic impedance differences. The acoustic homogeneity is not interpreted to be caused by scattering or absorption of the seismic signal, as a very strong sub-bottom reflector can be observed beneath the coral mound from which sediment core CS07 was recovered (Fig. 3.3.1-2), demonstrating that not all the seismic energy is absorbed or dispersed inside the mound structure. This prominent reflector is interpreted as the moundbase and can be seen in both the chirp lines.

The presence of this hard reflector surface at the base of the bioherms suggests it may have played a prominent role in mound initiation, which may have been facilitated by development of a hardground surface following a period of erosion and non-deposition. Studies in the northeast Atlantic have dated a similar feature (strong moundbase reflector) to the Late Pliocene–Pleistocene boundary (Van Rooij *et al.*, 2007a). This could suggest that the moundbase reflector does not represent the Quaternary scarps currently revealed at the surface (see Chapter 2); or that the surface scarps have incorrectly been interpreted as Quaternary. Chirp data also shows horst- and graben-like structures adjacent the mounds (for example see the eastern edge of Figs. 3.3.1-2). The relationship between these structures and the mounds has to be investigated but they may be the surface expression of underlying faults.

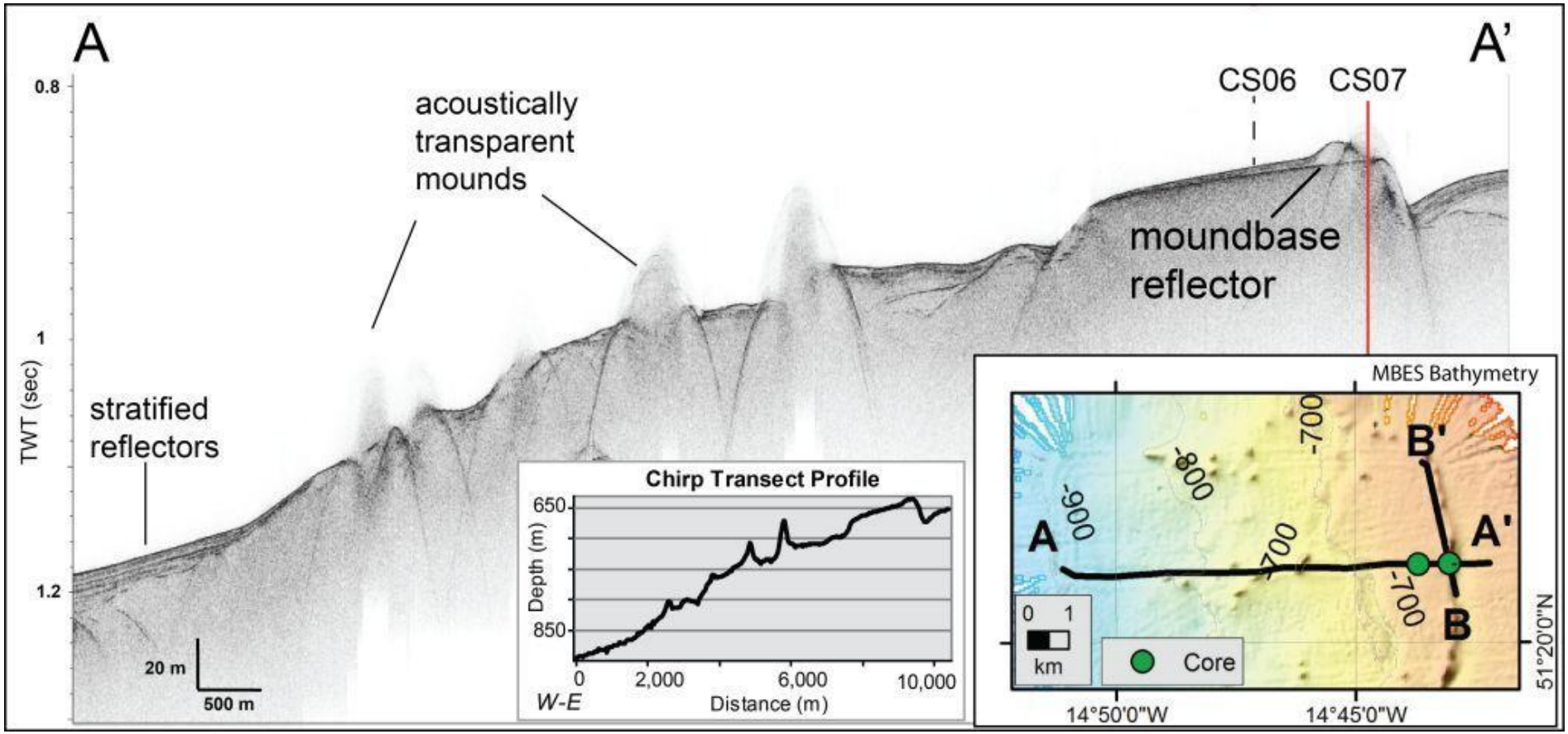

Figure 3.3.1: Chirp profile A-A' [line BOBECO122A] orientated west-east with bathymetric map inset and bathymetric profile. The acoustically homogenous hyperbolic features indicate the presence of mounds. The strong reflector underlying the mound structure (that core CS07 was acquired from) is interpreted as the hard moundbase. The dashed black line indicates core CS06 location; the red line indicates intersection of chirp line with profile B-B' (orientated south-north). TWT - two way travel time. Scales: horizontal 1/25000, vertical 50 cm/sec.

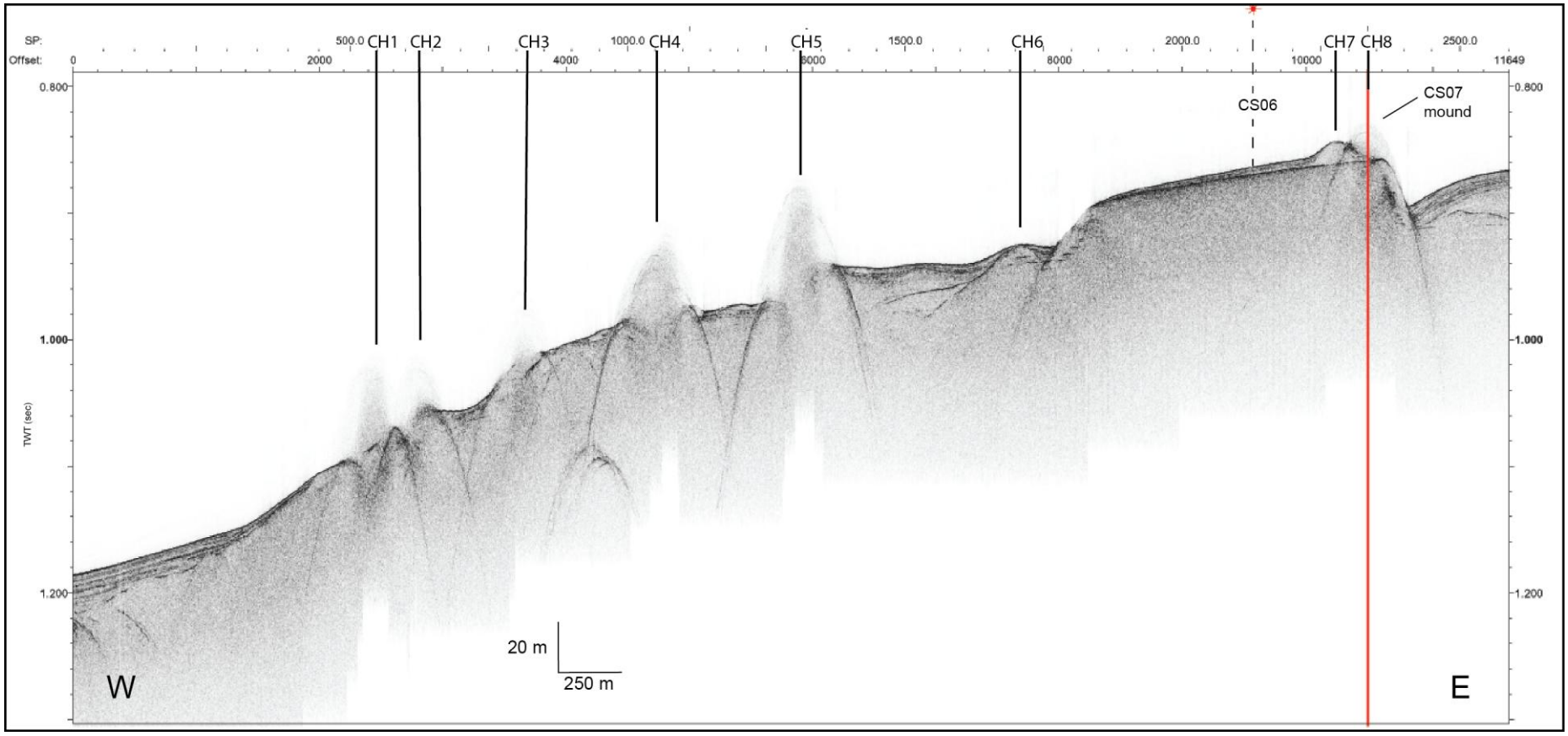

Figure 3.3.2: Chirp data for line BOBECO122A showing 8 mound-like features (named CH1-CH8; CH for Chirp). The navigation data was consulted in order to assign coordinates to the correlated shotpoints. CH6 may possibly represent a small buried mound. Location of sediment core CS06 indicated by red star and dashed line. Scales: horizontal 1/25000, vertical 50 cm/sec.

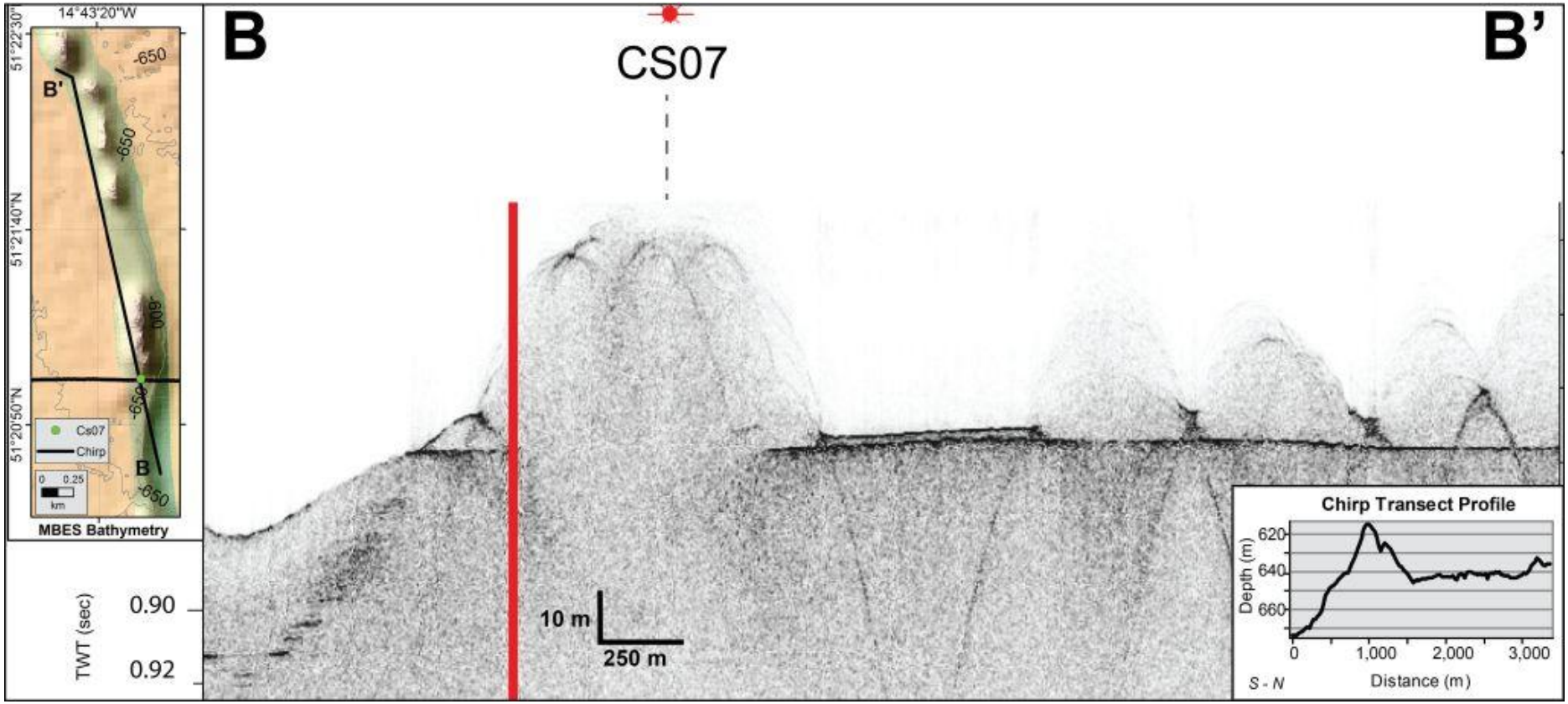

Figure 3.3.3: North-south Chirp profile B-B' with bathymetric map inset and bathymetric profile. Scales: horizontal 1/25000, vertical 50 cm/sec.

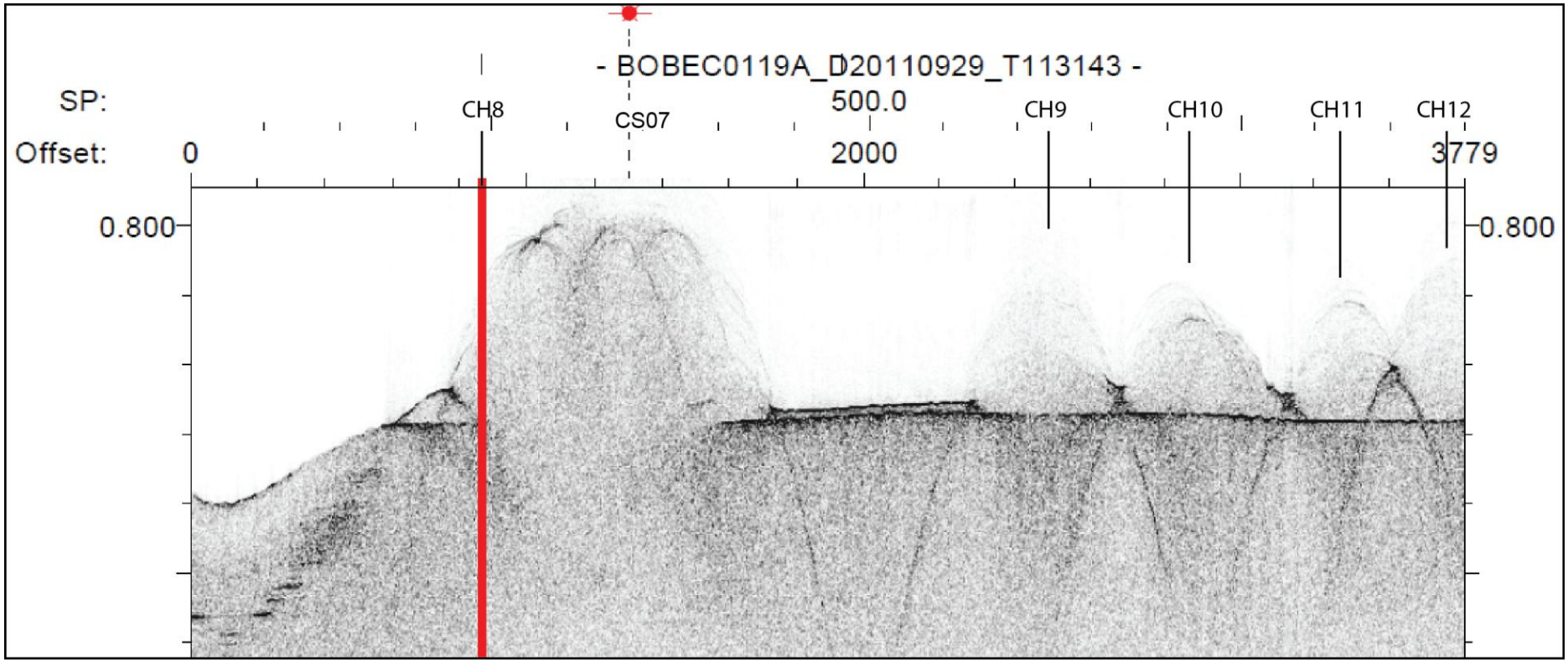

Figure 3.3.4: North-south Chirp data for line BOBECO119A showing 5 mound-like features (named CH8-CH12; CH for chirp). The navigation data was consulted in order to assign coordinates to the correlated shotpoints. Location of core CS07 indicated by red star and dashed line. Scales: horizontal 1/25000, vertical 50 cm/sec.

Mound-like feature	Chirp Line	SP	LAT	LONG
CH1	BOBEC0122A_D20110929_T125125	550	51.34843890	-14.81562780
CH2	BOBEC0122A_D20110929_T125125	625	51.34843890	-14.81038890
CH3	BOBEC0122A_D20110929_T125125	820	51.34852220	-14.79832220
CH4	BOBEC0122A_D20110929_T125125	1050	51.34903610	-14.78473330
CH5	BOBEC0122A_D20110929_T125125	1310	51.34985000	-14.77026940
CH6	BOBEC0122A_D20110929_T125125	1710	51.34986390	-14.74983610
CH7	BOBEC0122A_D20110929_T125125	2275	51.35039720	-14.72048330
CH8	BOBEC0122A_D20110929_T125125	2330	51.35036940	-14.71754170

Table 3.3.1: Coordinates of mound-like features identified in the chirp data for line BOBECO122A. SP-shotpoint

Mound-like feature	Chirp Line	SP	LAT	LONG
CH8	BOBEC0119A_D20110929_T113143	240	51.35116940	14.71754440
CH9	BOBEC0119A_D20110929_T113143	620	51.36309720	14.72141390
CH10	BOBEC0119A_D20110929_T113143	715	51.36611390	14.72249720
CH11	BOBEC0119A_D20110929_T113143	820	51.36938330	14.72385000
CH12	BOBEC0119A_D20110929_T113143	880	51.37111110	14.72466940

Table 3.3.2: Coordinates of mound-like features identified in the chirp data for line BOBECO119A. SP-shotpoint

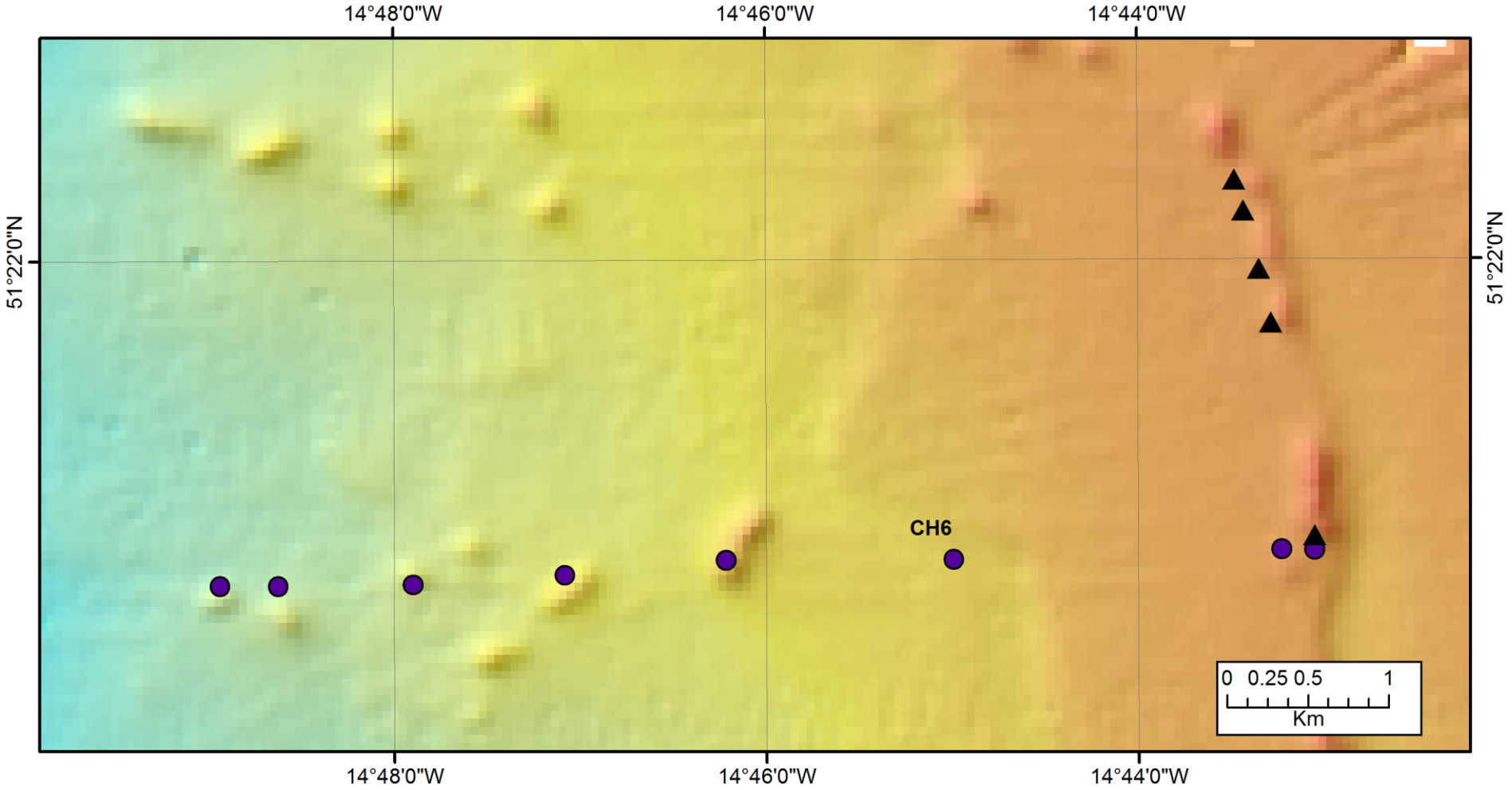

Figure 3.3.5: Composite plot of the coordinates of the mound-like features in the Chirp data with the mound structures imaged by the multibeam data. Both data sets correlate, but the precision of the match is not perfect. CH6 appeared to show a buried mound in the Chirp data and it does not show any surface representation. 7150 hillshaded shipborne multibeam data (24 kHz). Purple dots represent CH1-CH8 coordinates from line BOBECO122A (A-A'; West-East); black triangles represent CH8-CH12 coordinates from line BOBECO119A (B-B'; South-North)

Chapter 4: Sediment Core Analysis

4.1: Core Acquisition

Two Calypso piston cores [**CS06** and **CS07**] were acquired on the BobEco cruise on the 30th September 2011. The core depths are from the bathyal zone (500-2000 m below sea level [bsl]). Core **CS07** was acquired 584 m bsl from the summit of a carbonate mound which showed live coral cover (photo OTUS BobEco-474-290911-183940) and 625.5 cm of section was recovered. Core **CS06** was acquired at 655 m bsl from the adjacent seafloor sediments (750 m to the west and 420 m south), producing 297.5 cm of off-mound stratigraphy. Both 'whole' cores were cut into ~1 m or less sections onboard RV *Thalassa*. The core locations are shown in Fig 4.1.1 and the core attributes are provided in Table 4.1.1 (below).

Core ID	CS07	CS06
Lat	N 51 °21.243	N 51 °21.017
Long	W 014 °43.044	W 014 °43.693
Water depth	584 m	655 m
Section	Length (cm)	Length (cm)
1	97.5	100
2	100.5	100
3	100	97.5
4	100.5	N/A
5	100.5	
6	100.5	
7	26	
Core length	625.5	297.5

Table 4.1.1: CS06 and CS07 sediment core attributes.

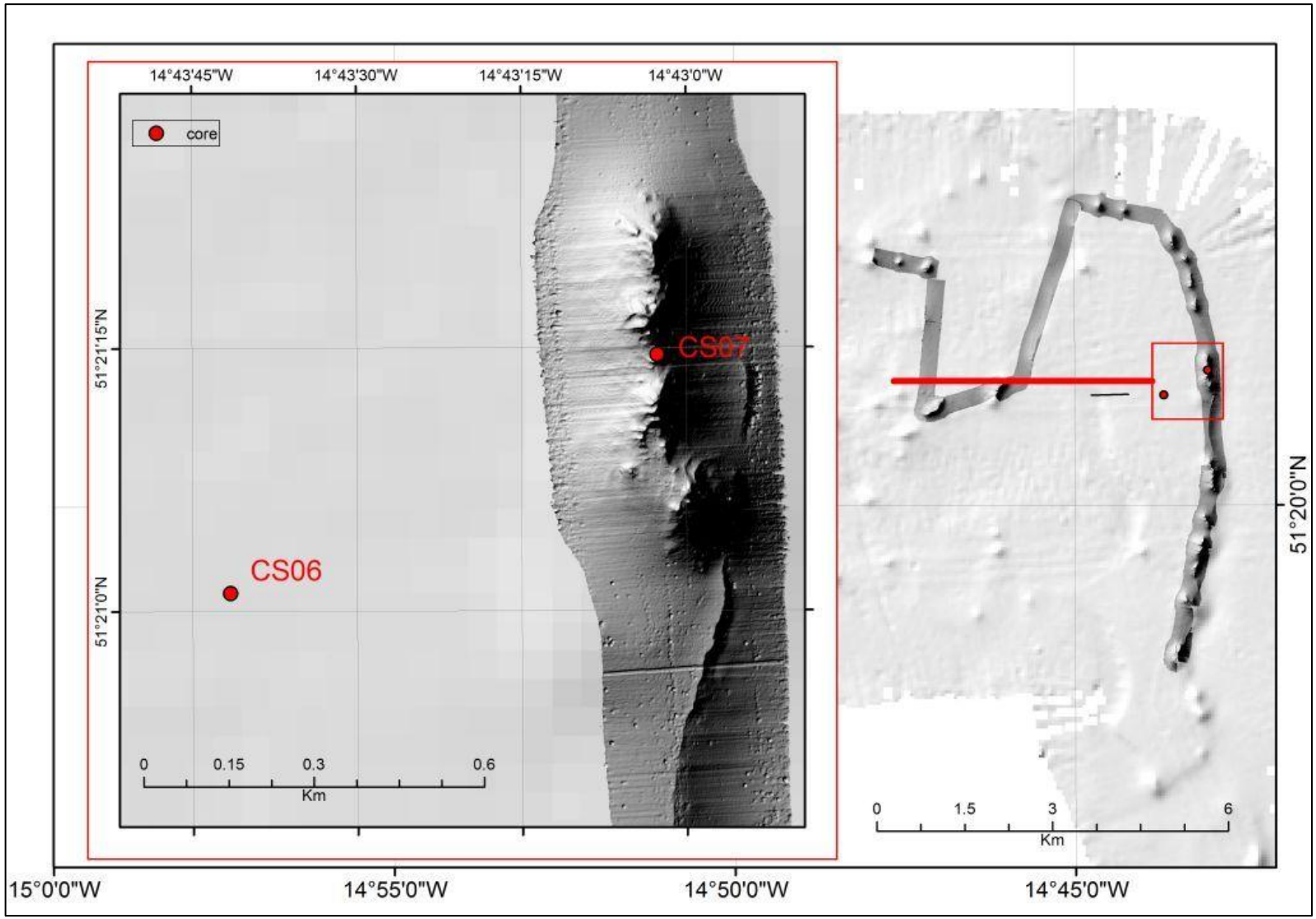

Fig 4.1.1: Seafloor locations of cores CS06 and CS07. ROV track, Reson 7125 400 kHz multibeam data (hillshaded BASE at 1m resolution), overlain on shipborne multibeam data, Reson 7150 24 kHz (hillshaded BASE at 50m resolution)

4.2: Closed core analysis [Multisensor Core Logger]

4.2.1: Method

The Multisensor Core Logger [MSCL] is a logging device which provides continuous measurements of:

- Gamma-ray attenuation,
- P-wave travel time, and
- Magnetic susceptibility.

The density (ρ) of the sediment indicates how tightly the material is packed together. Gamma density data provides a high-resolution record of bulk density, which may be used as a lithology indicator and highlight porosity changes. Sediment that contains a high percentage of ferro- or paramagnetic minerals has high magnetic susceptibility; biogenic material, such as silica, calcite, quartz and feldspar show low or even negative magnetic susceptibility values (Rothwell, 2006). Density and magnetic susceptibility may be used in conjunction to identify deposits rich in IRD and indicate Heinrich Events. MSCL results have also been used to identify possible accumulations of coral in the core by highlighting regions of higher density and p-wave velocity. Thus multi-sensor core logger values and trends can be important parameters relating to sediment character, provenance, and palaeoclimate.

The MSCL was deployed at the IFREMER institute in Brest to measure the three parameters (bulleted above) of the unopened core sections. The room temperature was measured and used to calibrate the MSCL. As the cores contained water saturated sediments the calibration section consisted of a cylindrical piece of aluminium of varying thickness surrounded completely by water in a sealed liner. Once calibrated, the core sections were carefully placed with the halfway horizontal line (marked during acquisition) parallel to the rack and scanned separately at a scanning interval of 1cm. It took approximately 22 minutes to scan 1m of sediment section.

The MSCL data was processed in the IFREMER institute in Brest to produce excel tables and graphs. Section 7 of core **CS07** (see Table 4.1.1) was rendered unusable due to anomalous p-wave velocity readings and was disregarded in data production. The resultant graphs were consulted in order to investigate whether the cores required freezing prior to splitting.

4.2.2: Results and discussion

The total MSCL gamma density, p-wave velocity and magnetic susceptibility readings for the complete length of core **CS07** are shown in Fig 4.2.1. More detailed views (from top and base of core) showing values of interest are shown alongside their respective core sections in Figs 4.2.2-3.

The magnetic susceptibility reading spikes with the onset of ice rafted debris [IRD] at 28 centimetres down-core (cmdc). A conspicuous granitic dropstone present at 56-72 cmdc is responsible for a significant spike in the gamma density, p-wave velocity and magnetic susceptibility readings at that particular level.

The increase in the magnetic susceptibility between 430–440 cmdc in Section 5 of **CS07** (Fig. 4.2.3) may be due to increased iron content, indicated by a distinct colour transition from dark brown muds to light pinkish brown muds. The yellowish brown coarse unit of Section 6 in **CS07** generates a large spike in all three readings, with an especially large magnetic anomaly (Fig. 4.2.3).

The variability in p-wave velocity in the top 20cm of core **CS07** (see very top of logged section in Fig. 4.2.2) may be explained by the localised accumulation of coral skeletons (branches/debris) at that level. This essentially corresponds to the uppermost surface layers of the coral mound itself.

Another p-wave velocity anomaly observed at 180 cmdc (Fig. 4.2.2) may also be explained by the observed increase of coral debris in this unit (Fig. 4.2.4).

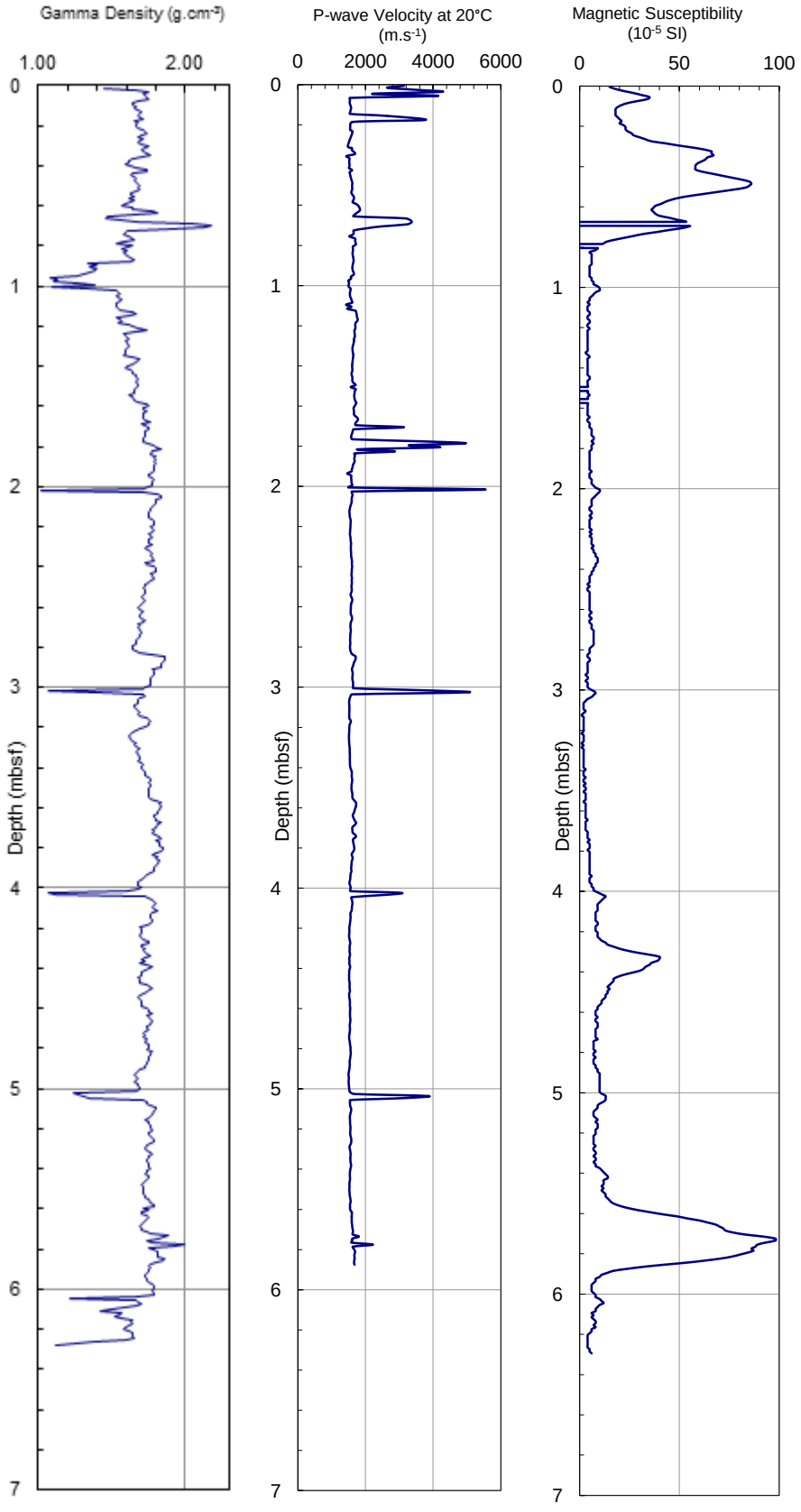

Fig 4.2.1: MSCL results for sediment core CS07.

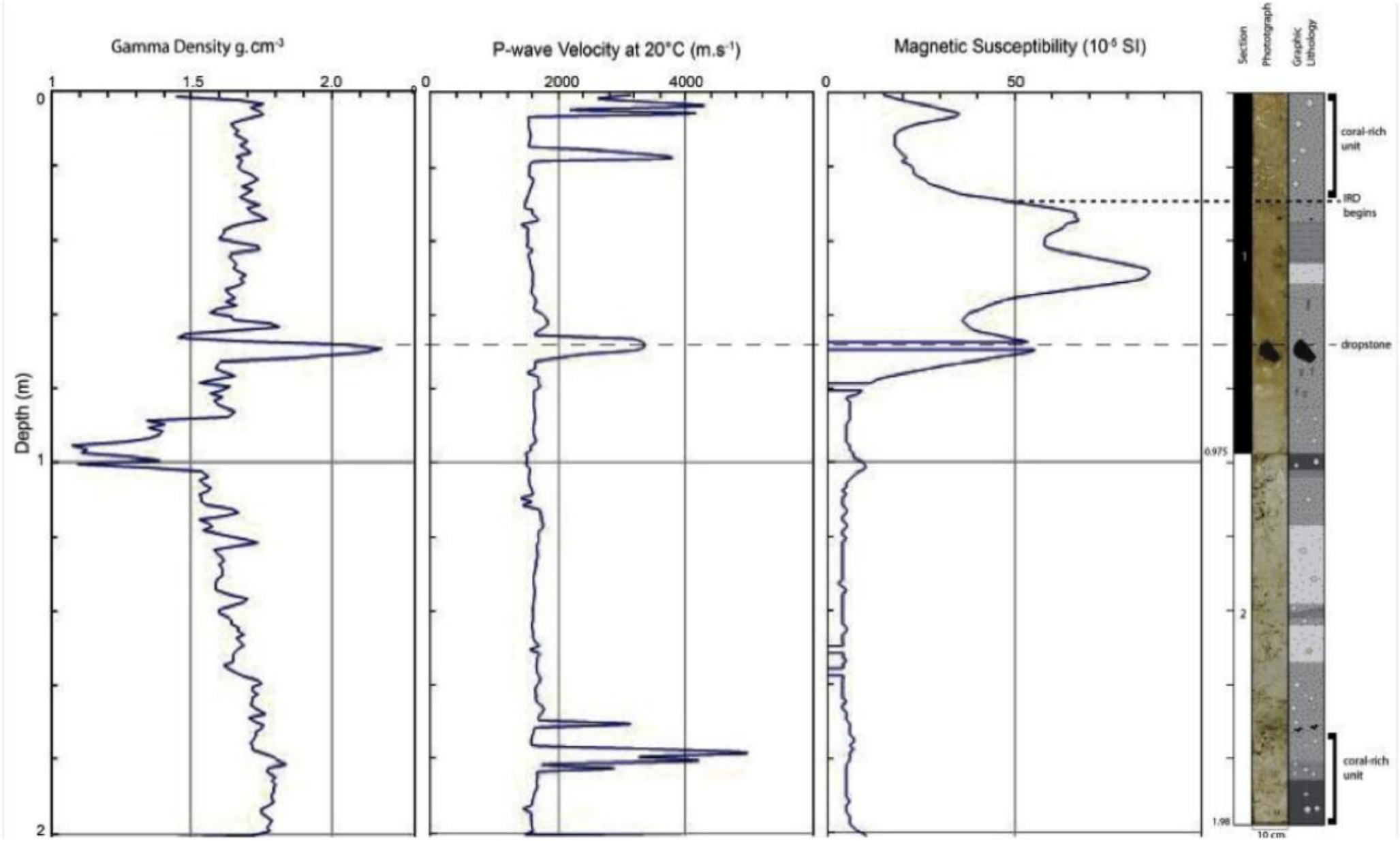

Fig 4.2.2: MSCL results for Section 1 and Section 2 of core CS07 with relevant core photographs and graphic log. For key to graphic log see Fig. 4.3.1.

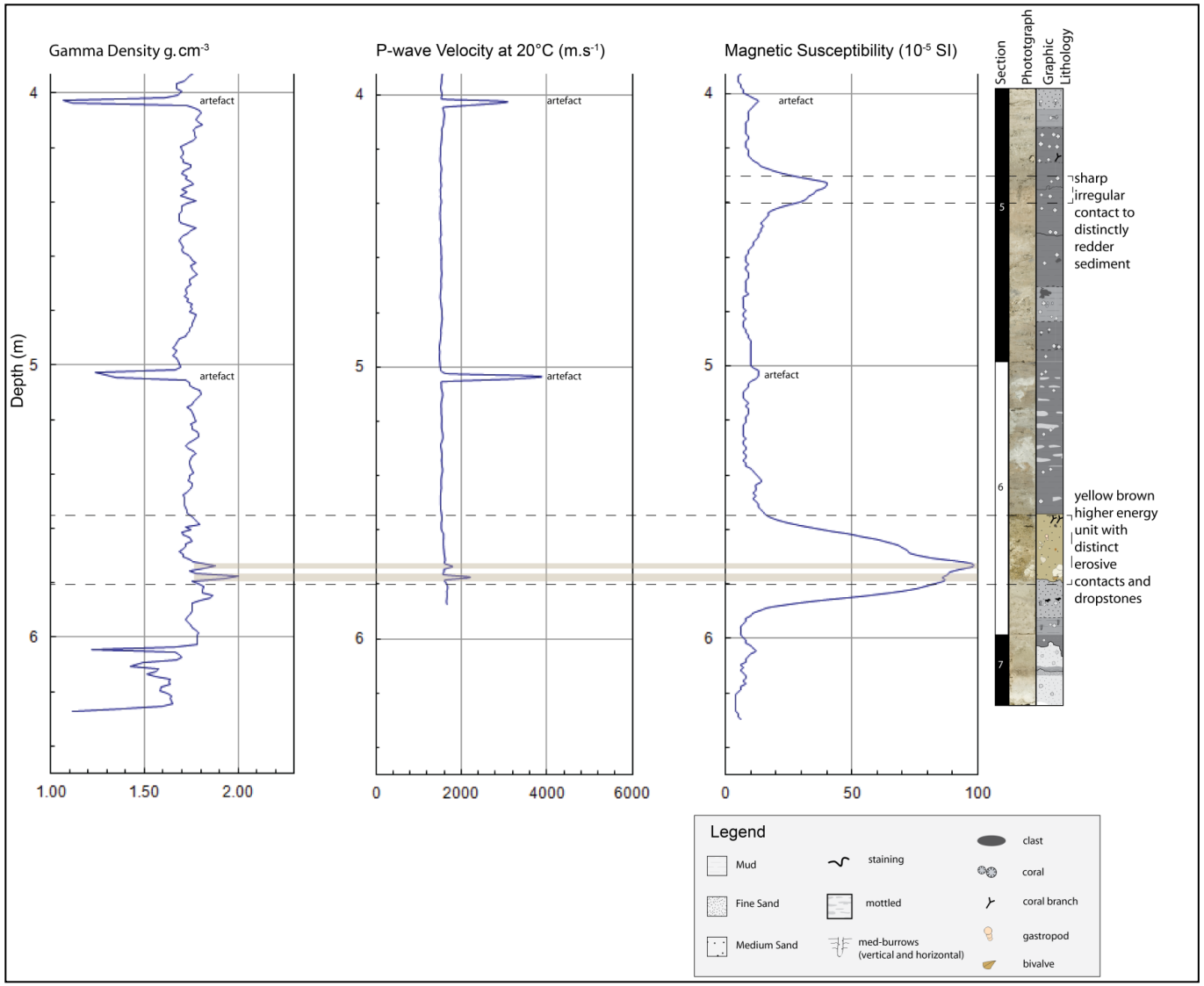

Fig 4.2.3: MSCL results for Section 4-7 core CS07 with photographs and graphic log.

Fig 4.2.4: Coral-rich unit located at 180 cmdc (indicated by arrow head) in CS07 S2. This unit may explain the p-wave anomaly seen in the MSCL data at this level in Fig. 4.2.2. Each scale bar line represents one cm.

Total MSCL gamma density, p-wave velocity and magnetic susceptibility readings for the entire length of core **CS06** are shown (alongside photographs of their respective core sections) in Fig 4.2.5. The spike in magnetic susceptibility 38 cmdc correlates to a void created by a missing clast. Further magnetic susceptibility spikes 75 and 180 cmdc correlate to concentrations of granule material noted in the sand units. There is a large magnetic susceptibility spike, and a rise in gamma density, associated with the granitic dropstone recovered from 235 cmdc (there are no results for p-wave velocity for this region; see base Fig. 4.2.5); however, there are no notable MSCL measurements associated with the dropstone noted 65 cmdc in Section one of **CS06**. Several muddy units occur in **CS06** and these show lower p-wave velocity and magnetic susceptibility readings.

4.2.3: Conclusion

MSCL results allowed identification of possible accumulations of coral skeletal material within the core, which dictated the strategy for opening the core (i.e. necessitating freezing the core beforehand). The magnetic susceptibility readings are particularly accurate at indicating potential IRD-rich units. Peaks in density in both cores may indicate poorly sorted ice-rafted debris. The p-wave velocity was also observed to increase with increasing grain-size.

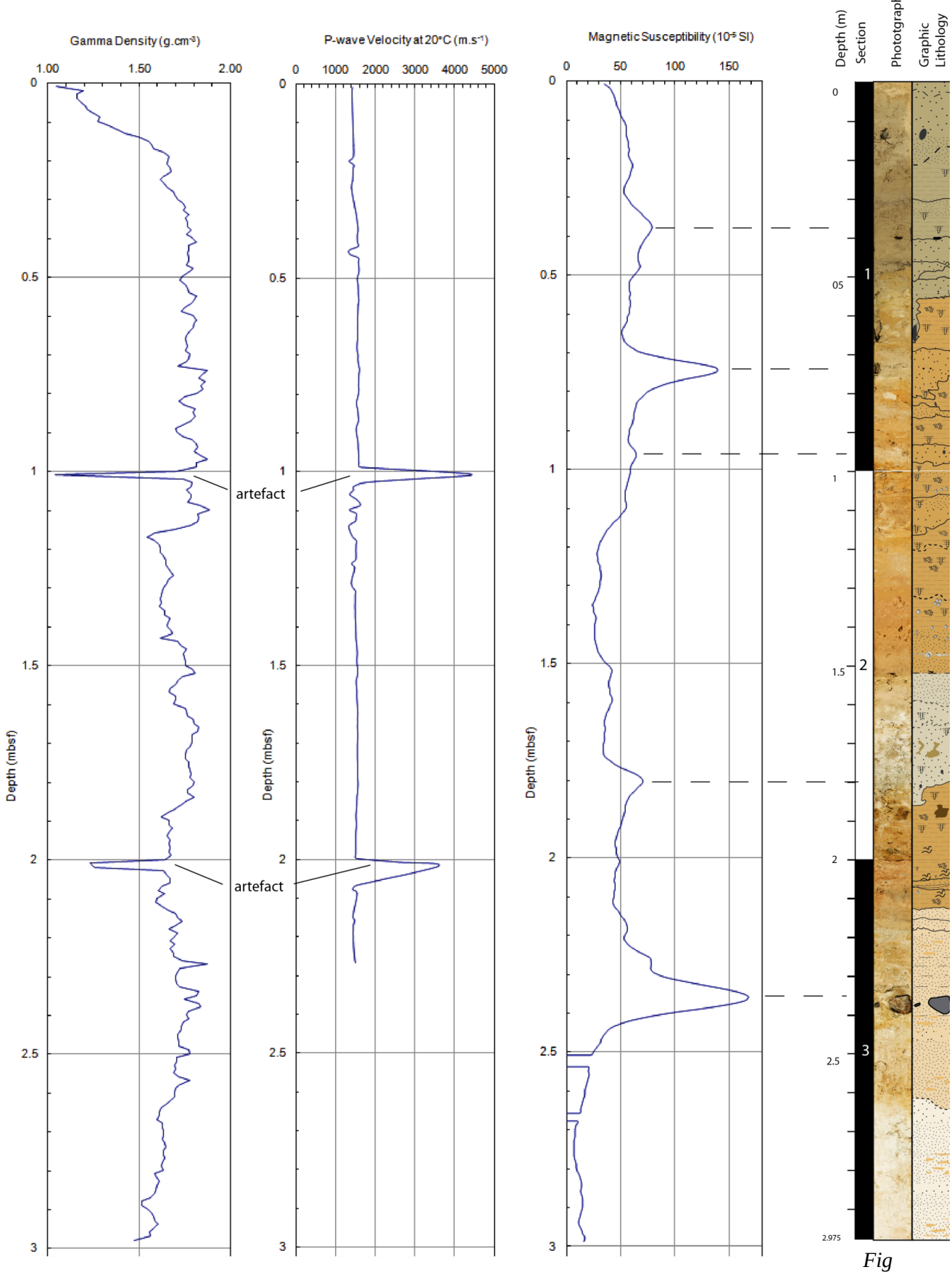

Fig 4.2.5: Comparative MSCL results and visual/graphic log for core CS06. For key to graphic log see Fig. 4.3.2.

4.3: Open core analysis

4.3.1: Sedimentological logging

Both cores were split in half lengthwise and visually logged in the IFREMER institute in Brest. Core **CS07** Section 1 was frozen before splitting due to the observed variability in the MSCL readings (see Section 4.2 and Fig. 4.2.2). Freezing prevented the coral branches from being dragged down the core by the wire cutter and thus destroying sedimentary structures and textures in the process. The rest of the core sections were split as per normal procedure using wire cutters. One half of each core was stored for archival purposes in the core store at IFREMER.

The 'working' split core section was laid out on a bench and the upper surface of the sediment skimmed (cleaned) using a broad palate knife to ensure accurate representation of sedimentological features. The working core section was then immediately photographed alongside a scale using a high-resolution camera.

Individual core sections were numbered according to their position in the core, from top to base. The nomenclature used utilised the core number first, followed by the section number, from the top to the base. Detailed (cm-scale) stratigraphic logging of the core was then undertaken. Lithology, colour and sedimentary structures were described as they appeared visually. As the sediments commonly included admixtures of secondary material the (Folk, 1954) classification, incorporating the modification of (Flemming, 2000) was used, which distinguishes six sediment types on the basis of mud and sand content:

Sand	<5% mud
Slightly muddy sand	5-25% mud
Muddy sand	25-50% mud
Sandy mud	50-75% mud
Slightly sandy mud	75-95% mud
Mud	>95% mud

The hand-drawn logs were subsequently digitised in NUI Galway using *Adobe Illustrator* (Fig 4.3.1).

Sediment samples (approximately 1 cm in stratigraphic width) were taken at 5 cm intervals for **CS06** and Section 1 of **CS07**. The exposed surface of each sampling area was first cleaned (skimmed) and placed in a small aluminium tray for laser grain size analysis. The material from the outer edges (~1 cm) was discarded in all cases, to avoid contamination by disturbed and reworked sediment due to friction from the metal coring cylinder during recovery. The sediment samples were removed using two semi-circular knives and stored in plastic *zip-lock* bags for later sieve-based grain size analysis and foraminiferal picking. The voids in the core section were refilled with foam blocks as sampling progressed down-core, to ensure minimal disturbance of the adjacent sediments. Coral fragments for stable isotope analysis and dating were also carefully extracted.

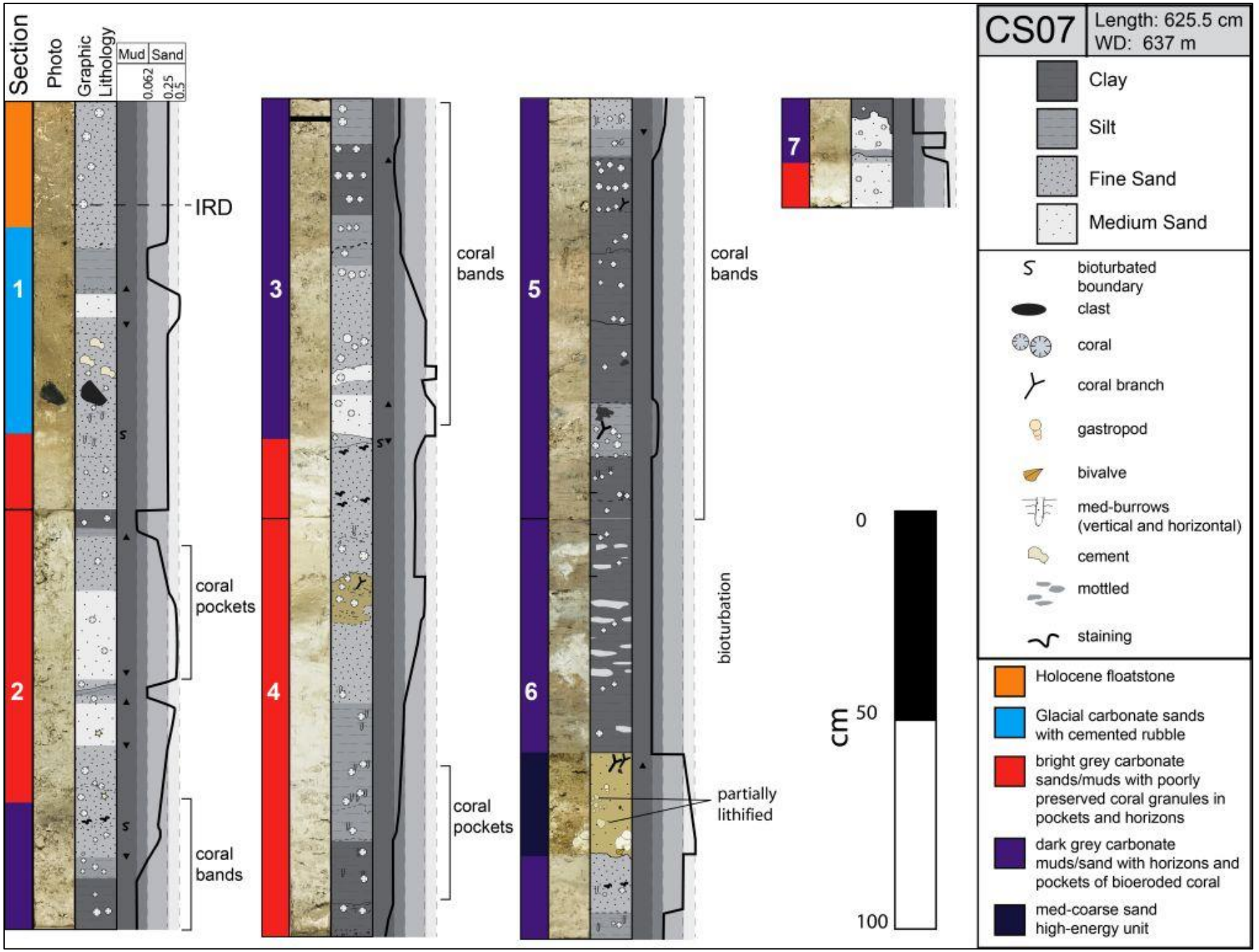

Fig 4.3.1: Detailed log of sediment core CS07.

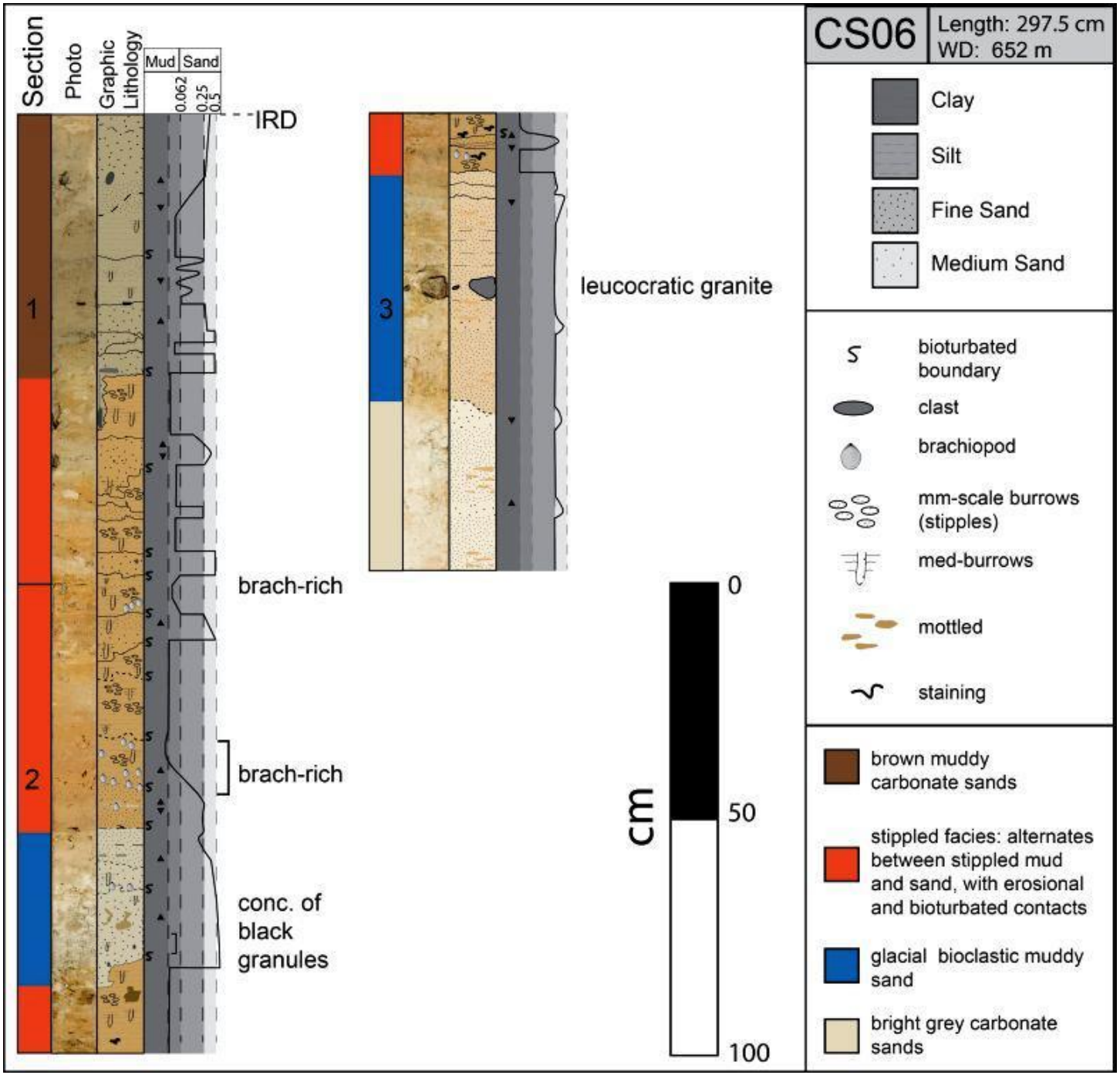

Fig 4.3.2: Detailed log of sediment core CS06.

4.4: Grain-size analysis

Grain-size analysis is based on the subdivision of the sediment into discrete grain-size fractions. The fractions discussed are based on the Udden-Wentworth grain-size classification of terrigenous sediments (Wentworth, 1922). The sediment is divided into its coarse (>63 µm) and fine (<63 µm) components, which separates the sand-sized sediment from the mud (silts and clays). Five subsequent subdivisions of the coarse fraction are differentiated:

	Udden-Wentworth term:	Scale:
Coarse component	Very coarse sand, granules, pebbles & above	>1000 µm
	Coarse sand	500-1000 µm
	Medium sand	250-500 µm
	Fine sand	125-250 µm
	Very fine sand	63-125 µm
Fine component	Silt & mud	<63 µm

Two grain-size analytical methods were used to assess the sedimentology:

4.4.1: Laser Diffraction Grain Size Analysis [LDGSA]

LDGSA was undertaken using the Granulometric Laser: Coulter LS200 for core **CS06** (**CS07** to be completed in 2013). Laser Diffraction Particle Size Analyzers measure particle size using the classic Mie theory of light scattering. The LS200 measures grain sizes within a size range from 17 nm to 2000 µm (i.e. it does not measure gravel). Each sample was rehydrated using a dropper and stirred to ensure a paste-like consistency. A spatula of sediment was added to a test-tube filled with distilled water and mixed by vibration for 30 seconds.

4.4.2: Sieve Based Grain Size Analysis [SBGSA]

SBGSA was carried out for both cores in order to fully assess the sedimentary characteristics of each sample (including particles >2000 µm) and allowed for the collection of the foraminiferal sample set.

Labelled beakers were weighed (on a scale sensitive to 0.1 g) before the samples were loaded for drying. The samples were then oven dried at 50-60°C (but never above 70°C as destruction of foraminiferal shells due to cracking may occur). The samples were dried until completely desiccated (i.e. there was no further loss of weight with time). The beakers with the dried samples were then reweighed. Subtraction of the original beaker weight from this value produced a weight for the sediment sub-sample.

Wet sieving was carried out in one run; Table 4.4.1 lists the sieve fractions used for this. The <63 µm fraction was not collected. This was due to the practical recovery problem of very long settling times required to recover this portion of each sample. Samples were poured onto the sieve stack and washed gently with water. The separated fractions from each sample were collected, dried (at 60°C) and weighed. The raw data were converted into weight percentages (wt%): (dry weight in g retained on a sieve/ dry weight in g of total sample) × 100. The size of the <63 µm fraction (silt and mud) was calculated by subtracting the combined weight of the separated coarser fractions from the overall weight of the dry sample.

Grade	Aperture (µm)	Aperture (Φ value)	
Coarse Sand	>500	1	*Top of stack*
Medium Sand	250-500	2	
Fine sand	63-250	4	*Base of stack*

Table 4.4.1: Wet-sieve stack configuration with Udden-Wentworth grade, µm and Phi (ϕ) values.

4.4.3: Results and Discussion

The mean grain size of the laser results for sediment core **CS06** is shown in Fig. 4.4.1. The sieving results (Table 4.4.2) and the ternary gravel sand mud diagram produced from the laser results (Fig. 4.4.1) show the sediment to be mainly made up of varying quantities of mud and fine sand, producing deposits of muddy sand and sandy mud.

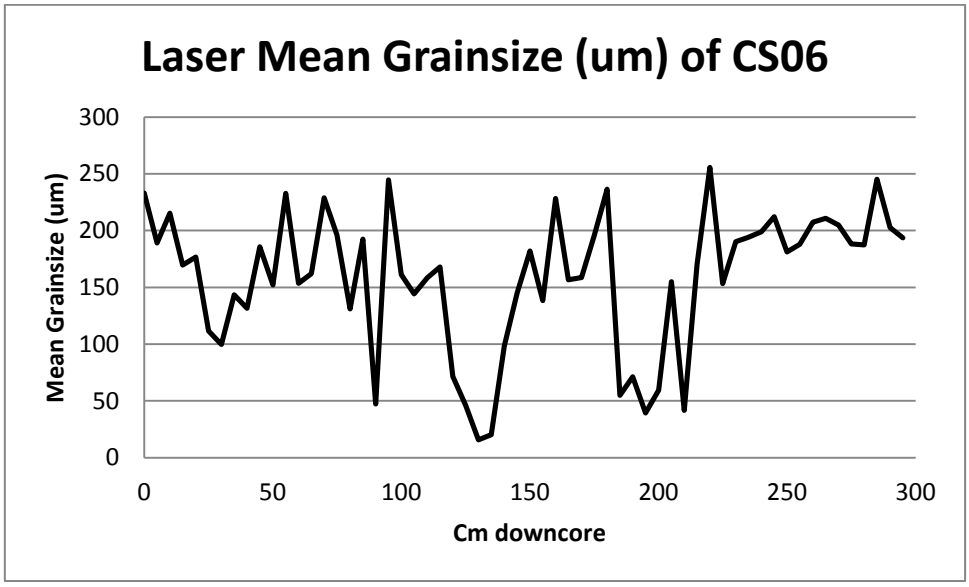

Fig. 4.4.1: CS06 laser diffraction mean grain size of core CS06.

At 60 and 65 cmdc the LDGSA measured **'muddy sand**'. This was probably due to large burrow structures present in the very fine mud (Fig. 4.4.3). SBGSA, by contrast, found these two sections to consist of **'sandy mud**'.

Graphing the variation of the wt% of the mud fraction down-core (Fig. 4.4.4) shows a generally high component of mud in Section 1 with lower values corresponding to the alternating sandier units. The excursion in the wt% of the mud fraction between 150-180 cmdc (Fig. 4.4.4b) corresponds to sand unit 18 in Section 2. Fig. 4.4.4c shows very clean deposits from 215 cmdc in Section 3, corresponding to the logged sand (Fig 4.3.2) and plotted sand in the laser ternary gravel sand mud diagram.

Core Section 1						Core Section 2						Core Section 3					
	CMDC	%MUD	% >63 µm	% 250 µm	% 500 µm		CMDC	%MUD	%>63 µm	%>250 µm	%>500 µm		CMDC	% MUD	%>63 µm	%>250 µm	%>500 µm
	0	19	62	16	2		**100**	46	35	11	8		**200**	68	20	5	7
	5	29	51	16	4		**105**	46	36	12	6		**205**	41	38	15	7
	10	27	47	19	7		**110**	28	50	15	6		**210**	77	13	3	7
	15	35	46	14	4		**115**	68	23	7	3		**215**	15	65	14	6
	20				3		**120**	58	31	7	4		**220**	32	43	22	5
	25	58	34	6	2		**125**	71	24	3	2		**225**	45	37	15	3
	30	60	30	8	2		**130**	87	10	2	2		**230**	31	48	16	4
	35	56	35	8	2		**135**	84	8	1	7		**235**	33	47	15	6
	40	67	23	8	2		**140**	72	24	3	1		**240**	35	44	14	7
	45	39	44	15	3		**145**	49	41	7	3		**245**	31	47	18	4
	50	43	40	12	5		**150**	43	44	9	4		**250**	35	50	14	1
	55	30	44	16	10		**155**	47	42	8	3		**255**	32	51	15	2
	60	50	37	9	4		**160**	37	42	16	5		**260**	26	55	18	2
	65	51	34	11	3		**165**	32	36	14	18		**265**	19	58	21	2
	70	38	39	16	8		**170**	37	42	13	7		**270**	26	53	20	1
	75	26	51	16	7		**175**	16	59	20	5		**275**	30	52	17	0
	80	43	40	13	4		**180**	21	46	23	10		**280**	25	58	16	1
	85	47	36	12	5		**185**	54	34	9	2		**285**	26	55	18	1
	90	67	25	6	3		**190**	56	31	9	5		**290**	25	60	14	2
	95	24	47	20	9		**195**	75	18	5	2		**295**	23	57	14	6

Table 4.4.2: Sieving results for sediment core CS06 (Sections 1-3) showing the sediment to comprise mainly mud and fine sands.

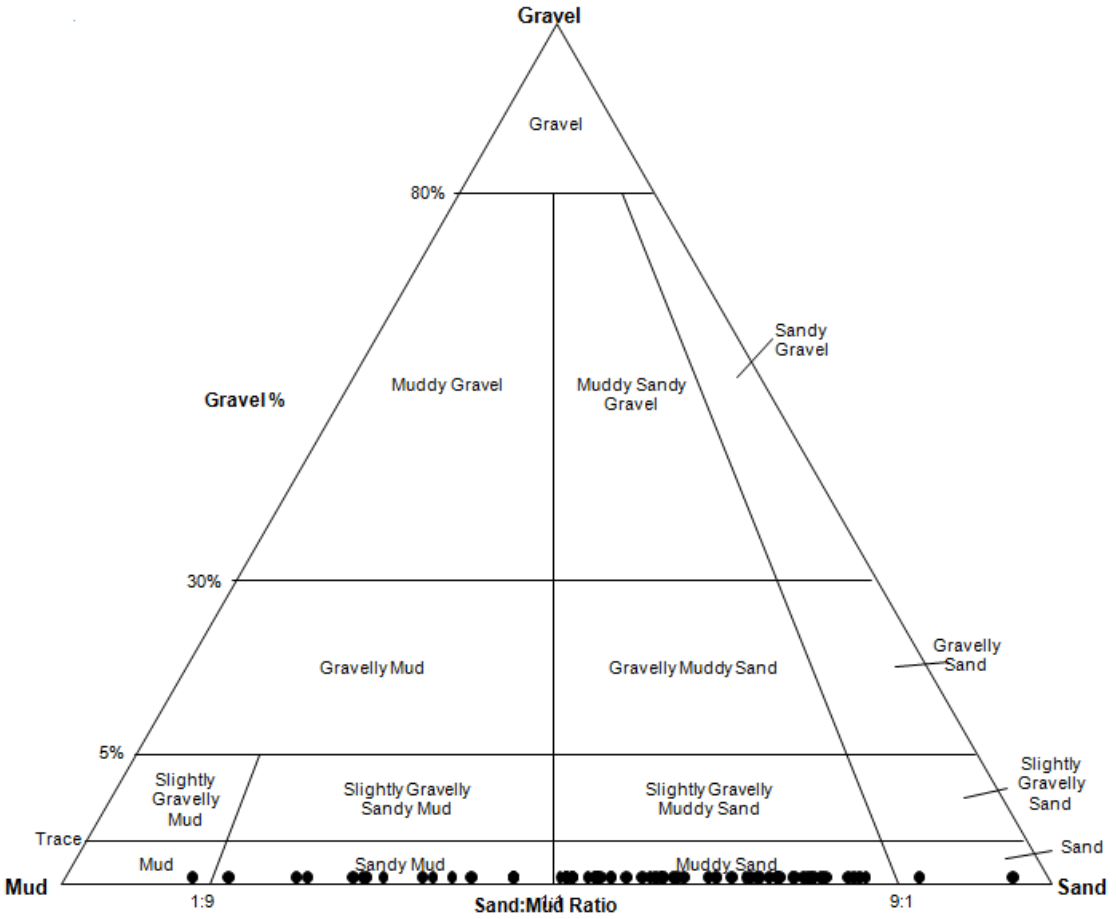

Fig. 4.4.2: CS06 laser diffraction grain size analysis results. Ternary gravel sand mud diagram showing the majority of the sediments fall within the muddy sand category.

Fig. 4.4.3: Sediment 60-65 cmdc in Core CS06 with burrows of lighter and coarser infill than the surrounding (enclosing) mud.

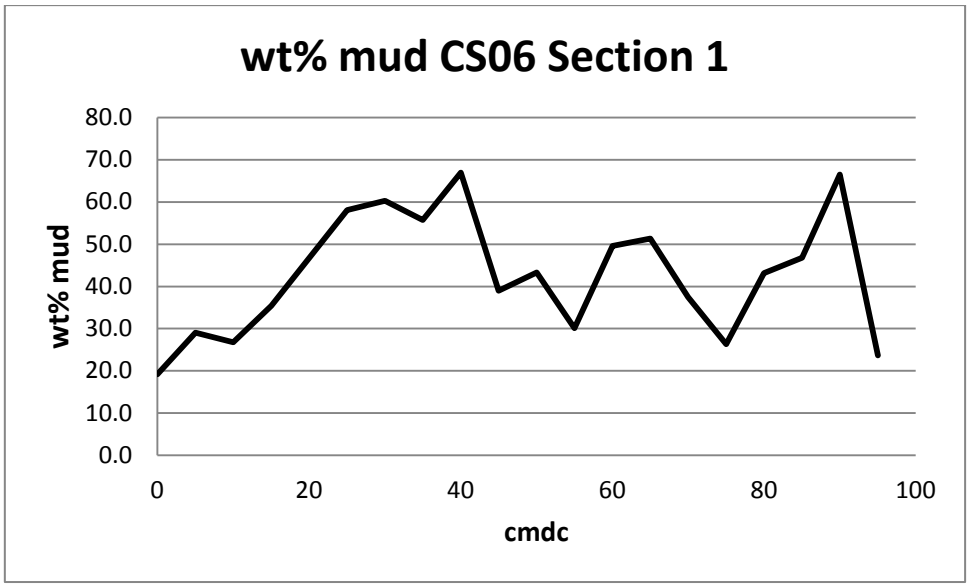

Fig. 4.4.4a: Graph showing variation in mud component down through core Section 1 in CS06.

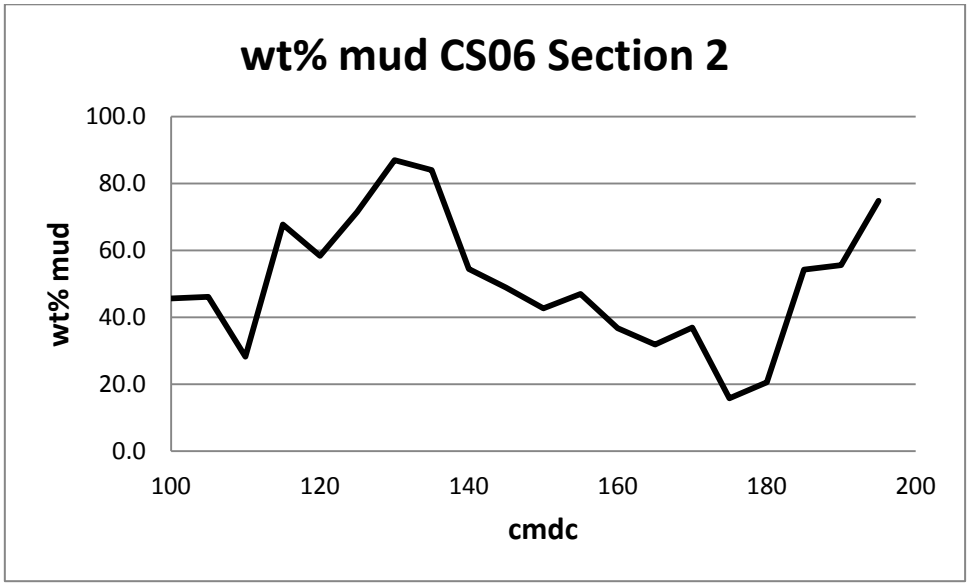

Fig. 4.4.4b: Graph showing variation in mud component down through core Section 2 in CS06.

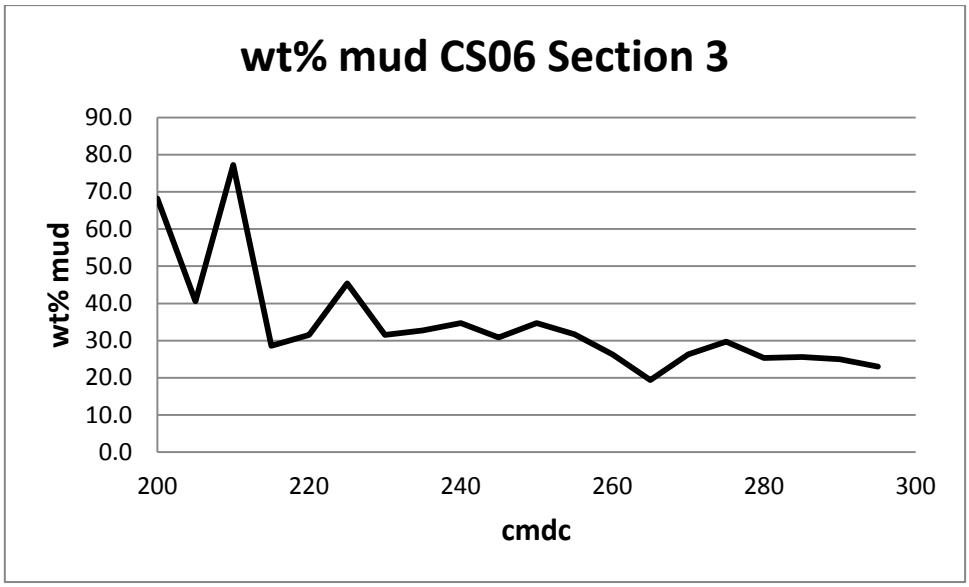

Fig. 4.4.4c: Graph showing variation in mud component down through core Section 3 in CS06.

The sieving results for Section 1 of **CS07** (Table 4.4.3) show the sediments to be composed of a much higher >500 µm component than core **CS06** due to the presence of gravel-size coral debris. The graph of wt% of the mud fraction (Fig. 4.4.5) shows that there is generally a high component of mud, producing deposits of gravelly sandy muds and gravelly muddy sands. The lower anomaly in the mud fraction at 60 cmdc in the graph is due to the purposeful sampling of a lithified irregularly shaped nodule 60-61 cmdc; this also explains the very high >500 µm component in the sieving results as the sediment consisted mainly of rubble.

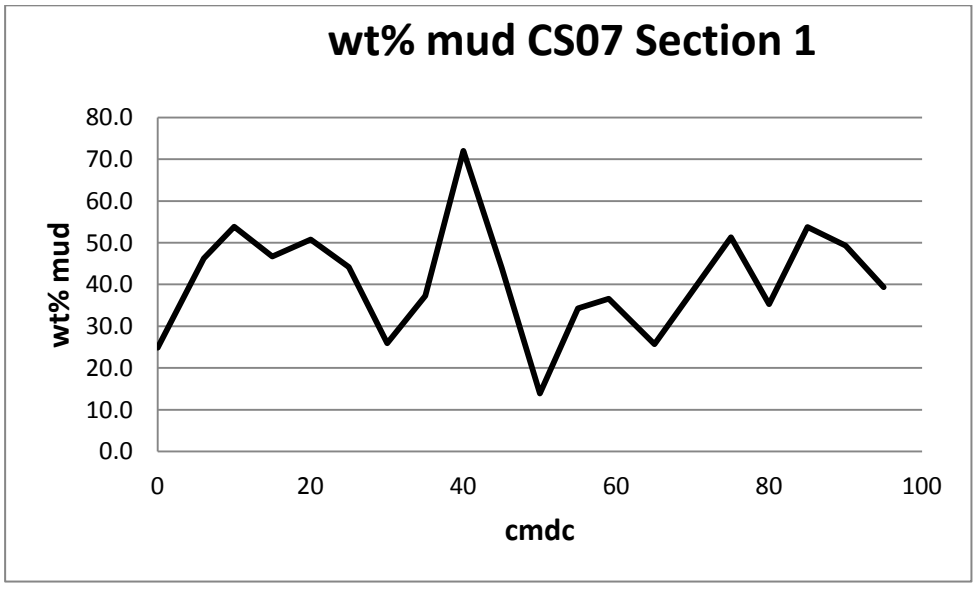

Fig. 4.4.5: Graph showing the variation in the mud fraction through Section 1 of core CS07. There is generally a high component of mud with lower excursions at 50 and 65 cmdc corresponding to sandier units.

Core Section 1	CMDC	%MUD	%>63 µm	%>250 µm	% >500um
	0	25	30	19	26
	6	46	17	10	28
	10	54	16	9	21
	15	47	21	8	24
	20	51	23	5	21
	25	44	33	8	15
	30	26	42	16	16
	35	37	29	18	16
	40	72	13	10	4
	45	44	13	16	27
	50	14	32	28	26
	55	34	20	19	27
	59	37	19	16	29
	60	14	8	6	72
	65	26	17	15	43
	75	51	28	10	12
	80	35	31	9	24
	85	54	33	7	6
	90	49	35	7	9
	95	39	31	11	19

Table 4.4.3: Sieving results for core CS07 Section 1. Note the generally high mud and silt fraction and of grains > 500 µm

In summary, the grain size analyses (LDGSA and SBGSA) agree broadly (and satisfactorily) to the logged cores (Figs. 4.3.1-2), which were determined essentially by visual inspection. As the LDGSA is based on a very small sample, the SBGSA (achieved by wet sieving) better represented the core units because it involves a comparatively larger and more representative sample size; as seen 60-65 cmdc in core **CS06** (Fig. 4.4.3).

4.5: Base Cutter Sediment (Bas Ogive)

Geotechnical results showed that the coring of **CS06** was abruptly stopped after 1.5 seconds due to encountering a firm and highly resistant layer. There was ~ 400-500 cm of penetration with sediment recovery of 297.5 cm. The depth of coring corresponds to the moundbase reflector previously highlighted in the chirp data (see Figs. 3.3.1-2). The base cutter sediment (named 'Bas Ogive'; BOg) contained moderately lithified reddish to green pebbly breccio-conglomeratic sediment. The presence of chalk was also noted. It is assumed that the rock broke up due to the release of pressure during coring. Carbonate cement was observed adhering to the pebbles and gravels that were encased in carbonate silty mud.

The BOg sediment was wet-sieved in NUI Galway for grain size analysis. In order to investigate the composition of the clasts and the nature of the carbonate cement 3 thin sections (BG1-BG3) were prepared from the >63 µm fraction of sieved sediment for analysis under normal and polarised light - plane polarised (PPL) and cross polarised (XPL).

4.5.1: Results and Discussion

Composition of Bas Ogive sediment

The wet-sieving results in Table 4.5.1 (below) show the BOg sediments to be composed mainly of gravel-pebble clasts >2 mm (69%). Of the remaining sediment 12% of the grains are greater than 500 µm (greater than or equal to coarse sand); 10% makes up the fine/medium sand and there is an 8% mud fraction.

CS06	% MUD	% >63 µm	% 250 µm	% 500 µm	% > 2mm
Bas Ogive	8	6	4	12	69

Table 4.5.1: Sieving results for Bas Ogive sediment from the base of core CS06.

The gravel and pebbles for the most part are angular with red and green staining (Fig. 4.5.1). The thin-sections show the clasts to be made up of bioclastic (predominantly foraminiferal) wackestone and packstone limestones or biomicrites (Figs. 4.5.1E, 4.5.2, and 4.5.3 - 4.5.3) cemented together, as well as chalks, and some intraclastic mud pebbles.

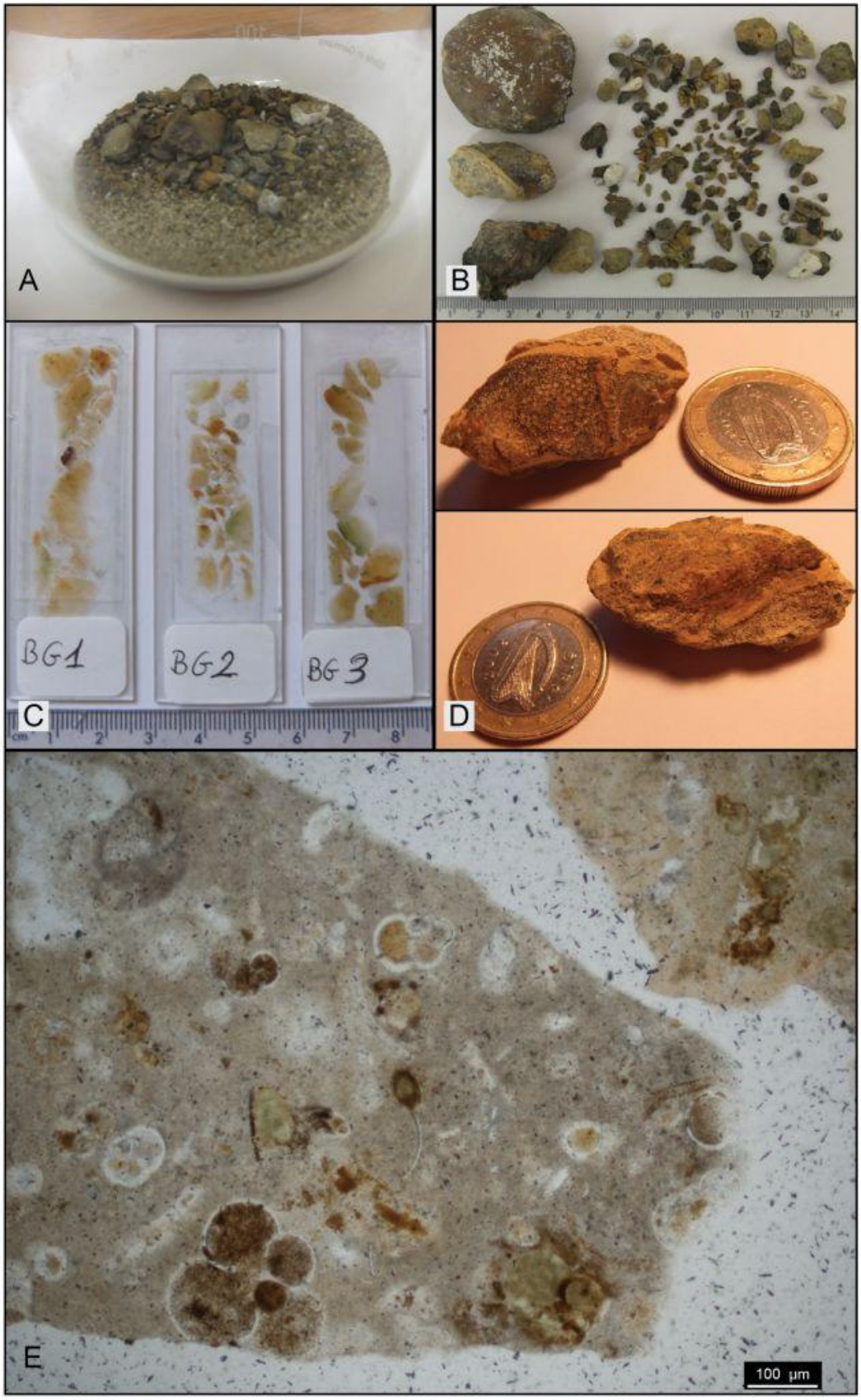

Fig. 4.5.1: Bas Ogive sediment A. The sieved sediment in beaker before thin sectioning (sediment >63µm); B. Lithics >2mm (ruler in cm), note the angularity (except large pebble in top left) and red and green colouration; C. Thin-sections; D. Top surface of pebble showing colonised surface and bottom surface showing cement; E. Foraminiferal wackestone clast in thin section (PPL).

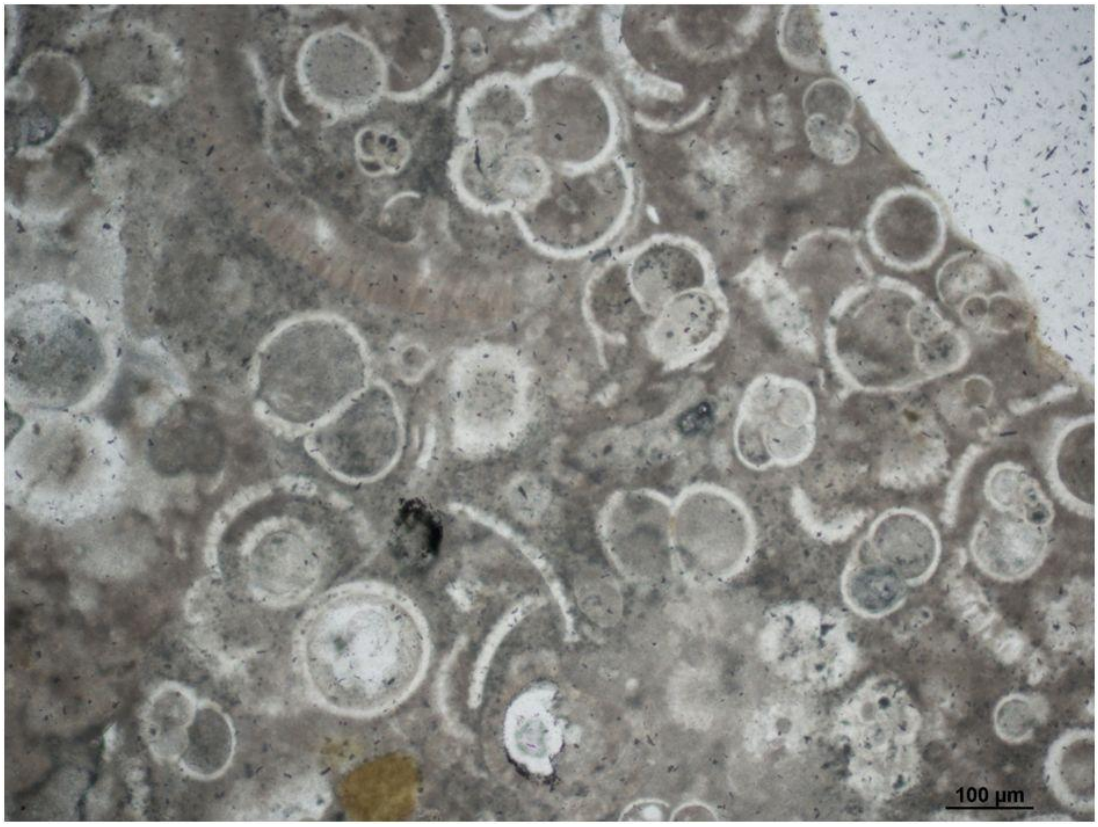

Fig. 4.5.2: Packstone with abundant planktonic foraminifera in BOg. Many thin shell fragments are also present. BG2 (PPL).

The carbonate grains are made up of planktonic foraminifera (Globigerinids are particularly abundant, Fig. 4.5.2), benthic foraminifera and admixed benthic invertebrate skeletons including bryozoans, brachiopods, bivalves, and coral (Fig. 4.5.3).

During the wet-sieving process the presence of a carbonate cement adhering to the pebbles and surrounding (loose) carbonate mud became apparent and indicated at least two generations of carbonate production. The thin-sections allowed the nature of this carbonate cement to be investigated. Some of the clasts showed an outer coating of bioclastic micrite as well as in-between clasts (Fig. 4.5.4), suggesting that two stages of carbonate formation occurred to generate the surrounding loose, wet, silty carbonate mud.

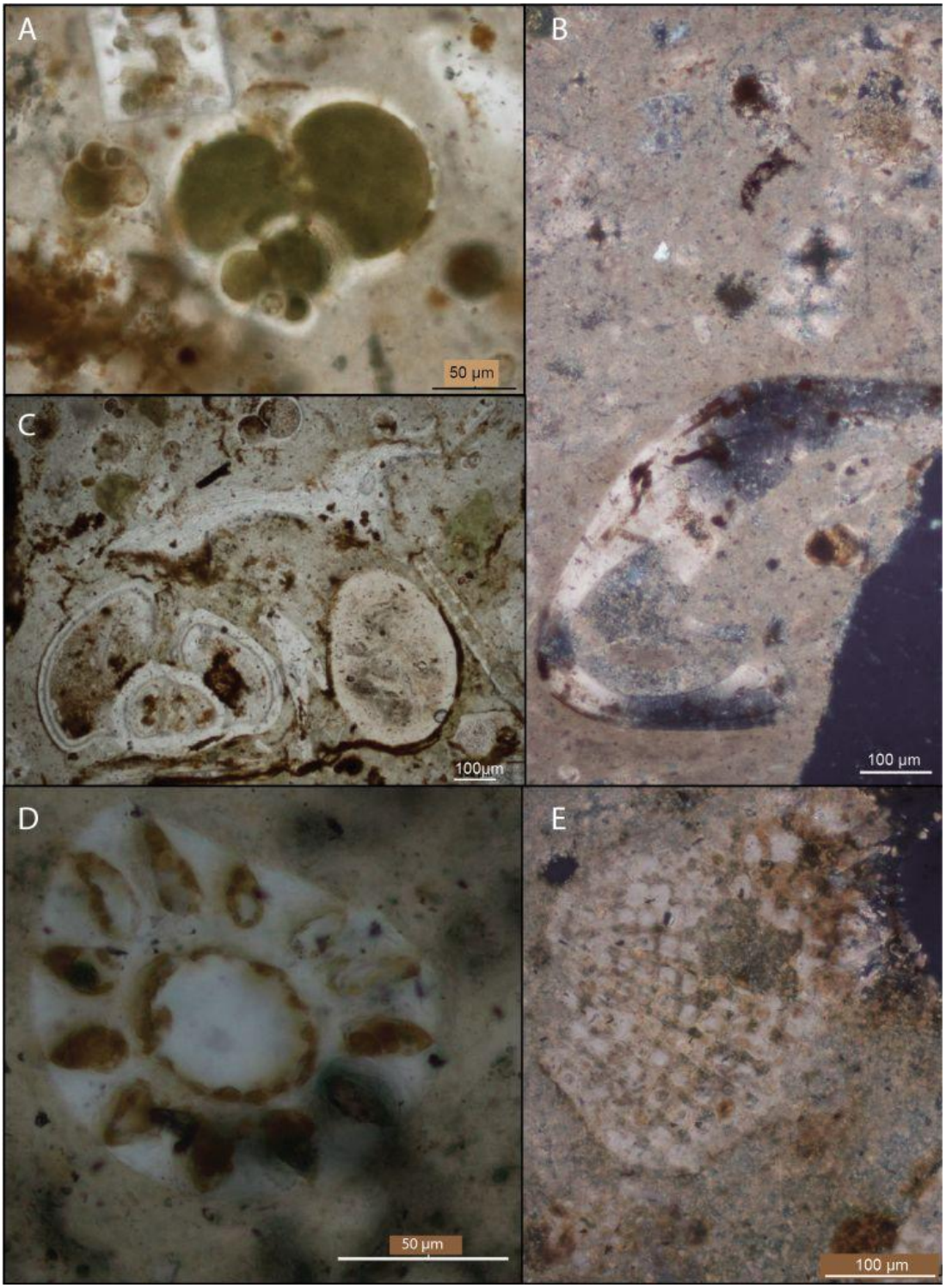

Fig. 4.5.3: Fossils in Bas Ogive. A, Globigerinid, BG1 (PPL); B. Brachiopod, BG1 10x XPL; C, Possible Cibicides benthic foram (left), mollusc shell (wavy elongated S form above) well-rounded chalk carbonate clast, BG 1 10x PPL. D, Coral (?) BG2 40x PPL; E. Bryozoan, BG3 20x XPL

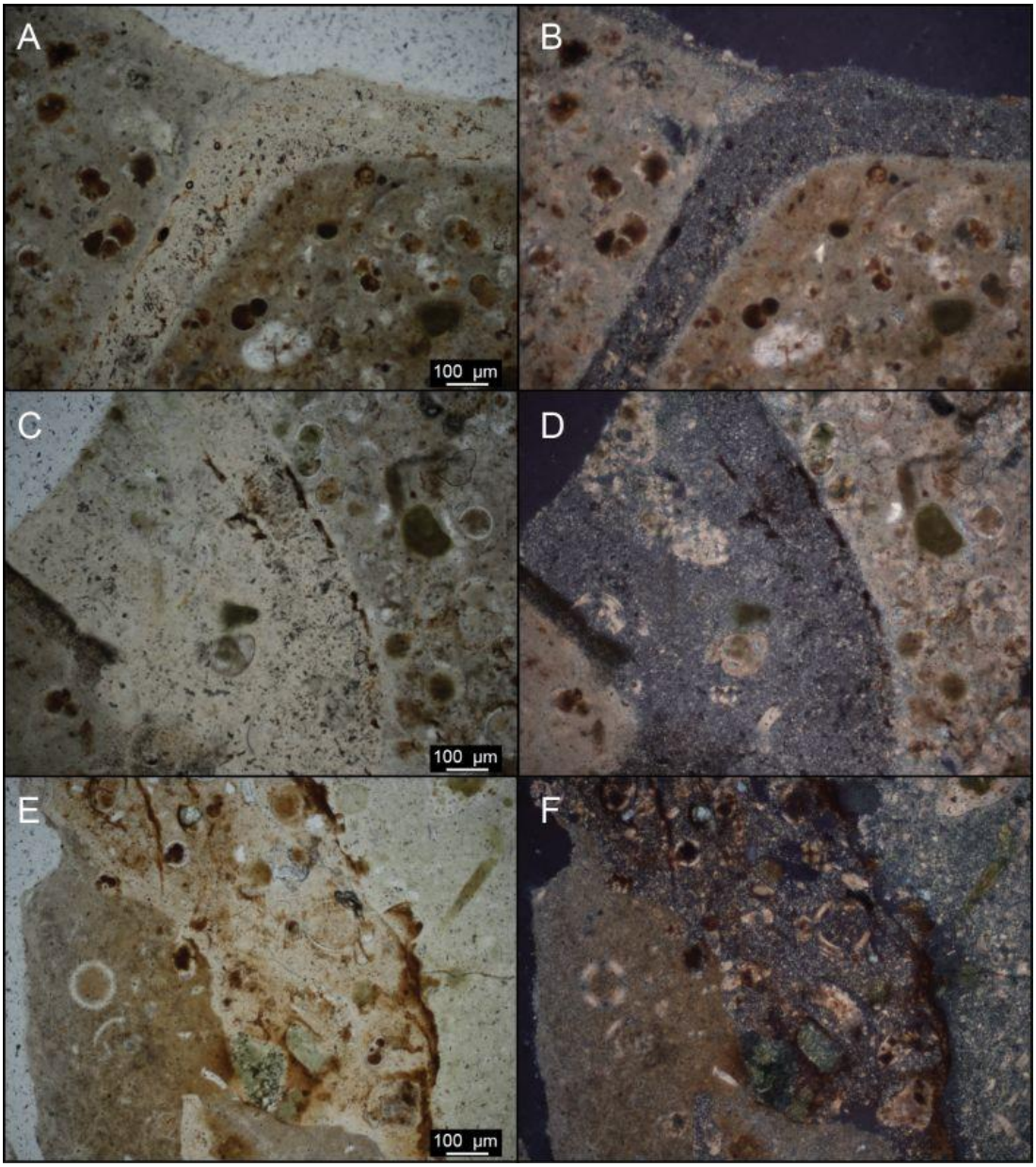

Fig. 4.5.4: Photomicrographs of the cement found between the Bas Ogive limestone clasts. Left – PPL, right XPL. A-D from thin-section BG3, E-F from thin-section BG2. Green coloration ascribed to glauconite.

The green colouration of the pebbles and small green clasts seen within the thin sections (e.g. Fig. 4.5.4) is ascribed to the formation of glauconite. Detrital glauconite grains are a typical feature of hardgrounds (Carson and Crowley, 1993). The red colouration is ascribed to iron-crust formation (Fig. 4.5.5). Manganese- and ferromanganese-rich horizons are often found in association with contourites (e.g.Faugères *et al.*, 2002) with the currents preventing the accumulation of other sediments. The interpreted glauconite also suggests that the region contained iron-rich muds where sedimentation rates were relatively low.

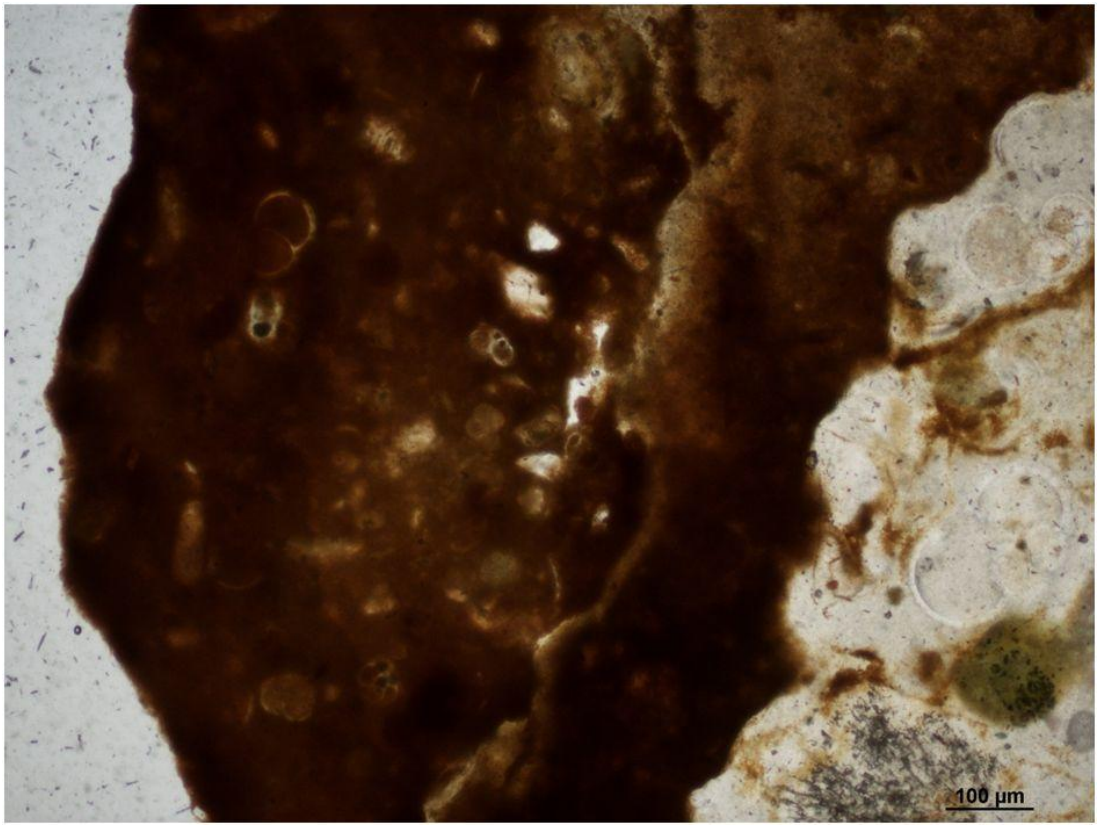

Fig. 4.5.5: Significant iron crust on clast in thin section.

Two of the recovered larger iron-stained clasts from the BOg have a surface covered in small circular impressions (e.g. Fig. 4.5.1D). These are interpreted as ichnofossils - essentially the remains of surface colonisation by benthic invertebrates. This feature has important implications because it means the pebbles were exposed at the surface for a sufficient period of time for colonisation to occur (which is corroborated by the iron-staining and glauconite, which both also require time to develop). The colonising animal may have been a cnidarian hydroid such as *Hydractinia echinata* with the individual hydranths joined to the colony by stems producing the circular pattern.

The BOg rock is composed of reworked wackestone and packstone clasts, which were later cemented together. It is not known, at present, whether hydrocarbon seepage and associated microbial activity were involved in the lithification of the resultant limestone breccio-conglomerate, or if it occurred abiogenically through oxidization by currents and a low sediment input. However, the BOg sediments are similar to the Mid-Pleistocene carbonates

described by Noé et al (2006) who ascribed lithification to be controlled by vigorous bottom currents Thus the diagenetic sequence of hardground formation may be similar to those specified by (Noé *et al.*, 2006):

Diagenetic sequence:	Seafloor stage	Subsurface stage	Event:	Age:
1	**(i)**		Sedimentation	Possibly Mid-Pleistocene
2		**(i)**	Physical compaction	
		(ii)	Rim and spar cementation	
		(iii)	Neomorphism	
3	**(ii)**		Exhumation & subsequent fragmentation of limestones into angular clasts	
4	**(iii)**		Hardground formation: cementation between limestone clasts	Holocene to Recent

Figure 4.5. 6: Diagenetic sequence of hardground formation as described by Noé et al., 2006.

A limestone clast from the BOg contained well-rounded chalk intraclasts (Fig. 4.5.7) implying a prior phase of exhumation and reworking to step 1 above. As chalk is fairly soft, the rounding of the clasts is not taken to necessarily imply particularly protracted transport distances.

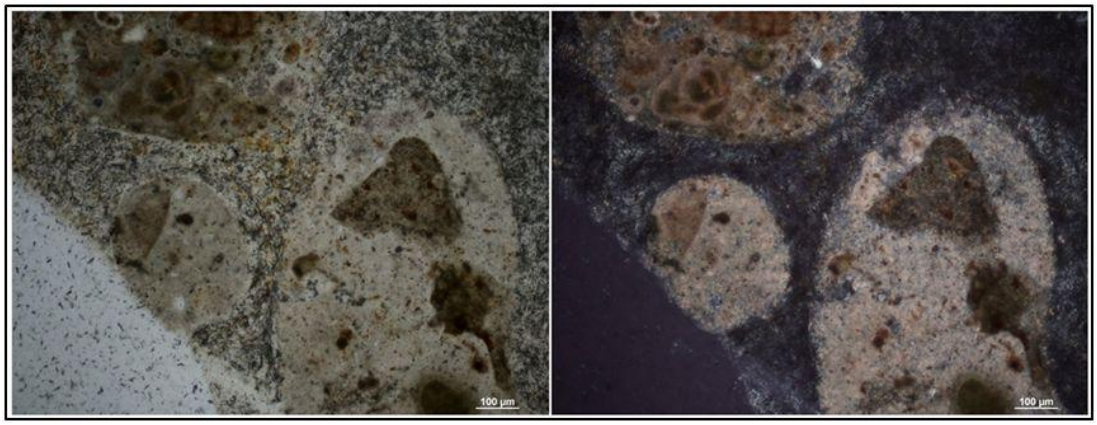

Fig. 4.5.7: Well-rounded intraclasts (within a larger clast) in the BOg. Left is PPL and right is XPL.

The proposed diagenetic sequence could suggest the rock relates to Quaternary scarp features presently found at the seafloor surface. Notwithstanding this, the BOg may be older than the surface scarps and could correlate to the Miocene erosional event associated with the reintroduction of the Mediterranean Ocean Water. It may also correlate with the 'iron-stained carbonate conglomerate' boulders collected on the Porcupine Bank by Scoffin and Bowes (1988) who assigned an upper Eocene to Lower Oligocene age based on fossil content. Scoffin and Bowes (1988) also postulated that the boulders represent the acoustic reflector reported by Roberts (1974) from the flanks of the Rockall Trough.

4.5.2: Conclusion

The BOg is believed to be a breccio-conglomeratic carbonate hardground. The recovered sample material disintegrated into its component lithic fragments upon release of pressure during sediment coring. To form the BOg sediment, pelagic oozes with admixed benthic skeletal grains were lithified to wackestones and packstones (or biomicrites), with some containing (previously reworked intraclastic mud pebbles). Wackestones with irregularly distributed planktonic foraminifera and benthic bioclasts form the predominant lithology type in the BOg. The glauconite and iron oxides suggests the sediments were deposited in an area of strong currents with low sedimentation rates.

The correlation of the BOg penetration depth to the (geophysically visualised) moundbase reflector indicates that the lithified carbonates provided a colonisation surface for the coral and stabilised the mound flanks as it developed.

4.6: Dropstone analysis

During logging two conspicuous granitic dropstones were recovered, one from **CS06** and one from **CS07**. Hand specimens were described and thin sections prepared to identify the minerals present, document their textural relationships and to classify the rocks.

4.6.1: Dropstone 1 (Granodiorite Gneiss)

This dropstone was recovered from brown coloured muddy fine-sand in core **CS07** Section 1 at 56-72 cmdc (see Fig. 4.3.1). In **hand specimen** it is a mottled dark grey phaneritic igneous rock which measures 6.5cm by 6cm, with sub-rounded edges. One face has a very smooth

surface and a gneissic fabric can be observed (Fig. 4.6.1). Medium-grained interlocking crystals are evident (white and beige-yellow feldspars, clear/vitreous dull grey quartz) along with abundant black biotite and hornblende amphiboles, giving the dark appearance.

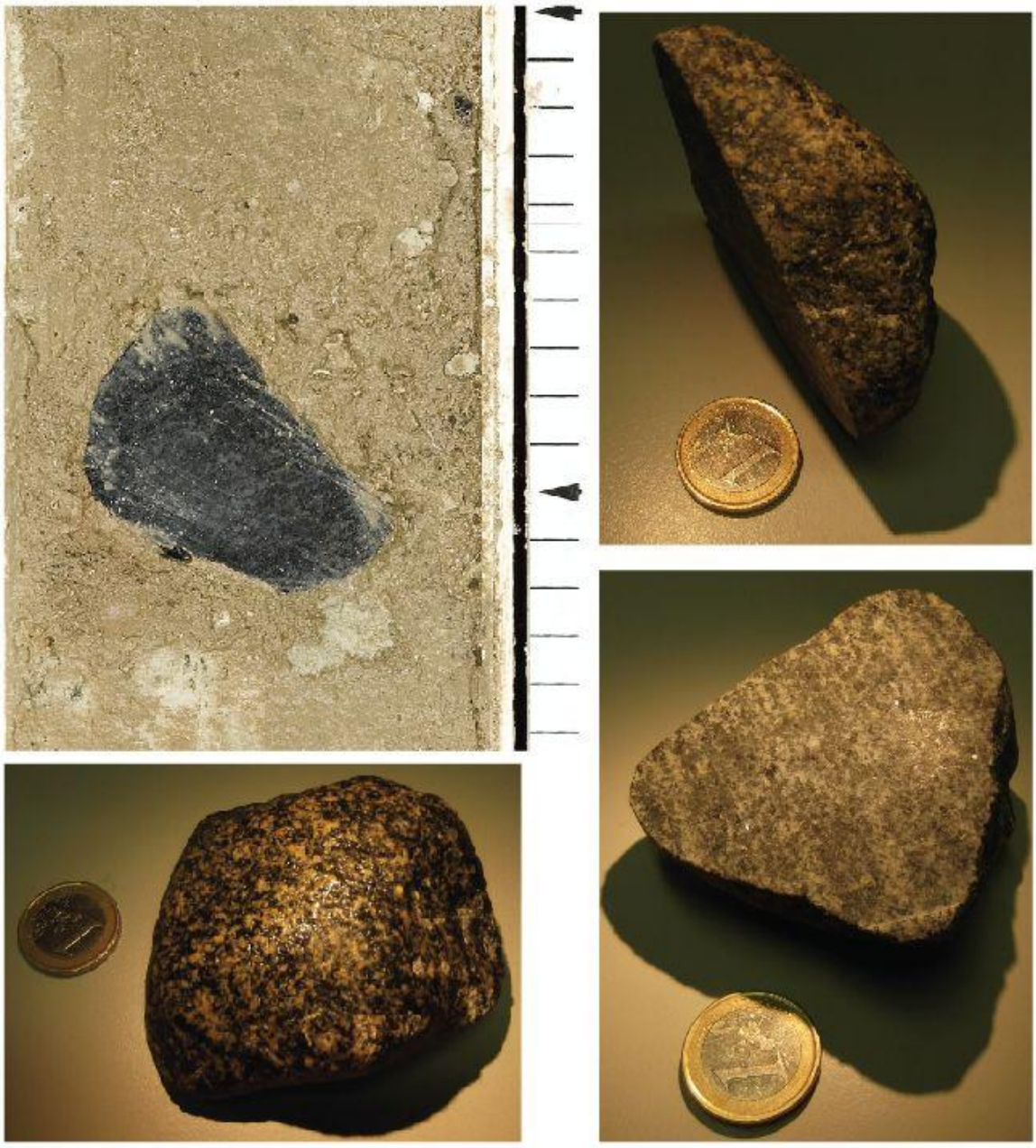

Fig. 4.6.1: Clockwise from left: Granodiorite gneiss as seen in-situ in core CS07; smooth surface of sample; aerial view of smooth face showing the gneissic fabric; smooth side facing down showing the sub-rounded nature of the rock.

In **thin section** (Figs. 4.6.2-4.6.6), feldspars (plagioclase and orthoclase) and quartz minerals make up more than 60% of the rock. Over 65% of the feldspar is plagioclase and approximately 40% is polysnthetically twinned. There is greater than 20 % Quartz.

Approximately 35% of the rock is made up of amphiboles. Other minerals include an appreciable amount of biotite and a very small amount of muscovite. A hypidiomorphic-granular texture is evident (Fig. 4.6.2)

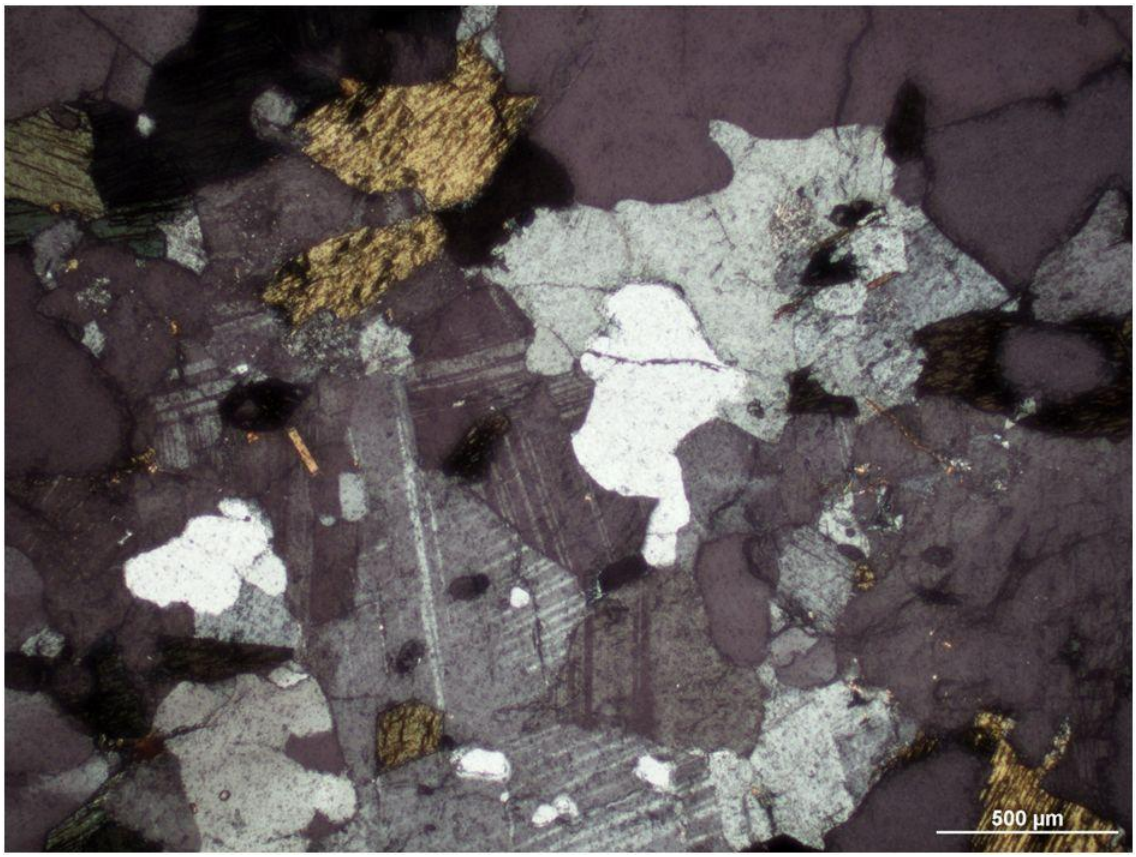

Fig. 4.6.2: Hypidiomorphic-granular texture in XPL. Euhedral and subhedral crystals of green and yellow amphiboles. Subhedral feldspar crystals with plagioclase displaying albite twinning. Clear and grey anhedral interstitial quartz. Smaller euhedral biotite crystals. Note the high percentage of plagioclase.

Quartz with diagnostic undulose extinction forms irregular shapes between the feldspars (Fig. 4.6.3) and provides evidence the rock has been strained. Biotite forms smaller euhedral crystals and is commonly found as composite crystals with the euhedral-subhedral hornblende (Fig. 4.6.5). The amphiboles are bluish green under PPL, but cross-polarization shows the two cuts have different XPL colours. The euhedral-subhedral amphibole crystals cut along the c-axis, show blueish-green to yellow-green pleochroism and are greenish-grey in XPL.

The basal cut amphiboles show blueish- green to straw yellow pleochroism and a strong yellow interference colour under XPL. There is also a small amount of muscovite with bright interference colours (Fig. 4.6.6).

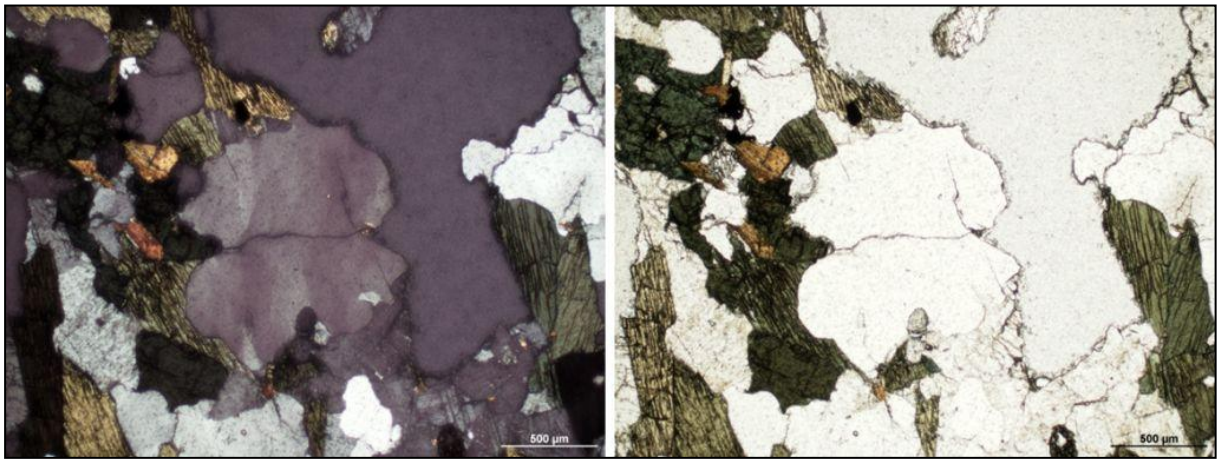

Fig. 4.6.3: Left: XPL; Right PPL. Anhedral quartz with undulose extinction. Euhedral & subhedral amphiboles (yellow and dark green in XPL; pale green and dark green in PPL). The two cleavage directions intersecting at 120 ° are clearly visible far right. Euhedral to subhedral biotite (yellowish brown – rusty red in XPL; brown in PPL). Large grey area in XPL is void due to thin-sectioning.

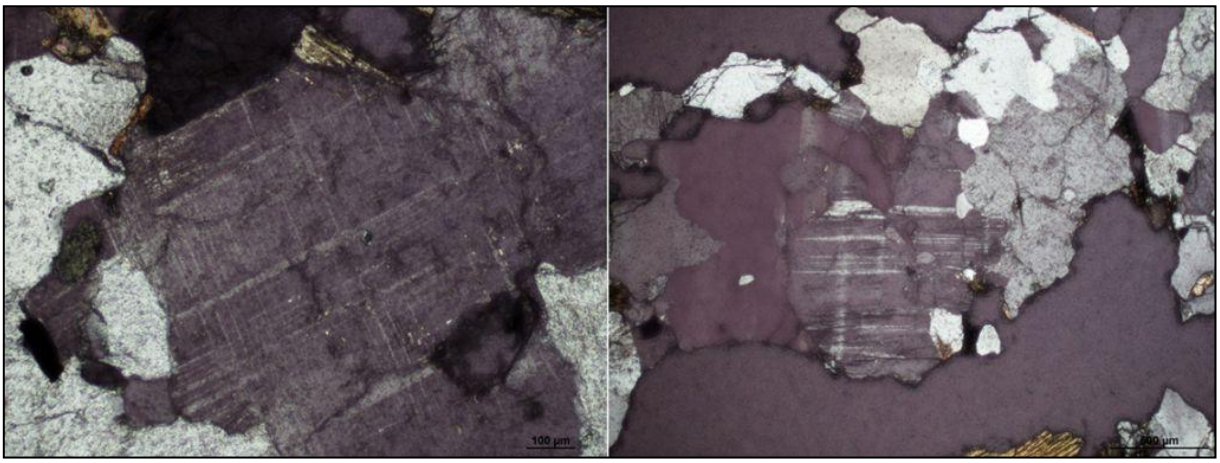

Fig. 4.6.4: Complex plagioclase twinning. XPL view.

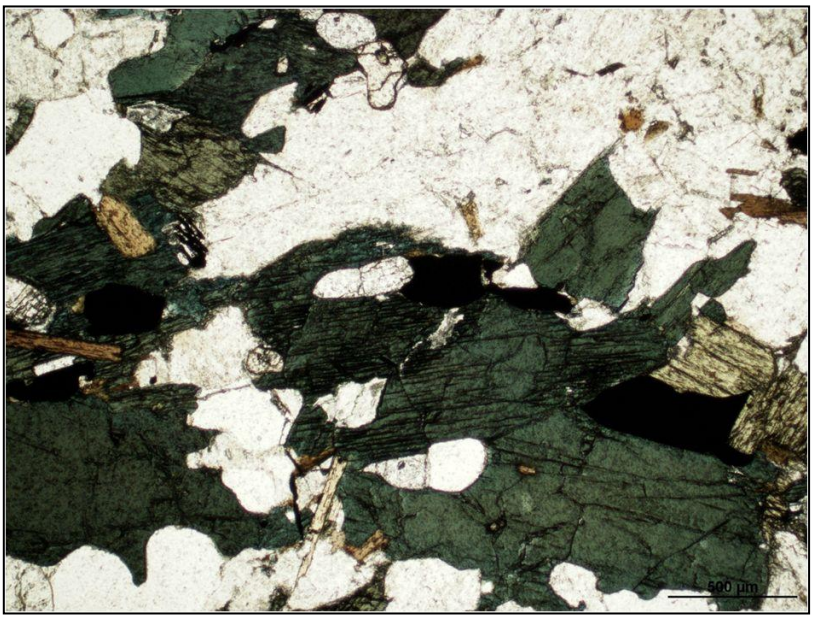

Fig. 4.6.5: Biotite (brown-light brown) is common in the sample; usually in association with hornblende (green) forming composite crystals. PPL view.

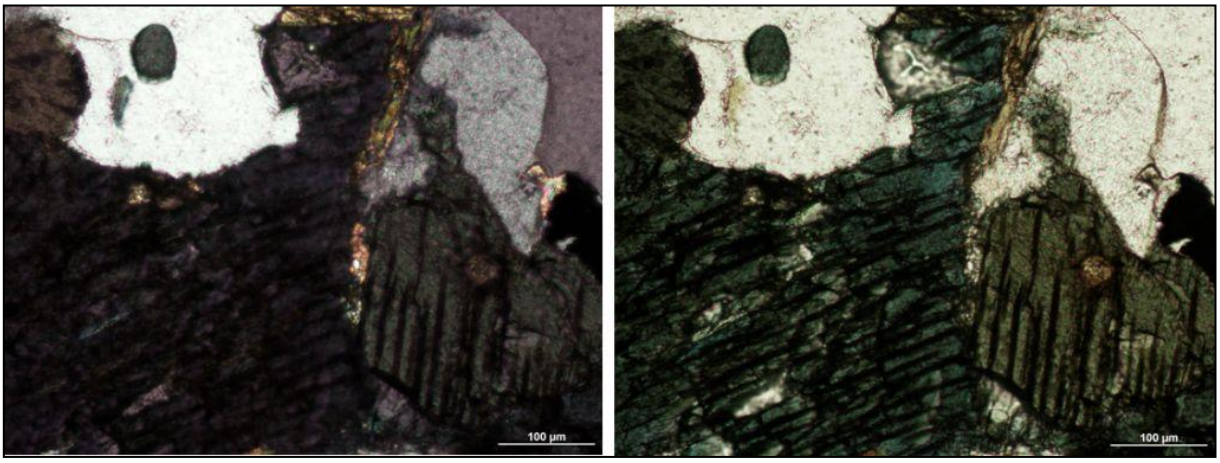

Fig. 4.6.6: Muscovite in between amphiboles; with bright interference colours in XPL (left) and colourless in PPL (right). Amphibole enclosed by interstitial quartz in top left.

In conclusion, most of Dropstone 1 is made up of feldspar, quartz and amphiboles with appreciable amount of biotite. The dominance of the plagioclase feldspar indicates a granodiorite and the fabric indicates a granodiorite gneiss, with the fabric (banding) a result of deformation. Possible provenances for this lithology include Connemara and Mayo (Belmullet) gneisses.

4.6.2: Dropstone 2 (Leucocratic granite)

This dropstone was recovered from beige, fine-grained, iron-stained, carbonate sands in core **CS06** Section 3, 235 - 239 cmdc (Fig. 4.6.7; see also Fig. 4.3.2).

Fig. 4.6.7: Dropstone recovered from core CS06 Section 3, 235 - 239 cmdc, as pictured in-situ in the core. Scale of 1cm interval to the right

In **hand sample**, Dropstone 2 was subrounded and measured 6 cm by 4 cm (Fig. 4.6.7). It was medium grained with a mottled yellowish pink colouration. The mottles are due to amalgamations of black crystals in the yellow-pink matrix. The crystals have a fabric of crystal alignment.

Thin section analysis (Figs. 4.6.8-4.6.11) reveals over 75% felsic minerals (quartz, alkali feldspar, plagioclase and also an appreciable amount of microcline) along with small amount of muscovite, biotite and some oxides. There is high quartz content (~30%) with stringers of quartz appearing as streams of anhedral grains (Fig. 4.6.9) and some strained quartz showing undulose extinction. Twinning was noted in plagioclase feldspars but it was not common (Fig. 4.6.10).

Dropstone 2 shows heavy alteration. The dark phenocrysts producing the porphyritic texture are amalgamations of highly altered green pleochroic biotites (some altered to chlorite) with epidote and sericite (Fig 4.6.11). Sericite is a common alteration mineral in areas that have been subjected to hydrothermal alteration.

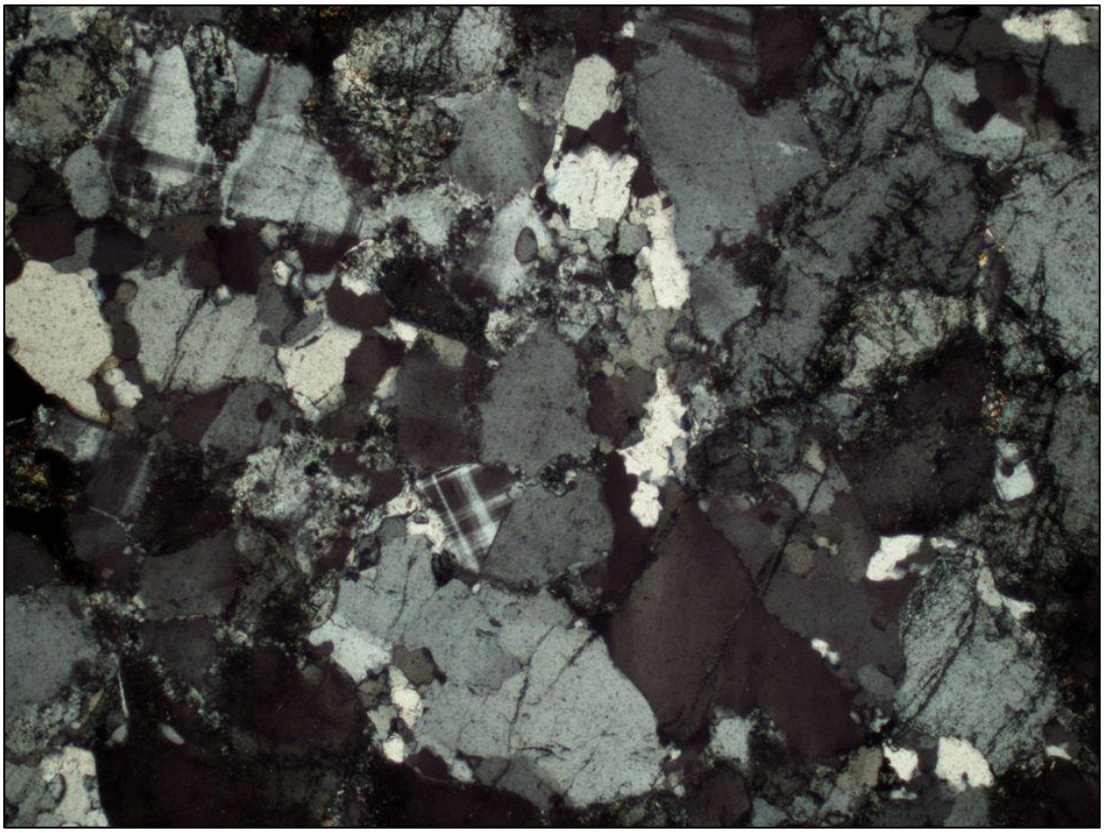

Fig. 4.6.8: General thin section (XPL) view of Dropstone 2. Microcline with cross-hatching evident, along with anhedral interstitial quartz

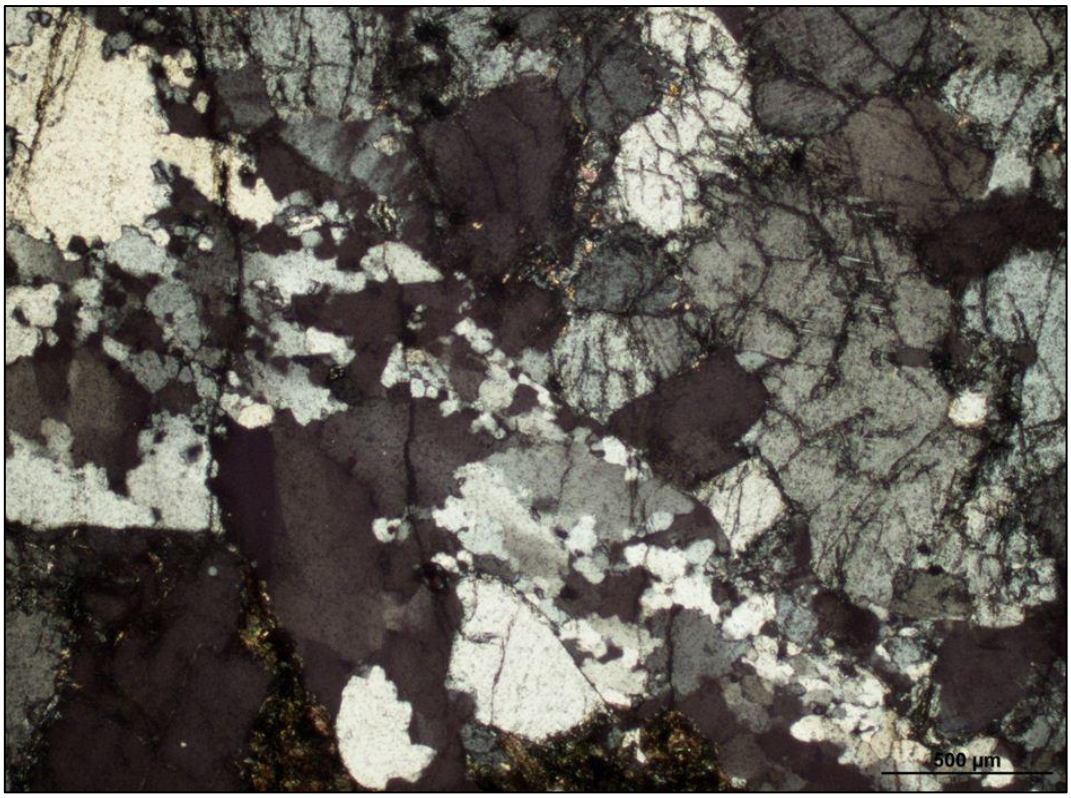

Fig 4.6.9: Dropstone 2 - smaller anhedral quartz alongside larger quartz grains.

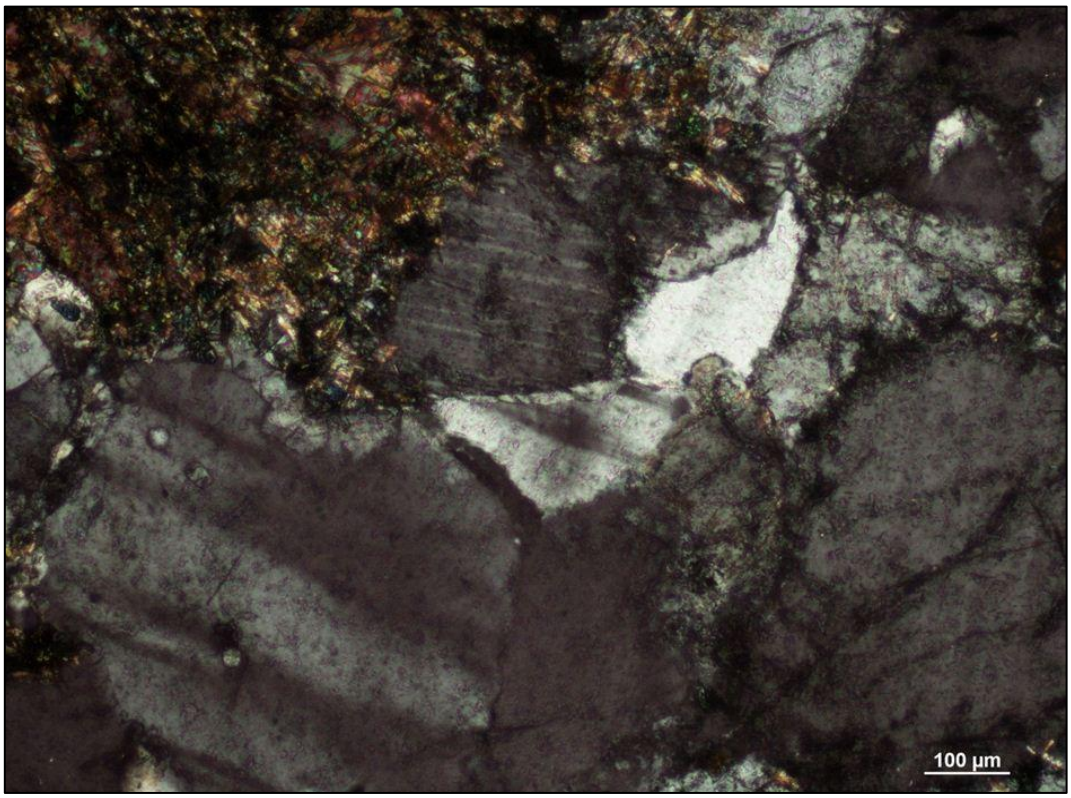

Fig. 4.6.10: Dropstone 2 - plagioclase feldspar with polysynthetic twinning.

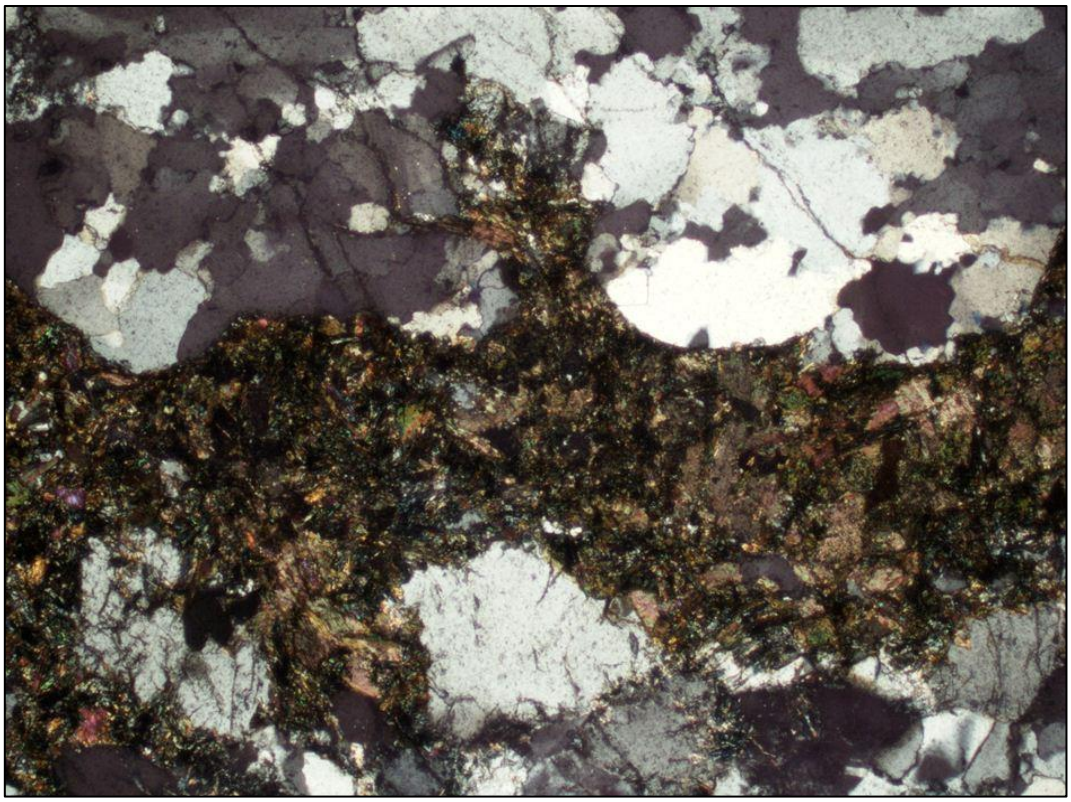

Fig 4.6.11 : Dropstone 2 - dark phenocrysts producing the porphyritic texture are amalgamations of highly altered green pleochroic biotites with epidote and sericite.

In summary, Dropstone 2 is a granite that appears to have undergone hydrothermal alteration. It is felsic rock as it has >75% felsic minerals and leucocratic as <30% minerals are mafic. Therefore its preliminary classification is that of leucocratic granite of indeterminate provenance.

4.7: Sediment composition

Sediment composition is described from the visual features noted during logging (Figs. 4.3.1-2) and characteristics of the faunal content during preliminary investigation under a microscope.

Both cores **CS06** and **CS07** are predominantly composed of (fairly cohesive) carbonate sediment due to a negligible flux of terrigenous sediment in the region (Øvrebø, 2005).

- In core **CS06** the carbonate sand-size material is predominantly composed of planktonic and benthic foraminifera.
- In contrast, in core **CS07**, Section 1, the carbonate sand-size material is predominantly made up of coral fragments, shells, calcite cement rubble and foraminifera.

The pelagic foraminifera are predominantly globigerinids with some samples containing many *Orbulina universa* and the deeper-water species *Globorotalia truncatulinoides* is also common. Preliminary investigation shows the benthic compositions are dominated by variations in assemblages of *Discanomalina coronata*, *Cibicides* sp., *Pyrgo* sp., *Uvigerina* sp., *Textularia* sp, and *Quinqueloculina* sp.

Other (macro and micro) fossils present in both cores include brachiopod shells, gastropods, echinoid spines, ostracods, sponge spicules and serpulids. The non-carbonate component of the sand in the cores is dominantly quartz with lithic fragments and glauconite. Glauconite present is presumed to be authigenically formed as casts within the chambers of foraminifera tests. The lithics comprise of a mixture of:

- Sedimentary (red sandstone and dark grey limestone)
- Metamorphic (schist) *and*
- Igneous (granite and diorite) rocks.

North Atlantic sediments enriched in coarse (>150 µm) lithic particles are generally regarded as ice-rafted debris (Thierens *et al.*, 2010). The lithics in the cores are interpreted to have been derived from west Ireland by ice-rafting during the Pleistocene. Neither core contained lithified horizons.

4.7.1: Sedimentological synthesis of CS07

Sediment core **CS07**, extracted from the mound, is mainly comprised of hemipelagic deposits of bioturbated structureless muds and sands with gradational to sharp contacts (Fig. 4.3.1). ROV video showed surface sediments near the top of the mound consisting principally of:

- Live corals
- Sediment-clogged dead coral framework
- Coral rubble *and*
- Other skeletal remains of various organisms.

Section 1 (Unit 1) consists of framework-building corals embedded in an unlithified sandy carbonate matrix. The sands suggest a strong current regime presently resides in this region.

Microscopic analysis showed the >500 µm fraction at the very top of the core (0 cmdc) to be characterized by sponge spicules and rich in foraminifera. Sponge and coral fragments, whole and broken bivalve mollusc shells and echinoderm spines provide a suitable habitat for the epifaunal *Textularia sagittula* foraminifera found in the >500 µm fraction. *Spirllina vivipara,* an epifaunal foraminifera that clings to hard substrates which Morigi *et al.* (2011) listed as a dominant species in CWC sediments, was also noted in this fraction.

Units 2 and 3 of Section 1 possibly represent glacial deposits as evidenced by the presence of IRD:

- Dropstone 1 is large and conspicuous and present at 56-72 cmdc *and*
- The >500 µm fraction of Unit 3 (65 cmdc) has a much higher lithic content than Unit 1. This particular fraction has a very high calcareous content but (in contrast to Unit 1) there is a low contribution by foraminifera with the calcareous grains comprising mainly of shell fragments and serpulid worms. Most notably there are no planktonic foraminifera at this level and the presence of *Orbulina* in the >250 µm fraction shows that this planktonic foraminiferan was settling at this period, but not growing to larger sizes. Bé *et al.* (1973) found the maximum diameter of the test in *Orbulina* increases towards the tropics i.e. directly with water temperature, thus reflecting the colder conditions.

Unit 3 of Section 1 (55.5-85 cmdc) consisted of brown muddy fine sand with large bright grey irregularly shaped ?nodules. The upper nodules showed moderate lithification of silty clay Sampling of these structures and subsequent sieving showed them to be composed of bright

grey subrounded granule and pebble grade elements (Fig. 4.7.1) with a white streak. This material *may* be calcite-cemented biogenic 'rubble' due to dissolution of coral debris and recycling of the dissolved carbon with precipitation as interstitial micrite (Mazzini *et al.*, 2012). Below Dropstone 1, the grey nodules are made up of soft (i.e. non-lithified) clay and the lowest in the unit have a soft silt-fine sand composition (Fig. 4.7.2). These may be unlithified representatives of the aforementioned features (described above) or, alternatively, possible burrow structures.

Fig. 4.7.1: Left: Lithified irregularly shaped ?nodules found in Section 1 in CS07 between 55 and 65 cmdc. Right: sieved fraction >500 µm, interpreted as calcite cemented biogenic rubble.

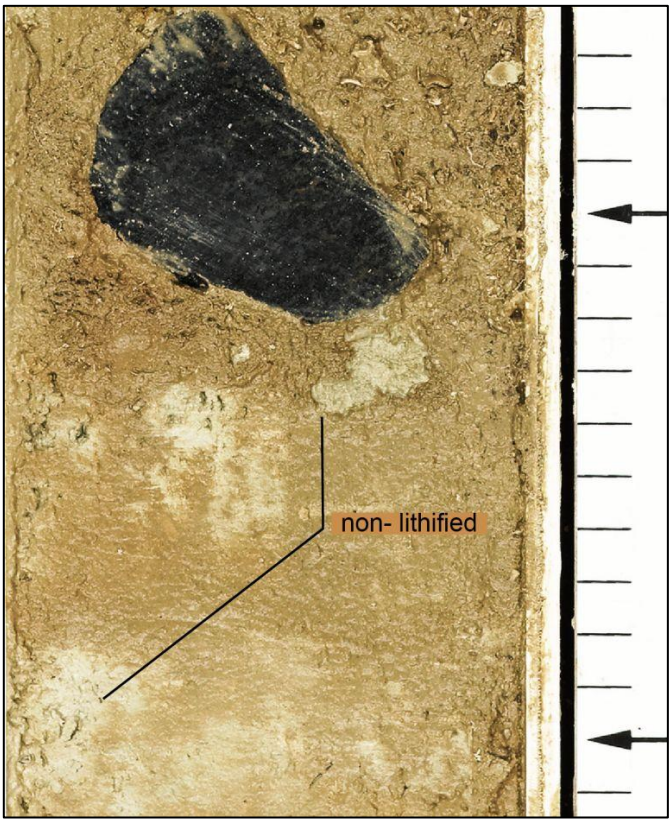

Fig.4.7.2: Irregularly shaped non-lithified bright grey nodules; upper nodules with clayey infill and lower with silt-fine sand.

The end of Section 1 along with most of Section 2 in **CS07** features homogeneous, bright grey muddy sands. The presence of *Gaudryina rudis* in the >500µm fraction at 90 cmdc in Unit 3 of Section 1 indicates that the environment was warm temperate. This suggests the sediments were *possibly* deposited during MIS 3 [60ka]. Like the surficial sediment at the very top of the core, coral branches, shell fragments and echinoderm spines provided a suitable habitat for *Textularia sagittula* foraminifera found in the sediment at this 90 level.

NOTE: Sections 2-7 of CS07 have yet to be sampled in detail. Therefore the following interpretations are based on visual results only. It is believed that further sampling will show pelagic oozes admixed with coral-fragments throughout the core.

The progressive darkening of the sediment in Section 2 through to the brownish grey sands of Section 3 (Fig. 4.3.1) coincides with better preservation of coral material and has been tentatively interpreted as indicative of glacial deposition. In Section 2 there is a change from light grey sands to olive grey silts and clays until a gradual coarsening to sands again 238.5 cmdc in Section 3, indicating corresponding changes in the energy regime (locally enhanced bottom currents).

At Unit 10 in Section 3 there is a sharp transition from the brownish grey sands to bright grey sands and the coral debris becomes conspicuously sparse which are interpreted as interglacial in nature. These deposits are sharply terminated (downsection) in Section 4 by a higher-energy unit with erosive upper and lower contacts (Fig. 4.7.3). The upper contact is irregular in outline and consists of a 3 cm thick layer of large coral fragments (granule-scale branches).

Fig. 4.7.4: Coarser unit in Section 4 showing erosive upper and lower boundaries; with an upper contact consisting of a 3cm thick layer of large coral fragments (granule-scale branches) that pinches to the left. Each line represents a cm in scale to right.

Below the coral boundary is an admixture of medium brown silty fine sand with coarse coral hash of 1-4 mm granules. Due to increased porosity at this level - there is a very high water content and the sediment is less cohesive.

Bright white silty sands continue following the coarser unit and reverse grade downcore to bright white carbonate muds indicating a lower energy regime. The darker coral-rich muddy sediments in Section 5 are interpreted as (potentially) interglacial and the conspicuous bright grey mottling in Section 6 is *possibly* due to bioturbation.

These muds lie directly and sharply above a very coarse higher-energy unit (Fig. 4.7.5) which is normally graded and contains:

- Partially lithified biogenic rubble
- Mud clasts,
- Large coral branches,
- Gastropod and barnacle shells.

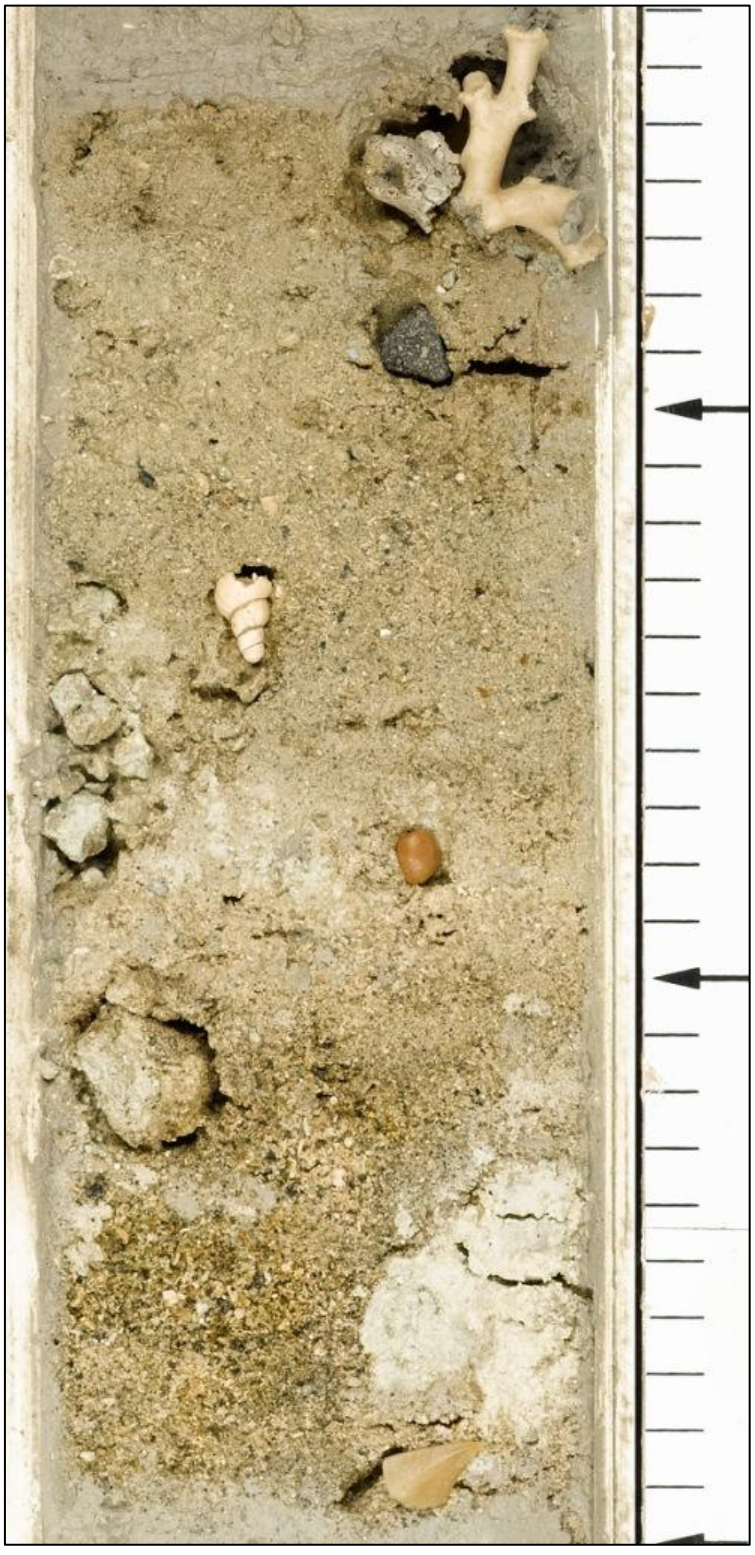

Fig.4.7.5: Coarse unit in Section 6 containing partially lithified possible biogenic rubble (middle left) and mud clasts (bright white in lower right) as well as branch size coral (a well preserved coral branch beside a heavily dissolved branch in upper right), a gastropod, and a mollusc shell (beneath mud clast) and pebbles.

The top 3.5 cm of this higher-energy unit is muddier; however, the mud in question may actually be clast which was ripped up and reworked. Like the higher-energy unit of Section 4 (above) there are coral branches concentrated at the upper boundary.

Shell material from this higher-energy unit in Section 6 in **CS07** (Fig. 4.7.5) has been examined by Patrick Collins, Marine Biologist of the Ryan Institute in NUIG:

- The **gastropod** has so far been identified as a *Troschelia ?berniciensis*. This predatory and scavenging omnivore has a wide range throughout the north-eastern Atlantic from 56°01'N, 32°42'W to north-west Norway and southwards to 25°N at depths of 90-2700 m (Bouchet and Warén, 1985). The creamy pink shell is 10×16 mm, comprises of swollen whorls and has a moderately high spire with a blunt tip. There are growth lines and spiral ridges. The aperture of the specimen is partially fragmented.
- The **barnacle** shell has so far been identified as a plate of *Scalpellum ?stroemi*. This suspension feeder belongs to a group known as acorn barnacles, which lack a peduncle and have the capitulum cemented directly to the substratum.

Olive grey sands (possibly glacial in nature and similar to those deposited in Section 2) lie beneath this higher-energy unit and grade (downwards) to olive grey muds. These muds are sharply terminated (at their base) in Section 7 by a conspicuously clean white sand deposit that, like the sands in Section 4, are interpreted as possibly representing warmer climatic conditions.

In conclusion, the predominantly grey and white sediments of **CS07** indicate a carbonate-rich depositional environment. During logging coral debris was noted as present throughout the entire 625.5 cm of the core (Fig. 4.3.1). The corals, mainly *Lophelia pertusa* and less frequently *Madrepora oculata*, occur as granule-sized fragments of branches. Rapid growth and breakdown of cold-water corals living in a very favourable environment may be the cause of the large amount of carbonate mud (Kenyon *et al.*, 2003).

The deposits from the base of Section 1 (Unit 4) downwards to Section 7 are primarily composed of bioturbated, poorly sorted, grey foraminiferal muddy sands and muds with thin, laterally discontinuous horizons, bands and pockets of bio-eroded coral. These deposits are interrupted by two conspicuously coarser units. Sandy facies dominate the upper and end parts of the core with silt and clay dominating 200 cm in the lower sections.

The growth and development of the coral mound consists of darker and lighter layers that may prove to be a response to environmental conditions, possibly glacial/interglacial intervals. Thus the darker deposits found at the bottom of Section 2 and throughout Section 3, Section 5 and 6 possibly represent colder periods. The coral appear to be better preserved in the darker sediments and more heavily dissolved in the lighter layers. The dissolution of the coral in lighter layers may be related to microbial sulphate reduction (Ferdelman *et al.*, 2006).

4.7.2: Sedimentological synthesis of CS06

Despite its relatively short length, the log of core **CS06** reveals a complex sedimentological history (Fig 4.3.2). It is probably that it records a fairly large amount of time (there *may* be a record of the last glacial and an interglacial stage (MIS 5) in section 3), due to a low sedimentation rate. Perhaps as much as 100,000 years may be represented in only 3m of the core.

Ice rafted debris [IRD] is observed at 13 cmdc in **CS06**. The >500 µm fraction at 20 cmdc was also found to have a high proportion of lithic fragments. There is an abrupt lithological change (downcore) from brown muddy sands to a stippled facies (StF) characterised by dark orange bioturbated stippled silty muds alternating with moderately sorted, bioturbated beige sands. The red coloration of the sediment indicates a well-oxygenated region with iron-rich minerals. The stipples are (very tentatively) interpreted as mm-scale burrows; they are beige and contain a coarser fill (from fine to coarse sand) than the surrounding orange mud matrix (Fig. 4.7.6).

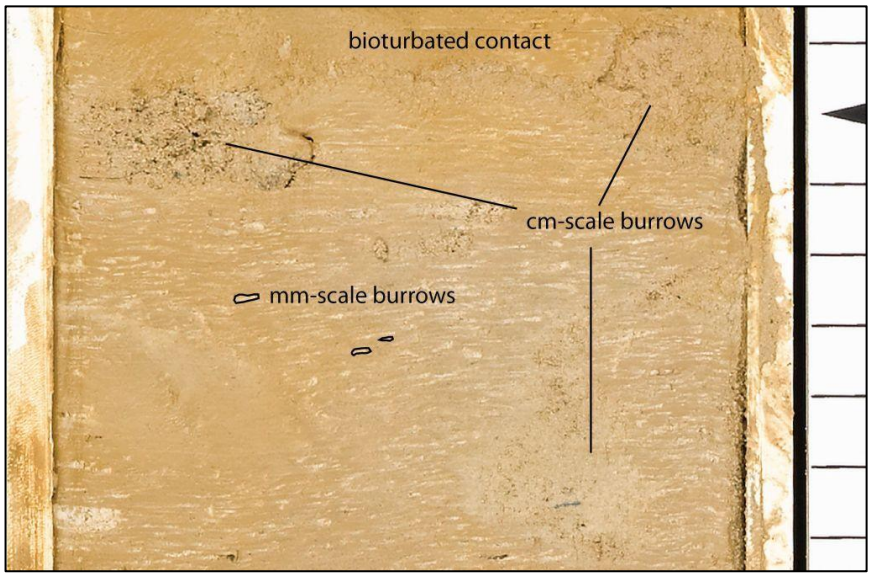

Figure 4.7.6: Photograph of stippled mud in core CS06. The stipples are interpreted as possible mm-scale burrows; they are beige and contain a coarser fill (from fine to coarse sand) than the surrounding orange mud matrix (three examples are outlined). The stippled facies is also characterised by cm-scale burrows and bioturbated contacts.

Syn-sedimentary structures in **CS06** are represented by normal and reverse graded-bedding. Erosive basal contacts and reactivation surfaces are common. Biogenic structures are very frequent, with the vertical burrows (of presumed crustacean origin) particularly conspicuous.

The StF also includes terebratulid brachiopods on at least two horizons (Fig. 4.3.2). The shells of these pedunculate brachiopods are quite thin and delicate and many are still intact and articulated. Coupled with the very fine-grained composition of the enclosing sediments, this indicates that these bioclasts represent an autochthonous colonisation surface.

The red poorly-sorted bioturbated sandy muds of the StF are tentatively interpreted as muddy contourites deposited by weak currents; the alternating sandier units of the StF are interpreted as the result of stronger currents winnowing and removing the fines to produce lags, now preserved as sandy contourite sequences. The silty mud facies have been interpreted (herein) to represent deposits during a colder period, perhaps glacial. This is corroborated by the conspicuous lack of *Orbulina universa* in the >500 µm fraction of the stippled mud deposit at 125 cmdc.

The StF sits stratigraphically above the 11 cm thick unit of light grey foraminiferal sand in Section 2 (at 153 cmdc). The contact between the two is very sharp. This light sand is tentatively interpreted as representing a Heinrich event and the >250 µm fraction of the unit is comprised mainly of planktonic foraminifera (90.5:1 planktonic: benthic ratio) with a very high lithic component and conspicuous low level of shell fragments, echinoderm spines and ostracods.

The StF reappears downcore from 186 cmdc in Section 2 to 212.5 cmdc in Section 3, where there is a sharp change in lithology from the StF silty mud sediments to poorly sorted reddish fine to medium sand with dispersed black granules. These sands are interpreted as glacial due to the presence of IRD with the large granitic Dropstone 2 found between 235.5-239 cmdc. These reddish sands quickly transition downwards into bright white fine to medium sands at 263 cmdc. These sands (thus far) interpreted as potentially representing warmer conditions. This contention was supported by the discovery of a noticeable abundance of large globigerinids in the > 500 µm fraction at 270 cmdc.

Discanomalina coronata is present throughout the > 500 µm fraction of core **CS06** (apart from in the possible interglacial unit at 175 cmdc). Margreth *et al.* (2009) proposed *D. coronata* as an indicator species to identify mounds and/or living coral ecosystems. It could be argued that its prevailing presence is due to the proximity to the surrounding mounds.

The muddy sediments of **CS06** contain thin-shelled *Dentalina* forms. The small pore spaces of muddy substrates are often rich in organic debris and allow bacterial blooms, explaining why such sediments often support large populations of thin-shelled, delicate and elongate foraminifera (Armstrong and Brasier, 2005).

Chapter 5: Summary

5.1: Discussion

Multibeam data has shown the study area in the Porcupine Bank to be characterised by elongated mounded complexes over 50 m high and over 100 m in length in water depths of between 630–850 m. The mounds thus occur in a depth range close to the permanent thermocline where enhanced seabed dynamics are likely to occur.

The high resolution of the ROV bathymetric map imaged 17 mounds/mound complexes in great detail (Fig. 3.1.18-26) along an ~18 km transect. The shipborne multibeam imaged >40 mounds in lower resolution in an area approximately 110 km^2.

The CHIRP data showed the mounds to have a different geophysical structure to the surrounding (adjacent) sediment, indicating a different composition. This was verified by the two recovered sediment cores, showing the depositional regime to differ greatly between two areas that are located ~750 m apart. The mound unit (**CS07**) is distinct from the lateral sediments in terms of its of its varying quantities of coral fragments embedded in unlithified, grey calcareous sediments, as opposed to the predominantly red calcareous muds of the off-mound sediment (**CS06**).

Both cores contained hemipelagic deposits comprised of foraminifera, invertebrate skeletons and varying amounts contributed by siliciclastics, with the faunal assemblages differing between the cores. Most of the sediments from the on-mound core correlate very well to the buried facies predicted by Scoffin and Bowes (1988):

''On burial this facies would eventually consolidate to form bioturbated, poorly sorted, foraminiferal sandstones and greensands, with thin, laterally discontinuous horizons of bioeroded coral branches''.

The location of the Arc Mounds invokes a strong interaction of topography with local current dynamics. Coral mound development in this area seems to be related to the local topographic features, as most of the mounds are north-south elongated in shape, parallel to seafloor scarps. However, the N-S water current direction indicates that the coral mound morphology is influenced by the local current regime as well as the surrounding seabed morphology. The mounds therefore probably exhibit both inherited and developed morphologies and division of cold-water coral mounds into these discrete categories does not accurately represent the nature of cold-water coral mound growth.

The moderately lithified basal calcareous conglomerate hard-ground recovered from the off-mound core (**CS06**) can be confidently correlated to a mound base reflector shown in the chirp data indicating the mounds developed above an erosional surface. Cold water corals have been documented thriving under scarps (De Mol *et al.*, 2011) where they are protected from sand-scour. It is postulated that initiation of the mound growth occurred by colonisation of the scarps, and that this was followed by accumulation of coral debris and sediment to allow vertical development. If the cored rock represents the scarps documented at the surface then it is believed to be Quaternary in age. This suggests a younger colonisation surface than the *Challenger* Miocene moundbase where the first settlement of cold-water coral larvae is thought to result from the (re)introduction of the MOW into the Porcupine Seabight (Raddatz *et al.*, 2011).

5.2: Conclusions

- The multidisciplinary approach taken in this study combined aspects of marine sedimentology, geophysical remote sensing, and GIS for the holistic study of the Arc Mounds cold-water coral environment and its governing (geological and oceanographical) processes. The mound structures are interpreted as coral carbonate mounds, based on their biological, sedimentological and surficial seismic characteristics.
- The sediment cores recovered and logged provide information on depositional history and environmental change. The analysis of the lithofacies indicates a discontinuous depositional regime, characterized by long periods of medium and low energy, with intervening high-energy events. Thus deposition at the Arc Mounds appears to be influenced by bottom currents, ice rafting, and slope instability.
- Only core **CS07** (extracted from the mound) contained coral. This observation supports the hypothesis that corals are intrinsic in the generation of these deep water bioherms found in the NE Atlantic.
- The correlation of the base cutter sediment (Bas Ogive) penetration depth to the moundbase reflector in the CHIRP data indicates that lithified carbonates provided an initial colonisation surface for the coral and stabilised the mound flanks as it developed. This erosive surface may be Quaternary, if it is a buried representative of

the scarps currently revealed at the surface. However, it could also be of an older origin, if it correlates to the Miocene Challenger moundbase deposits.

- The initial genesis of the mound may be related to hydrocarbon seeps if the base cutter sediment proves to contain authigenic methanic cement and the relationship between the mounds and the horst and graben structures has to be investigated. However it is most likely that the development of the mound was controlled by oceanic circulation and associated dynamics in nutrient supply.
- The grain size analyses agree satisfactorily to the visually logged cores. As the Laser-based grain size analysis is based on a very small sample, the secondary grainsize analysis achieved by wet sieving better represented the core units because it involves a larger sample size. The magnetic susceptibility measurements were particularly accurate at indicating IRD-rich units. Preliminary investigation of the foraminiferal content yielded information on key depositional units.
- Hillshaded multibeam data best imaged the scarp features, but sidescan data augmented the multibeam by proving the irregular linear features were not a source of noise.

5.3: Recommendations

- The deep-sea sediment dynamics could be further investigated. Current meter measurements could be taken in order to combine this information along with seabed samples, cores and bedform morphologies; so as to determine current strengths, directions and periodicities at the seabed. This would aid in qualifying the currents' influence on the resulting sedimentary deposits, and in relation to the benthic habitat.
- It remains to be tested whether the where the base of the mound is correlated to the acoustic reflector that corresponds to the hardground retrieved from core **CS06**; as the on-mound core (**CS07**) only penetrates 6.26 m. Ideally the entire mound would be cored.
- Investigation into nepheloid layers as the possible food source for these deep-water suspension feeders.

5.4: Future Work

Sampled coral branches and fragments have been sent for dating to the CNRS laboratory, Gif Sur Yvette in France. It is postulated that U-series dating will show corals of Holocene age developed on an ancient reef surface. Based on the relationship of coral ages and depth in the core we will be able to estimate Vertical Mound Growth Rates (VMGRs).

The taxonomic approach of foraminiferal analysis throughout the core will provide the most detailed interpretation as this will infer the palaeoenvironments based on the known environmental preferences of modern species or genera. It will be investigated, for example, whether the cold-water coral ecosystem from core **CS07** offers a better ecological niche for the benthic foraminifera, in comparison to the adjacent sediments from core **CS06**.

The fossils found in the Bas Ogive will be analysed for fossils indicative of Paleogene and mid-Pleistocene age. Cathodoluminescence and fluorescence measurements will be undertaken in order to investigate a microbial component of the cement of this hard basal horizon. Iron oxides are often associated with hydrothermal sources and this will be investigated further.

References

ARMSTRONG, H. & BRASIER, M. 2005. *Microfossils*, Wiley.

BÉ, A. W. H., HARRISON, S. M. & LOTT, L. 1973. Orbulina universa d'Orbigny in the Indian Ocean. *Micropaleontology*, 151-192.

BOUCHET, P. & WARÉN, A. 1985. Revision of the northeast Atlantic bathyal and abyssal Neogastropoda excluding Turridae (Mollusca, Gastropoda). *Boll Malacol Suppl* 1, 296.

CARSON, G. & CROWLEY, S. 1993. The glauconite-phosphate association in hardgrounds: examples from the Cenomanian of Devon, southwest England. *Cretaceous research,* 14, 69-89.

CONNELL, J. 1997. Disturbance and recovery of coral assemblages. *Coral reefs,* 16, 101-113.

DALY, J. S., TYRRELL, S., BADENSZKI, E., HAUGHTON, P. D. W., SHANNON, P. M. & WHITEHOUSE, M. 2008. Mesoproterozoic orthogneiss from the north Porcupine High, offshore western Ireland. Abstract. *51st Irish Geological Research Meeting.* University College Dublin.

DE MOL, B., VAN RENSBERGEN, P., PILLEN, S., VAN HERREWEGHE, K., VAN ROOIJ, D., MCDONNELL, A., HUVENNE, V., IVANOV, M., SWENNEN, R. & HENRIET, J. 2002. Large deep-water coral banks in the Porcupine Basin, southwest of Ireland. *Marine Geology,* 188, 193-231.

DE MOL, L., VAN ROOIJ, D., PIRLET, H., GREINERT, J., FRANK, N., QUEMMERAIS, F. & HENRIET, J.-P. 2011. Cold-water coral habitats in the Penmarc'h and Guilvinec Canyons (Bay of Biscay): Deep-water versus shallow-water settings. *Marine Geology,* 282, 40-52.

DICKSON, R. R. & MCCAVE, I. N. 1986. Nepheloid layers on the continental slope west of Porcupine Bank. *Deep Sea Research Part A. Oceanographic Research Papers,* 33, 791-818.

DORSCHEL, B., HEBBELN, D., RÜGGEBERG, A., DULLO, W. C. & FREIWALD, A. 2005. Growth and erosion of a cold-water coral covered carbonate mound in the Northeast Atlantic during the Late Pleistocene and Holocene. *Earth and Planetary Science Letters,* 233, 33-44.

DORSCHEL, B., WHEELER, A. J., MONTEYS, X. & VERBRUGGEN, K. 2010. *Atlas of the deep-water seabed: Ireland*, Springer.

FAUGÈRES, J. C., ZARAGOSI, S., MÉZERAIS, M. & MASSÉ, L. 2002. The Vema contourite fan in the South Brazilian basin. *Geological Society, London, Memoirs,* 22, 209-222.

FERDELMAN, T., KANO, A., WILLIAMS, T. & HENRIET, J. 2006. the IODP Expedition 307 Scientists. *IODP expedition,* 307, 11-16.

FLEMMING, B. 2000. A revised textural classification of gravel-free muddy sediments on the basis of ternary diagrams. *Continental Shelf Research,* 20, 1125-1137.

FOLK, R. L. 1954. The distinction between grain size and mineral composition in sedimentary-rock nomenclature. *The Journal of Geology*, 344-359.

FRANK, N., RICARD, E., LUTRINGER-PAQUET, A., VAN DER LAND, C., COLIN, C., BLAMART, D., FOUBERT, A., VAN ROOIJ, D., HENRIET, J. P. & DE HAAS, H. 2009. The Holocene occurrence of cold water corals in the NE Atlantic: Implications for coral carbonate mound evolution. *Marine Geology,* 266, 129-142.

GUINOTTE, J. M., ORR, J., CAIRNS, S., FREIWALD, A., MORGAN, L. & GEORGE, R. 2006. Will human-induced changes in seawater chemistry alter the distribution of deep-sea scleractinian corals? *Frontiers in Ecology and the Environment,* 4, 141-146.

GYORY, J., MARIANO, A. J. & RYAN, E. H. 2003. *"The Slope/Shelf Edge Current." Ocean Surface Currents* [Online]. Available: http://oceancurrents.rsmas.miami.edu/atlantic/slope.html 2013].

HACKETT, B. & PETTER RØED, L. 1998. A numerical study of the slope current northwest of the British Isles. *Continental Shelf Research,* 18, 1-30.

HALL-SPENCER, J., ALLAIN, V. & FOSSÅ, J. H. 2002. Trawling damage to Northeast Atlantic ancient coral reefs. *Proceedings of the Royal Society of London. Series B: Biological Sciences,* 269, 507-511.

KENYON, N. H., AKHMETZHANOV, A. M., WHEELER, A. J., VAN WEERING, T. C. E., DE HAAS, H. & IVANOV, M. K. 2003. Giant carbonate mud mounds in the southern Rockall Trough. *Marine Geology,* 195**,** 5-30.

KLAGES, M., THIEDE, J. & FOUCHER, J. 2004. Reports on Polar and Marine Research. *The Expedition ARKTS XIX/3 of the Research Vessel Polarstern in 2003; Reports of Legs 3a, 3b and 3c.* Germany: Alfred Wegener Institute for Polar and Marine Research.

MARGRETH, S., RÜGGEBERG, A. & SPEZZAFERRI, S. 2009. Benthic foraminifera as bioindicator for cold-water coral reef ecosystems along the Irish margin. *Deep Sea Research Part I: Oceanographic Research Papers,* 56**,** 2216-2234.

MASSON, D., DOBSON, M., AUZENDE, J. M., COUSIN, M., COUTELLE, A., ROLET, J. & VAILLANT, P. 1989. Geology of Porcupine Bank and Goban Spur, Northeastern Atlantic—Preliminary results of the Cyaporc submersible cruise. *Marine Geology,* 87**,** 105-119.

MAZZINI, A., AKHMETZHANOV, A., MONTEYS, X. & IVANOV, M. 2012. The Porcupine Bank Canyon coral mounds: oceanographic and topographic steering of deep-water carbonate mound development and associated phosphatic deposition. *Geo-Marine Letters***,** 1-21.

MORIGI, C., SABBATINI, A., VITALE, G., PANCOTTI, I., GOODAY, A., DUINEVELD, G., DE STIGTER, H., DANOVARO, R. & NEGRI, A. 2011. Foraminiferal biodiversity associated with cold-water coral carbonate mounds and open slope of SE Rockall Bank (Irish continental margin-NE Atlantic). *Deep Sea Research Part I: Oceanographic Research Papers*.

NAYLOR, D. & MOUNTENEY, S. N. 1975. *Geology of the North-West European continental shelf. 1.,* London, Graham Trotman Dudley Publ, , .

NEW, A. & SMYTHE-WRIGHT, D. 2001. Aspects of the circulation in the Rockall Trough. *Continental Shelf Research,* 21**,** 777-810.

NOÉ, S., TITSCHACK, J., FREIWALD, A. & DULLO, W.-C. 2006. From sediment to rock: diagenetic processes of hardground formation in deep-water carbonate mounds of the NE Atlantic. *Facies,* 52**,** 183-208.

ORR, J. C., FABRY, V. J., AUMONT, O., BOPP, L., DONEY, S. C., FEELY, R. A., GNANADESIKAN, A., GRUBER, N., ISHIDA, A. & JOOS, F. 2005. Anthropogenic ocean acidification over the twenty-first century and its impact on calcifying organisms. *Nature,* 437**,** 681-686.

ØVREBØ, L. K. 2005. *Spatial and temporal variations in sedimentary slope processes along the margins of the Rockall Trough, offshore West Ireland.* PhD, University College Dublin.

ØVREBØ, L. K., HAUGHTON, P. D. W. & SHANNON, P. M. 2006. A record of fluctuating bottom currents on the slopes west of the Porcupine Bank, offshore Ireland—implications for Late Quaternary climate forcing. *Marine Geology,* 225**,** 279-309.

POLLARD, R. T., GRIFFTTHS, M. J., CUNNINGHAM, S. A., READ, J. F., PÉREZ, F. F. & RÍOS, A. F. 1996. Vivaldi 1991 - A study of the formation, circulation and ventilation of Eastern North Atlantic Central Water. *Progress in Oceanography,* 37**,** 167-192.

RADDATZ, J., RÜGGEBERG, A., MARGRETH, S. & DULLO, W.-C. 2011. Paleoenvironmental reconstruction of Challenger Mound initiation in the Porcupine Seabight, NE Atlantic. *Marine Geology,* 282**,** 79-90.

ROTHWELL, R. G. 2006. *New techniques in sediment core analysis*, Geological Society Publishing House.

SCOFFIN, T. P. & BOWES, G. E. 1988. The facies distribution of carbonate sediments on Porcupine bank, northeast Atlantic. *Sedimentary Geology,* 60**,** 125-134.

SHANNON, P. M., CORCORAN, D. & HAUGHTON, P. 2001. The petroleum exploration of Ireland's offshore basins: introduction. *Geological Society, London, Special Publications,* 188**,** 1-8.

SMEULDERS, G. 2011. Cold-water coral habitats of Rockall and Porcupine Bank, NE Atlantic Ocean: sedimentary facies and benthic foraminiferal assemblages.

STETSON, T. R., SQUIRES, D. F. & PRATT, R. M. 1962. Coral banks occurring in deep water on the Blake Plateau. American Museum novitates; no. 2114.

TATE, M. & DOBSON, M. 1989. Late Permian to early Mesozoic rifting and sedimentation offshore NW Ireland. *Marine and Petroleum Geology,* 6**,** 49-59.

THIERENS, M., TITSCHACK, J., DORSCHEL, B., HUVENNE, V. A. I., WHEELER, A. J., STUUT, J. B. & O'DONNELL, R. 2010. The 2.6 Ma depositional sequence from the Challenger cold-water coral carbonate mound (IODP Exp. 307): Sediment contributors and hydrodynamic palaeo-environments. *Marine Geology,* 271**,** 260-277.

TITSCHACK, J., THIERENS, M., DORSCHEL, B., SCHULBERT, C., FREIWALD, A., KANO, A., TAKASHIMA, C., KAWAGOE, N. & LI, X. 2009. Carbonate budget of a cold-water coral mound (Challenger Mound, IODP Exp. 307). *Marine Geology,* 259**,** 36-46.

VAN DER LAND, C. 2011. *Impact of diagenesis on carbonate mound formation.* Royal Netherlands Institute for Sea Research (NIOZ).

VAN ROOIJ, D., BLAMART, D., KOZACHENKO, M. & HENRIET, J. P. 2007a. Small mounded contourite drifts associated with deep-water coral banks, Porcupine Seabight, NE Atlantic Ocean. *Geological Society Special Publication,* 276.

VAN ROOIJ, D., BLAMART, D., RICHTER, T., WHEELER, A., KOZACHENKO, M. & HENRIET, J. P. 2007b. Quaternary sediment dynamics in the Belgica mound province, Porcupine Seabight: ice-rafting events and contour current processes. *International Journal of Earth Sciences,* 96**,** 121-140.

VAN WEERING, T. C. E., DE HAAS, H., DE STIGTER, H., LYKKE-ANDERSEN, H. & KOUVAEV, I. 2003. Structure and development of giant carbonate mounds at the SW and SE Rockall Trough margins, NE Atlantic Ocean. *Marine Geology,* 198**,** 67-81.

WENTWORTH, C. K. 1922. A scale of grade and class terms for clastic sediments. *The Journal of Geology***,** 377-392.

WHEELER, A., BECK, T., THIEDE, J., KLAGES, M., GREHAN, A. & MONTEYS, F. 2005. Deep-water coral mounds on the Porcupine Bank, Irish Margin: preliminary results from the Polarstern ARK-XIX/3a ROV cruise. *Cold-water Corals and Ecosystems***,** 393-402.

WHEELER, A., KOZACHENKO, M., HENRY, L. A., FOUBERT, A., DE HAAS, H., HUVENNE, V., MASSON, D. & OLU, K. 2011. The Moira Mounds, small cold-water coral banks in the Porcupine Seabight, NE Atlantic: Part A—an early stage growth phase for future coral carbonate mounds? *Marine Geology,* 282**,** 53-64.

WHEELER, A. J., BEYER, A., FREIWALD, A., DE HAAS, H., HUVENNE, V. A. I., KOZACHENKO, M., OLU-LE ROY, K. & OPDERBECKE, J. 2007. Morphology and environment of cold-water coral carbonate mounds on the NW European margin. *International Journal of Earth Sciences,* 96**,** 37-56.

WHITE, M. & BOWYER, P. The shelf-edge current north-west of Ireland. Annales Geophysicae, 1997. Springer, 1076-1083.

WHITE, M. & DORSCHEL, B. 2010. The importance of the permanent thermocline to the cold water coral carbonate mound distribution in the NE Atlantic. *Earth and Planetary Science Letters,* 296**,** 395-402.

WHITE, M., MOHN, C., STIGTER, H. & MOTTRAM, G. 2005. Deep-water coral development as a function of hydrodynamics and surface productivity around the submarine banks of the Rockall Trough, NE Atlantic Cold-Water Corals and Ecosystems. *In:* FREIWALD, A. & ROBERTS, J. M. (eds.). Springer Berlin Heidelberg.

WOOD, R. 1999. *Reef evolution*, Oxford University Press, USA.